

Native H₂ exploration in the western Pyrenean foothills

Nicolas Lefevre¹, Laurent Truche², Frederic Victor DONZE¹, Maxime Ducoux³, Guillaume Barré⁴, Rose-Adeline Fakoury⁵, Sylvain Calassou⁶, and Eric Gaucher⁷

¹Université Grenoble Alpes

²ISTerre

³M&U sasu

⁴Université de Pau et Pays de l'Adour

⁵Total SA

⁶TOTAL

⁷Centre Scientifique et Technique

November 21, 2022

Abstract

Native hydrogen (H₂) may represent a new carbon free energy resource, but to date there is no specific exploration guide to target H₂-fertile geological settings. Here, we present the first soil gas survey specifically designed to explore H₂ migration in a region where no surface seepage has been documented so far. We choose the Pyrenean orogenic belt and its northern foreland basin (Aquitaine, France) as a playground to test our strategy. The presence of a mantle body at shallow depth (< 10 km) under the Mauléon Basin connected to the surface by major faults is considered as a preliminary pathfinder for H₂ generation and drainage. On this basis, more than 1,100 in situ soil gas analysis (H₂, CO, CO₂, CH₄, H₂S, and ²²²Rn) were performed at ~1 m depth at the regional scale along a 10 x 10 km grid spanning over 7,500 km². The analysis campaign reveals several hot spots to the north of the Mauléon Basin where H₂, CO₂ and ²²²Rn concentrations exceed 1000 ppmv, 10 vol% and 50 kBq m⁻³, respectively. Most of these hot spots are located along the North Pyrenean Frontal Thrust and other related faults rooted in the mantle body. These results, together with evidence of fluid migration at depth, suggest that H₂ may be sourced from mantle rocks serpentinization and carried to the surface along major thrusting faults. Hydrogen traps remain unidentified up to now but the presence of salt-related structures (diapirs) near these hot spots could play this role.

1 **Native H₂ exploration in the western Pyrenean foothills**

2 **Nicolas Lefeuvre^{1,2,*}, Laurent Truche¹, Frédéric-Victor Donzé¹, Maxime Ducoux³,**
3 **Guillaume Barré^{2,4}, Rose-Adeline Fakoury², Sylvain Calassou², Eric C Gaucher²**

5 ¹ Université Grenoble Alpes, CNRS, ISTerre, F-38058 Grenoble Cedex 9, France

6 ² Total SA, CSTJF, F-64018 Pau Cedex – France

7 ³ M&U SAS, 38120 Saint-Egrève - France

8 ⁴ Université de Pau et Pays de l'Adour, E2S UPPA, CNRS, Total, LFCR, 64000, PAU,
9 France

10 *Corresponding author: Nicolas Lefeuvre (nicolas.lefeuvre@univ-grenoble-alpes.fr)

11 **Key Points:**

- 12 • Soil gas mapping for H₂ targeting
- 13 • Fertile area for H₂ production, migration
- 14 • Multiple gas analysis

15

Abstract:

Native hydrogen (H_2) may represent a new carbon free energy resource, but to date there is no specific exploration guide to target H_2 -fertile geological settings. Here, we present the first soil gas survey specifically designed to explore H_2 migration in a region where no surface seepage has been documented so far. We choose the Pyrenean orogenic belt and its northern foreland basin (Aquitaine, France) as a playground to test our strategy. The presence of a mantle body at shallow depth (<10 km) under the Mauléon Basin connected to the surface by major faults is considered as a preliminary pathfinder for H_2 generation and drainage. On this basis, more than 1,100 in situ soil gas analysis (H_2 , CO, CO₂, CH₄, H₂S, and ²²²Rn) were performed at ~1 m depth at the regional scale along a 10 × 10 km grid spanning over 7,500 km². The analysis campaign reveals several hot spots to the north of the Mauléon Basin where H_2 , CO₂ and ²²²Rn concentrations exceed 1000 ppmv, 10 vol% and 50 kBq m⁻³, respectively. Most of these hot spots are located along the North Pyrenean Frontal Thrust and other related faults rooted in the mantle body. These results, together with evidence of fluid migration at depth, suggest that H_2 may be sourced from mantle rocks serpentinization and carried to the surface along major thrusting faults. Hydrogen traps remain unidentified up to now but the presence of salt-related structures (diapirs) near these hot spots could play this role.

33

Plain language Summary:

Native hydrogen (H_2) is currently considered as a possible energy resource for the development of a carbon-free society. Throughout the world, and for over a century, numerous natural H_2 -bearing geological fluids have been discovered, but to date, there is neither exploration strategy nor any resource assessment, as practical guidelines for hydrogen targeting are still missing. Here, we propose a new integrated approach dedicated to native H_2 exploration, using the Pyrenean orogenic belt and its northern foreland basins as a playground. On this basis, a soil gas (H_2 , CO₂, CH₄, radon) exploration campaign, encompassing the major tectonic structures identified in the region has been carried out. This survey reveals several hotspots where H_2 , CO₂ and radon concentrations are by two orders of magnitude above the regional background. These hotspots are mainly located along major faults deeply rooted in the mantle body (~10 km depth) that is well imaged by geophysical data. Therefore, the combined presence of soil gases significantly enriched in H_2 , CO₂, and radon, a dense mantle body below the foreland basin potentially subject to active hydrothermal alteration, and deep faults, represents a favorable geological setting for H_2 generation and drainage.

49

1 Introduction

Several water-rock interaction processes producing molecular hydrogen (hereafter “hydrogen” or “ H_2 ”) in the Earth are now well identified (Klein et al., 2020). Among these processes, serpentinization of ultramafic rocks (Malvoisin et al., 2011; Marcaillou et al., 2011; Mayhew et al., 2013; McCollom et al., 2016) and water radiolysis (Lin et al. 2005a; Truche et al., 2018) have drawn most of the scientific attention so far because they may fuel deep microbial subsurface ecosystems and trigger the abiotic synthesis of organic molecules (Etiope et al., 2015; Fiebig et al., 2007; Johnson et al., 2015; Lin et al., 2005b; McCollom, 2013; Sauvage et al., 2021; Schrenk et al., 2013; Sherwood Lollar et al., 2006; Sherwood Lollar et al., 2021; Truche et al., 2020; Vandenborre et al., 2021). Recently, the growing demand for carbon-free energy has sparked an unprecedented interest in naturally occurring H_2 , as it could represent a potential alternative resource to fossil fuels (Donzé et al., 2020;

61 Gaucher, 2020; Murray et al., 2020; Prinzhofer et al., 2018; Truche and Bazarkina, 2019,
62 Smith et al., 2005).

63 The discoveries of hundreds of natural H₂ seepages, generally connected with
64 circulation of hydrothermal fluids through ultramafic rocks both through seafloors (Donval et
65 al., 1997; Charlou et al., 2010) and on continents (Abrajano et al., 1988; Deville & Prinzhofer,
66 2016; Monnin et al., 2009; Neal & Stranger, 1983; Vacquand et al., 2018; Zgonnik et al.,
67 2020), raise important questions regarding the energy potential of natural hydrogen. Current
68 estimates of global H₂ flux, even if poorly constrained (reported value ranges from ~0.2 to 2.1
69 Tg yr⁻¹; Cannat et al., 2010, Charlou et al., 2010; Merdith et al., 2020; Sherwood Lollar et al.,
70 2014; Truche et al., 2020; Worman et al., 2020) seems to be too low to support an industrial
71 production (~70 Tg of H₂ are manufactured annually worldwide). However, the recent
72 observations of intra-cratonic seepages with no obvious relationship with ultramafic
73 formations (Donzé et al., 2020; Larin et al., 2014; Moretti et al., 2021; Prinzhofer et al., 2019;
74 Zgonnik et al., 2015) have challenged our understanding of H₂ production and behavior in the
75 crust. Despite these questionings, the recent discovery of a H₂-rich (>90 mol% H₂), over-
76 pressurized gas field from the shallow Bougou-1 well, Taoudenit Basin, Mali (Prinzhofer et
77 al., 2018) that is used for small-scale electricity generation, attests to the niche potential of
78 commercial H₂ exploitation.

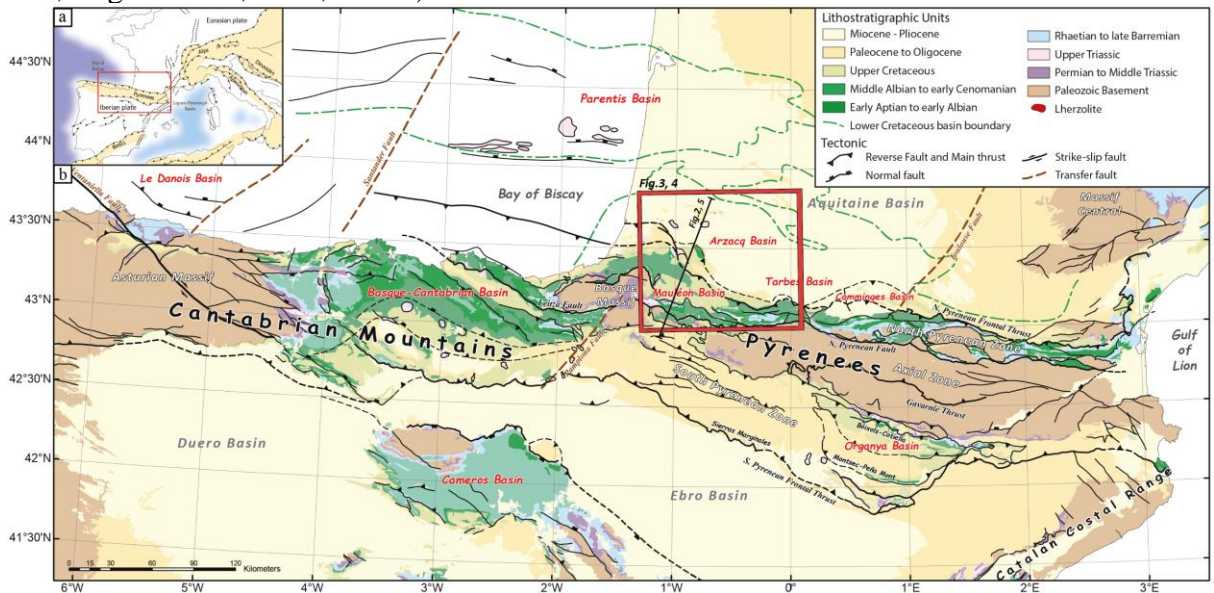
79 Currently, there is neither specific exploration guide to target H₂ fertile geological
80 settings, nor robust resource assessment that can promote industrial interests. Identification of
81 circular depressions in intra-cratonic basins, ultramafic bodies exhumed at the surface (e.g.
82 ophiolites, greenstones belts) or buried under a sedimentary cover represents a promising
83 starting point for exploration, but our knowledge of the hydrogen system is still insufficient to
84 design on purpose drilling campaigns based solely on this information. A combination of
85 geophysical, geochemical and geological data is definitively needed, but in the absence of
86 clearly established exploration guidelines, the direct detection of H₂ seepages remains one of
87 the most straightforward and effective pathfinders. Indeed, the existence of focused seepages
88 at the surface testifies to the presence of active H₂ flux driven by conduits or faults connecting
89 potential leaking reservoirs or draining diffuse sources at depth. This can be done visually by
90 observing H₂-rich gas bubbles in rivers or streams (Chavagnac et al., 2013; Deville et al.,
91 2011), or eternal flame burning H₂ like in Chimaera, Turkey (Etiope et al., 2011), but also by
92 monitoring soil gas emissions. Such a technique has already proven to be useful for the
93 detection of H₂ degassing in surface rounded depressions located in intra-cratonic basins
94 (Donzé et al., 2020; Larin et al., 2014; McCarthy et al., 1986; Moretti et al., 2020; Prinzhofer
95 et al., 2019; Zgonnik et al., 2015). Soil gas monitoring (e.g. ²²²Rn, He, CH₄, CO₂, COS, CS₂,
96 H₂S and light hydrocarbons) combined with geophysical methods enables large areas survey
97 and has already been applied with great success for targeting mineral, geothermal, and
98 hydrocarbons resources (Disnar & Gauthier, 1988; Gao et al., 2011; Hinkle, 1994; McCarthy
99 and Reimer, 1986; Noble et al., 2018; Pereira et al., 2010; Polito et al., 2002). Furthermore,
100 the geochemical characteristics and behavior of soil gases (²²²Rn, Hg, He, H₂, H₂S and CO₂)
101 in volcanic and seismically active areas have been investigated widely for correlating
102 geochemical variations with faults and earthquake activities (Ciotoli et al., 1999, 2007; Du et
103 al. 2008; Li et al., 2013; Lombardi & Voltattorni, 2010; Wiersberg & Erzinger, 2008;
104 Woodruff et al., 2009; Xiang et al., 2020).

105 Here, we present the results of a soil gas regional monitoring campaign dedicated to
106 H₂ exploration. Following synergies and results from the Convergence project, we use the
107 Pyrenean orogenic belt and his northern foreland basins as a case study. This area gathers
108 several promising characteristics that may define a H₂-fertile geological province such as the
109 presence of mantle rock at shallow depth connected to the surface by several deeply rooted
110 faults. The objective of this study is to identify the presence of a H₂ fertile zone through the

111 direct observation of H₂ and associated gas (CH₄, CO₂, ²²²Rn) emissions, and the comparison
 112 of soil gas maps with georeferenced structural and geophysical data.

113 2 Targeting H₂ emissions in the NW Pyrenees foothills

114 The Pyrenees is an E-W-trending orogenic belt (Fig. 1) resulting from the inversion of
 115 a series of rift basins that formed along the Iberia-Europe divergent boundary during the late
 116 Jurassic to Early Cretaceous time (e.g., Clerc et al., 2012, 2013; Ducoux et al., 2019; Jammes
 117 et al., 2009, 2010a; Lagabrielle and Bodinier, 2008; Lagabrielle et al., 2010; Lagabrielle et al.,
 118 2016; Lescoutre and Manatschal, 2020; Masini et al., 2014; Mouthereau et al., 2014; Teixell
 119 et al., 2018; Tugend et al., 2014, 2015b).



120
 121 **Figure 1.** Tectonic setting of the Pyrenean-Cantabrian belt (modified from Pedrera et
 122 al., 2017 and Ducoux et al., 2019). (a) insert show the Iberian Peninsula and the Pyrenean belt
 123 in-between France and Spain. (b) Geological map of the Cantabrian Mountains and the
 124 Pyrenees, with location of the studied area (red rectangle) displayed on Figures 3 and 4. The
 125 black line corresponds to the trace of the cross section displayed on Figure 2 and 5.

126 After the Variscan orogeny, this area records several extensional phases, but the main
 127 phase of divergence between the Iberian and European plates occurs during early Aptian to
 128 early Cenomanian time. This main phase of divergence leads to hyperextension and mantle
 129 exhumation as suggested by remnants of rift basins and several pieces of mantle exposures
 130 now exposed in the North Pyrenean Zone (NPZ) of the Pyrenees (e.g. Jammes et al., 2009;
 131 Clerc et al., 2012, 2013; Fabries et al., 1991, 1998; Lagabrielle and Bodinier, 2008;
 132 Lagabrielle et al., 2016; Masini et al., 2014; Tugend et al., 2014; 2015b). Hyperextension and
 133 mantle exhumation related to a major lithospheric thinning were evidenced by a high
 134 temperature and low pressure metamorphism (Azambre and Rossy, 1976; Bernus-Maury,
 135 1984; Clerc and Lagabrielle, 2014; Clerc et al., 2015; Dauteuil and Ricou, 1989; Ducoux et
 136 al., 2019; Golberg and Leyreloup, 1990; Lescoutre et al., 2019; Ravier, 1959) as well as
 137 emplacements of alkaline magma along the rift axis (Azambre and Rossy, 1976; Azambre et
 138 al., 1992; Le fur-Ballouet, 1985; Rossy et al., 1992). The end of rifting was rapidly followed
 139 by the onset of contractional deformation during the late Santonian with the deposition of the
 140 early-orogenic sequence related to the inversion of the hyperextended rift system (García-
 141 Senz 2002; Garrido-Megias & Ríos 1972; Gómez-Romeu et al., 2019; McClay et al., 2004;
 142 Mouthereau et al., 2014; Muñoz, 1992; Teixell, 1998; Vergés et al., 1995; Vergés & García-
 143 Senz, 2001). The main convergence phase (i.e. collision) occurred in Eocene-Oligocene times

(Mouthereau et al., 2014; Muñoz 1992, 2002; Vergès et al. 2002) and ended during the Chattian (Ortiz et al., 2020). The present-day structure of the Pyrenean belt (Fig. 2) shows an asymmetric double-verging tectonic wedge composed of Paleozoic rocks above the northward underthrusting Iberian continental lithosphere inherited from the Cretaceous hyperextended Pyrenean rift system (e.g., Chevrot et al., 2018; Choukroune and ECORS Team, 1989; Mouthereau et al., 2014; Muñoz, 1992; Roure et al., 1989; Teixell, 1998; Teixell et al., 2016; Vergès et al., 1995; Wang et al., 2016; Fig. 2)..

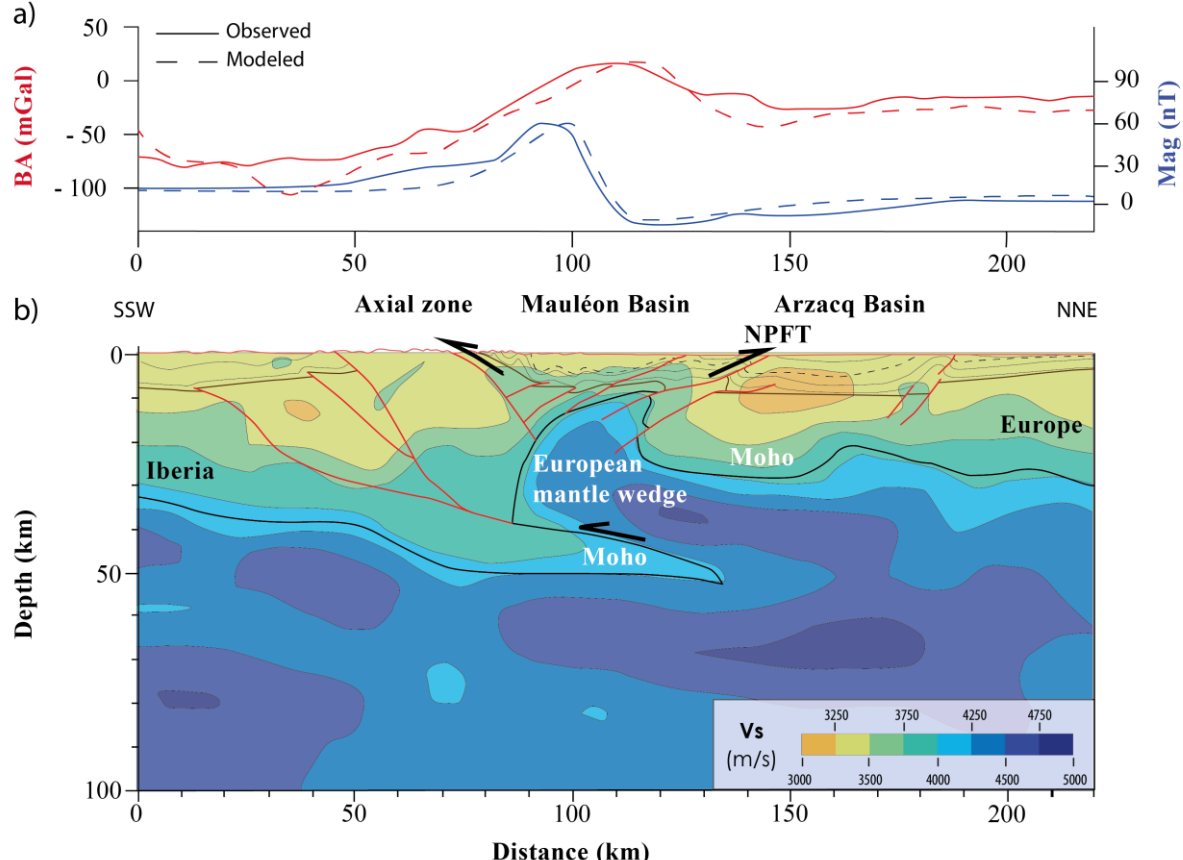


Figure 2. (a) Bouguer (Ayala et al., 2016) and magnetic anomalies (García-Senz et al., 2019), and (b) Vs model obtained by full waveform inversion (modified from Wang et al., 2016) along the same transect shown in Figure 1. NPFT – North Pyrenean Frontal Thrust

In this study we focus on the Mauléon and Arzacq Basins, located in the western NPZ of the Pyrenees. During the rifting phase, these two rift basins bounded by detachment faults were separated by the Grand Rieu ridge made of Paleozoic basement (Jammes et al., 2009; Lecoutre et al., 2019; Masini et al., 2014; Saspiurry et al., 2020; Tugend et al., 2014). The Arzacq Basin sat on the hyperthinned continental crust whereas the Mauléon Basin lied directly on top of exhumed mantle. At present-day, the rift architecture of the Arzacq Basin is relatively well preserved, while the Mauléon Basin was highly deformed during subsequent orogenesis. This latter corresponds to a pop-up structure (e.g., Labaume and Teixell, 2020; Teixell et al., 2016;) that overthrusts the Arzacq Basin towards the north along the North Pyrenean Frontal Thrust (NPFT) and the Axial Zone towards the south along the North Pyrenean Fault (NPF) (Fig. 2b).

Several geophysical studies have also revealed interesting characteristics of the deepest structure of the western Pyrenees (i.e. beneath the Mauléon Basin) by processing gravimetric (Lacan, 2008), magnetic (Garcia-senz et al., 2019) and seismic data (Chevrot et al., 2015, 2018; Wang et al., 2016). First, a strong positive Bouguer gravity anomaly (> 20 mGal; Fig. 2) is observed below the Mauléon Basin. This anomaly is interpreted as the

presence of dense materials at relatively shallow depth such as lower crust or mantle pieces (Grandjean, 1994; Pedreira et al., 2007, Pedrera et al., 2017; Vacher & Souriau, 2001). Second, a significant positive magnetic anomaly (> 60 nT; Fig. 2) is located right below the Mauléon Basin (Garcia-Senz et al., 2019). This magnetic anomaly, which is well correlated with the Bouguer anomaly previously mentioned, provides key information on the nature of mantle rocks because the magnetic susceptibility might be correlated to the serpentinization degree (Oufi et al., 2002; Toft et al., 1990). Indeed, the ultra-mafic rocks such as lithospheric mantle acquire their para-magnetism during the serpentinization reaction, and the associated formation of magnetite. Third, high seismic velocities ($V_p \approx 7.3$ km s $^{-1}$, $V_s \approx 4.2$ km s $^{-1}$) were calculated by full waveform inversion under the western part of Mauléon Basin and are attributed to an exhumed serpentinized mantle body located at 8 to 10 km depth (Christensen, 2004, Wang et al., 2016).

All together, these geophysical data support the presence of a dense mantle body at ~8 km depth below the Mauléon Basin inherited from the Cretaceous pre-collision hyperextended rift system. This dense mantle body was further incorporated into the accreting wedge during the orogenesis of the Pyrenean belt (e.g. Casas et al., 1997; Jammes et al., 2010a; Wang et al., 2016; Lescoutre and Manatschal, 2020; Saspiturry et al., 2020). Therefore, the combination of all these data indicating both the presence of a potential source of H₂ through mantle rocks serpentinization and the existence of preferential conduits for fluid migration makes the north Pyrenean foothills a promising geological setting for H₂ exploration.

3. Materials and Methods

3.1 Soil gas analysis

The investigated area for soil gas analysis is located in the southwest of France (Aquitaine region) along the Pyrenean belt and corresponds to approximately 7500 km 2 (Fig. 1). It encompasses the NPZ, the Mauléon Basin, the Arzacq Basin and the Grand Rieu ridge. A total of 1106 soil gas in-situ measurements have been performed over 131 different locations (Table A2). The sampling mesh was defined along a $\sim 10 \times 10$ km grid (Fig. 3a). The concentration and nature of gases measured in soils may vary according to meteorological (e.g. temperature, hygrometry) and pedological factors (e.g. soil composition, vegetation, microbiology). The present regional soil gas survey is not intended to document the effect of such parameters on soil gas composition. However, all the measurements have been done during spring and summer seasons (April to August 2018, 2019 and 2020) in order to limit the amplitude of hygrometry and temperature variation. Soils affected by anthropogenic activities, such as ploughed soils, gardens or industrial areas have not been sampled. Most of the sampling sites located to the western part of the NPZ have altitudes between 50 to 400 meters above sea level and are mainly composed of grasslands and forest soils. The sampling sites located in the Axial Zone have altitudes ranging from 400 to 1500 meters and are mostly composed of forests and meadows.

At each sampling site, 7 small boreholes were drilled in the soil over an area of 100 m 2 - 5 of them were devoted to H₂, CO, CO₂, CH₄, H₂S, and O₂ measurement using a GA-5000 (GeoTech[®]) multi-gas analyzer and the remaining 2 were dedicated to radon (²²²Rn) measurement using an AlphaGuard DF2000 radon analyzer (Bertin instrument[®]). Additional series of measurements have been carried out over time (2018, 2019 and 2020) on hot spots where H₂ concentration was > 200 ppmv. Each borehole has a depth of ~1 m and a diameter of 1 cm. A portable drill (DH36DBL, Hitachi[®]) operating in percussion mode only (no rotation of the drill bit) was used for this purpose. Numerous tests were conducted using various drilling procedures on different lithologies and soils to determine the optimal drill

218 configuration. Thus, a specific drilling procedure was selected to minimize and even prevent
 219 any production of H₂ through drill bit metamorphism and “mechano–radical” processes.
 220 Indeed, the increase in temperature of the drill bit may induce the cracking of the organic
 221 matter and trigger H₂ production (Lewan et al., 1997; Li et al., 2017; Lorant et al., 2002). The
 222 mechanical dissociation of the covalent Si-O bond in silicate minerals creates surface radicals
 223 which react with water to produce H₂. This process, referred to as “mechano–radical”, has
 224 been experimentally demonstrated by friction experiments involving various silicate bearing
 225 rocks saturated with water (Hirose et al., 2011) and is supposed to be at the origin of high
 226 concentration of H₂ in soil gas associated with active tectonic faults (Kita et al., 1982; Sato et
 227 al., 1984). Drilling boreholes in soils without drill bit rotation clearly prevent artificial
 228 generation of H₂ as demonstrated by Halas et al. (2021), and by our plethora of measurements
 229 where H₂ concentrations in soil gas is lower than 5 ppmv (Table A1). Immediately after
 230 drilling, a stainless-steel sampling probe was tightly inserted inside the borehole and
 231 connected to one of the two gas analyzers either for ²²²Rn or for H₂, CO₂, CH₄ and O₂
 232 measurements. Each gas analyzer is equipped with a pump set to operate at the same flow rate
 233 of 550 mL min⁻¹.

234 The multi-gas detector GA-5000 is equipped with two different sensors: 1) an
 235 electrochemical cell for H₂, CO, H₂S, and O₂ concentration measurements, and 2) a dual
 236 wavelength infrared sensor for CO₂ and CH₄ concentration measurements. Uncertainties and
 237 interferences are documented in Table 1. Galvanometric measurement of a gas mixture of H₂,
 238 CO, and H₂S is subject to potential cross-interferences (Korotcenkov et al., 2009).

Gas	Range	Typical accuracy	
CH ₄	0 - 100 vol%	0 - 70 ± 0.5 vol%	70 - 100 ± 1.5 vol%
CO ₂	0 - 100 vol%	0 - 60 ± 0.5 vol%	60 - 100 ± 1.5 vol%
O ₂	0 - 25 vol%	0 - 25 ± 1 vol%	
H ₂	0 - 1000 ppmv	2 ppmv	

239 **Table 1.** Gas concentration range and measurement accuracy for CH₄, CO₂, O₂ and H₂
 240 analysis by the GA-5000 instrument.

241 However, H₂ concentration measurement over the 0 – 1000 ppmv range is weekly
 242 impacted (< 10 ppmv) by the combined presence of CO and H₂S provided their
 243 concentrations remain < 300 ppmv and < 15 ppmv, respectively. Other species like HCN,
 244 NO_x or C₂H₄ may also interfere with the H₂ measurement, but their concentrations have never
 245 been detected in the prospected soils. For all measurements done in the field, H₂S has never
 246 been detected in the soil gases during our exploration campaign, neither using the GA-5000
 247 gas analyzer nor by gas chromatography (see below), nor olfactorily for H₂S (human can
 248 smell H₂S at few tens of ppb in the air). In addition, for every H₂ concentration recorded with
 249 the GA-5000 analyzer at a value above 500 ppmv, a separate soil gas sample was taken in a
 250 gas tight Swagelok® stainless steel gas cylinder (40 mL). The cylinder was put under vacuum
 251 first using a primary vacuum pump and then connected to the soil gas probe for sampling. The
 252 gas composition was further analyzed in the lab regarding H₂, CO₂, CO, CH₄ using a Perkin
 253 Elmer® CLARUS 500 Gas Chromatograph (GC) equipped with a thermal conductivity
 254 detector (TCD) and a 2 m long column (RESTEK® Shin Carbon ST 80/100) with Ar as a
 255 carrier gas. The GC was calibrated using several Ar + H₂ + CH₄ + CO₂ + CO gas mixtures of
 256 different concentrations injected with a gas syringe of calibrated volume. The estimated
 257 analytical error is ± 5%.

258 The AlphaGuard DF2000 device is equipped with a pulsed ionization chamber
 259 (internal volume of 0.62 L) and a fiberglass selective filter. The radon (²²²Rn) measurement

range is between 2 to 2×10^6 Bq·m⁻³ with uncertainty variability of 5 cpm at 100 Bq·m⁻³. The analysis is based on the decay of ²²²Rn to ²¹⁸Po resulting in the emission of α -particles which can be measured by the instrument. Relative humidity, atmospheric pressure and temperature are simultaneously measured.

3.2 Soil gas data processing

The statistics of the soil gas concentration sampled during the survey are reported in Table 2. The averaged concentrations of H₂, CO₂ and ²²²Rn were then interpolated and mapped using ArcGIS Pro (ESRI®) geographical information software (GIS). The natural neighbor interpolation method was used to define lines of equiconcentration of H₂, CO₂ and Radon. This method is based on the Voronoï tessellation of our discrete set of spatial gas concentration measurements (Sibson, 1981).

Gas	N	Mean	Standard deviation	Min	Max
H ₂ (ppmv)	1106	33	104	0	> 1000
CO ₂ (vol%)	1106	0.85	1.2	0	10.5
²²² Rn (Bq m ⁻³)	893	1002	9343	0	57316

Table 2. Main statistics of soil gas data acquired during this study.

4 Results

4.1 Soil gas mapping

The localization of each sampling site is shown in Figure 3a (red cross). These 131 locations constitute a sampling grid where a total of 1106 soil gas analyses have been carried out over 3 years (Table A1). This sampling grid is superimposed to the geological map of the targeted area (Fig. 3a) and the associated H₂, CO₂, and ²²²Rn gas concentration contour maps are also plotted (Fig. 3b, c and d, respectively). When looking at these 3 latter maps (Fig. 3b, c and d), one can observe that most of the highest H₂, CO₂, and ²²²Rn concentrations are located along the NPFT or to the south of this major fault. In addition, these high gas concentration data define 12 hot spots, with some of them being superimposed.

4.2 Hydrogen

Regarding H₂ concentrations, their values range from 0 to > 1000 ppmv. Among the 1106 concentration values reported in Table A1, 958 data (87 %) are < 50 ppmv, 146 data (6 %) are \geq 50 ppmv, with 73 data (7 %) being > 100 ppmv and 5 data being above the sensor saturation (1000 ppmv) of the GA-5000 instrument. The high H₂ concentration values can be grouped into three main hot spots (Fig. 3b). The most significant hot spot is located between a triangle defined by Orthez to the north east, Peyrehorade to the east and Sauveterre-de-Béarn to the south. In this zone (133 km²), 10 neighboring sampling sites display mean H₂ concentration values above 50 ppmv. In more details, among 298 measurements carried out over 3 years in this area, 89 (30 %) display H₂ concentration above 50 ppmv. Four sampling sites exhibit high H₂ concentrations: Le Bourguet (up to 547 ppmv), north and east Baigts-de-Béarn (up to 734 and 481 ppmv, respectively), Sauveterre-de-Béarn (up to 632 ppmv) and Laborde (above the quantification limit of 1000 ppmv). At Sauveterre-de-Béarn, H₂ concentration was independently measured by GC and was found to be as high as 822 ppmv. The second hot spot is located to the south west of Asasp Arros. It corresponds to a single location where 5 independents gas measurements were > 50 ppmv. The third hot spot, located to the south of Pau, corresponds to two neighboring locations close to the NPFT. There, 6

300 independent measurements were > 50 ppmv of H₂ with a maximum value of 129 ppmv. In
301 addition to these 3 H₂ hotspots, it was found that the soils surrounding two outcropping bodies
302 of lherzolite at Urdach and Turon de La Técouère (red squares on Fig. 3b) also display high
303 H₂ concentrations, but with high heterogeneities among the values. At Urdach, over the 9
304 measurements carried out, 2 were > 1000 ppmv. At Turon de la Técouère, 2 measurements
305 were > 1000 ppmv, 18 measurements were in-between 100 and 800, and the other 11 were <
306 100 ppmv. These two locations are both very singular and very specific because of their
307 geological context. Thus, they are not included into the interpolation in order to avoid bias in
308 the interpretation of the map.

309 4.3 Carbon dioxide

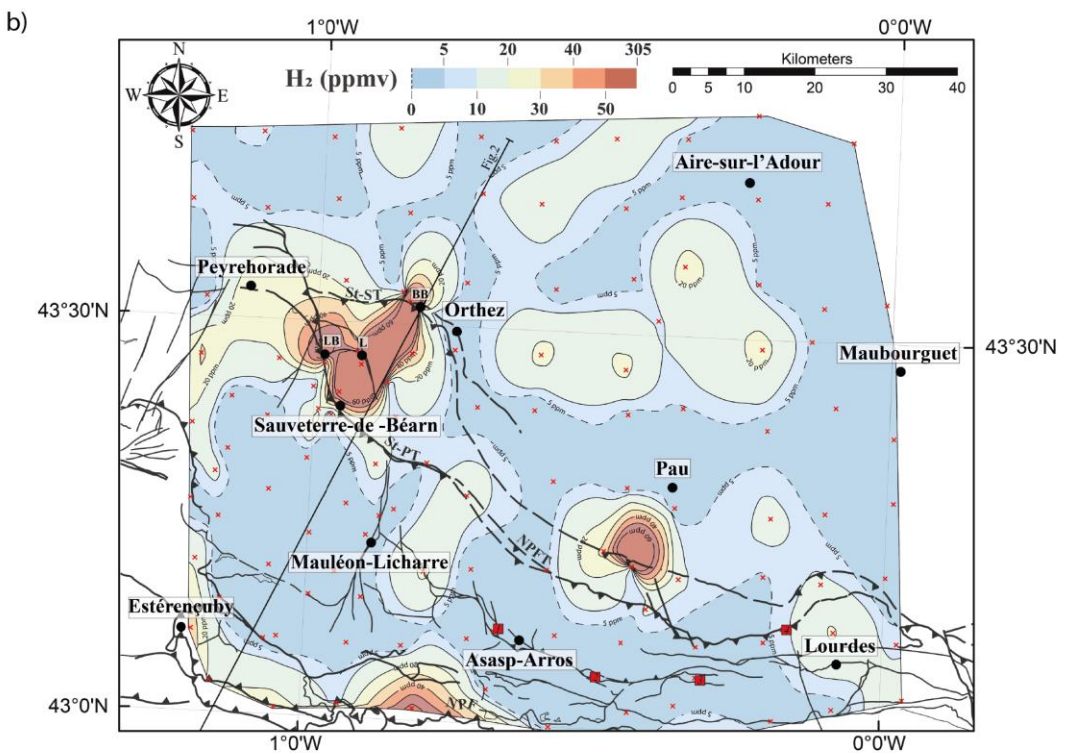
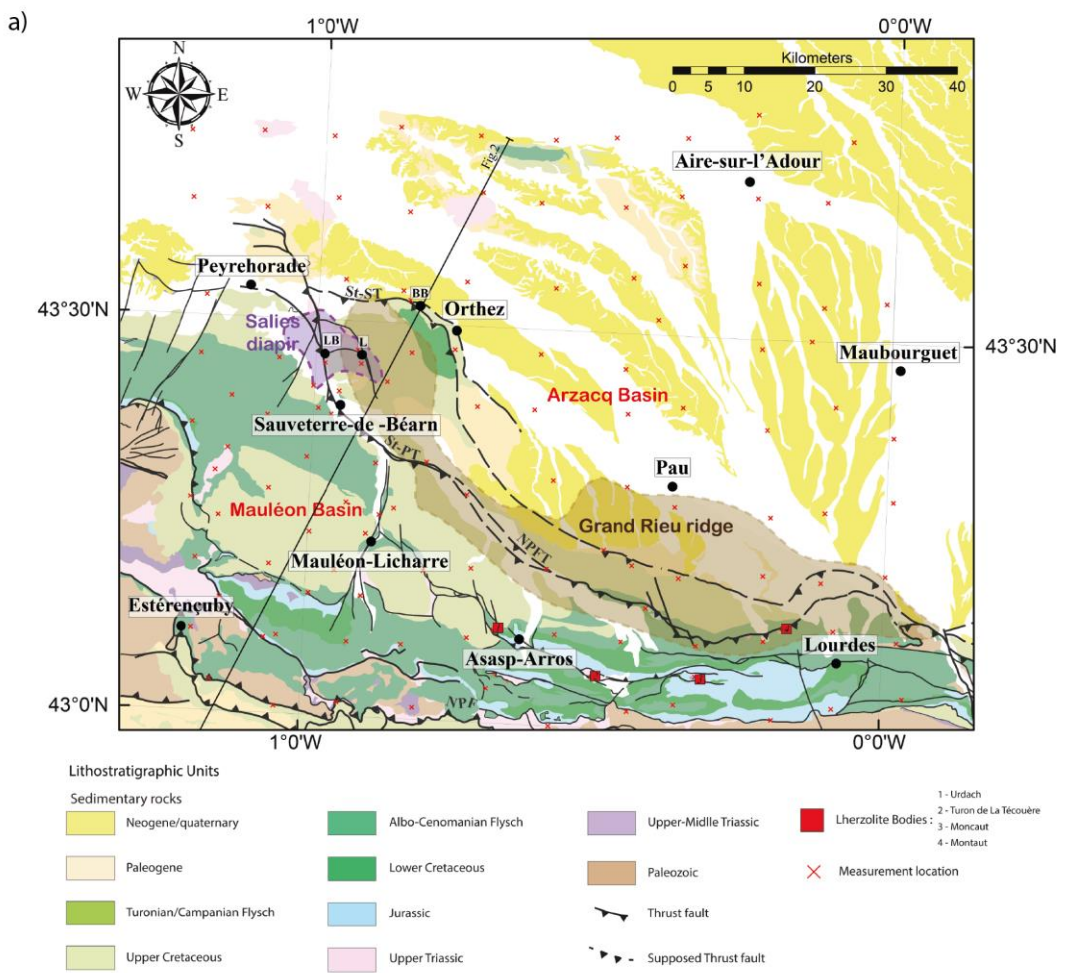
310 Regarding the CO₂ concentrations, their values range from 0 to 10.3 vol% with the
311 following distribution: 815 values (74 %) are ≤ 1 vol%, 233 values (21 %) are in the range 1
312 to 3 vol% range, and 58 values (5 %) are > 3 vol% with a maximum at 10.3 vol% (Table A1).
313 The spatial distribution of CO₂ concentration is less contrasted than for H₂, but the high
314 concentrations zones lie mostly to the south of the NPFT (Fig. 3b). Among the five detected
315 hotspots where CO₂ concentration exceed 3 vol%, one display some overlaps with the
316 previously described H₂ hot spot located on the NPFT: i.e. close to Peyrehorade with a
317 maximum of 3.05 vol%. Another was located near Sauveterre-de-Béarn with a maximum of
318 10.3 vol%. Two others hot spots were located along faults, to the east of Asasp-Arros, and to
319 the south-east of Lourdes. Their maximum CO₂ concentrations are 2.9 and 3.8 vol%,
320 respectively. The last hot spot is located in the Arzacq Basin to the east of Orthez. It exhibits a
321 maximum CO₂ concentration of 2.5 vol%.

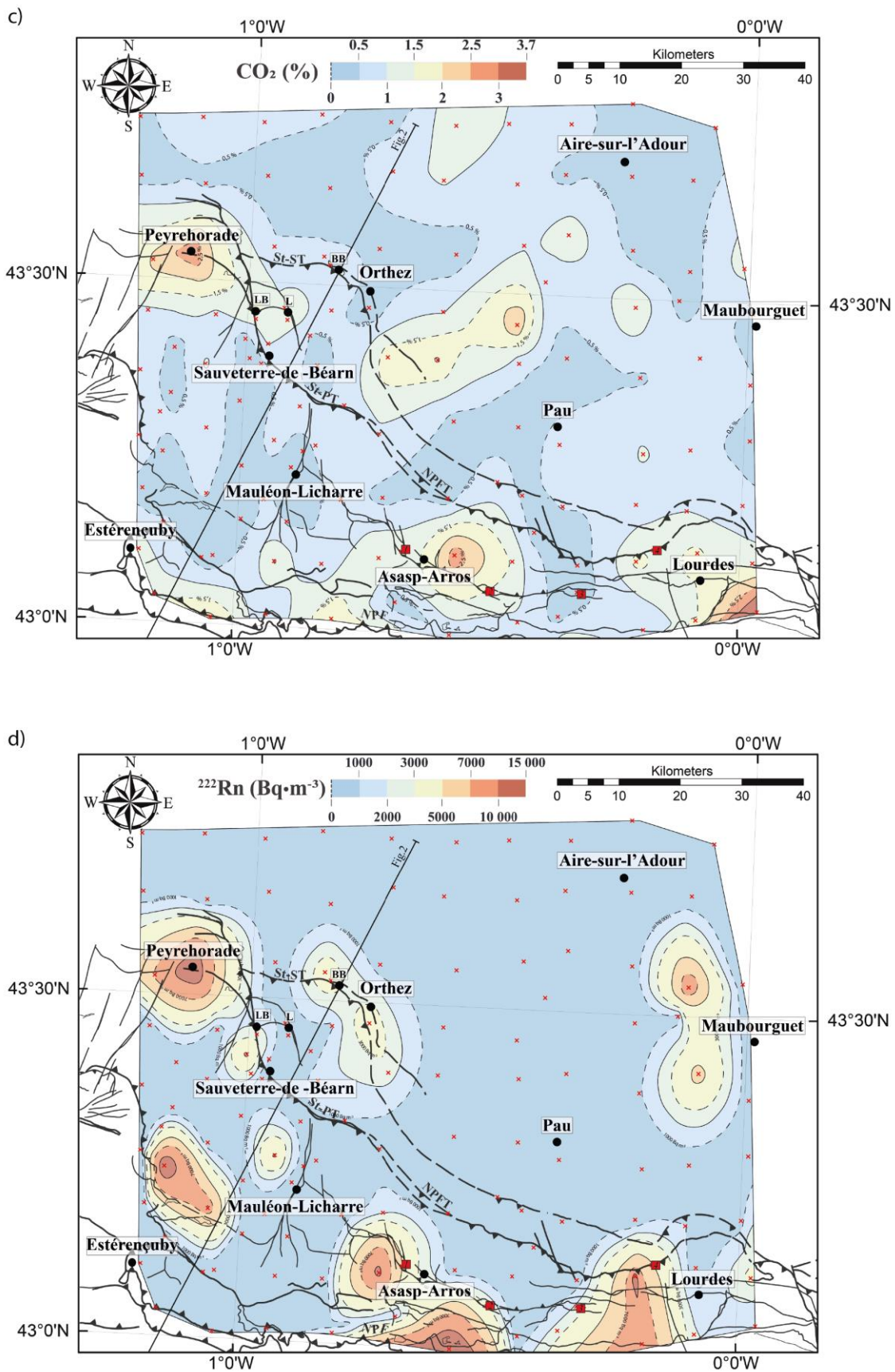
322 4.4 Methane, carbon monoxide and hydrogen sulfide

323 Methane (CH₄) was also measured with the GA-5000 instrument, but its concentration
324 was always below the quantification limits (0.5 vol%) and was not detected by GC analysis at
325 Sauveterre-de-Béarn. Hydrogen sulfide (H₂S) was never detected, and carbon monoxide (CO)
326 was rarely detected (38 values ≥ 10 ppmv, maximum 79 ppmv), with a random spatial
327 distribution. The oxygen (O₂) concentration was very close to 20 vol% (except when CO₂
328 concentration was > 5 vol%) indicating that all our samples were dominated by air.

329 4.5 Radon

330 Finally, the radon soil gas map (Fig. 3d) can be nicely superimposed to the H₂ and
331 CO₂ zones (Fig. 3b, and d, respectively). Among the 893 ²²²Rn concentration values (Table
332 A1), 177 (20 %) are ≥ 1 kBq m⁻³, with a very high value of 57.3 kBq m⁻³ recorded at
333 Sauveterre-de-Béarn. Most of the highest ²²²Rn concentrations are located along the NPFT
334 and to the south of this major fault. Seven hot spots exceeding ²²²Rn concentration of 5
335 kBq m⁻³ can be easily identified: 1) Peyrehorade with a maximum at 28.6 kBq m⁻³, 2) to the
336 north of Sauveterre-de-Béarn with a maximum at 57.3 kBq m⁻³, 3) to the north of Estérençuby
337 with a maximum at 13.4 kBq m⁻³, 4) to the west of Asasp-Arros with a maximum of 33.2
338 kBq m⁻³, 5) to the south of Asasp-Arros with a maximum at 20 kBq m⁻³, 6) to the west of
339 Lourdes with a maximum at 14.4 kBq m⁻³, and 7) to the north-east and south-east of
340 Maubourguet with maximums of 12 and 8.2 kBq m⁻³, respectively. Interestingly, the large H₂
341 and CO₂ hotspot previously identified in between Orthez, Peyrehorade and Sauveterre-de-
342 Béarn, also corresponds to an area of high ²²²Rn concentration.
343





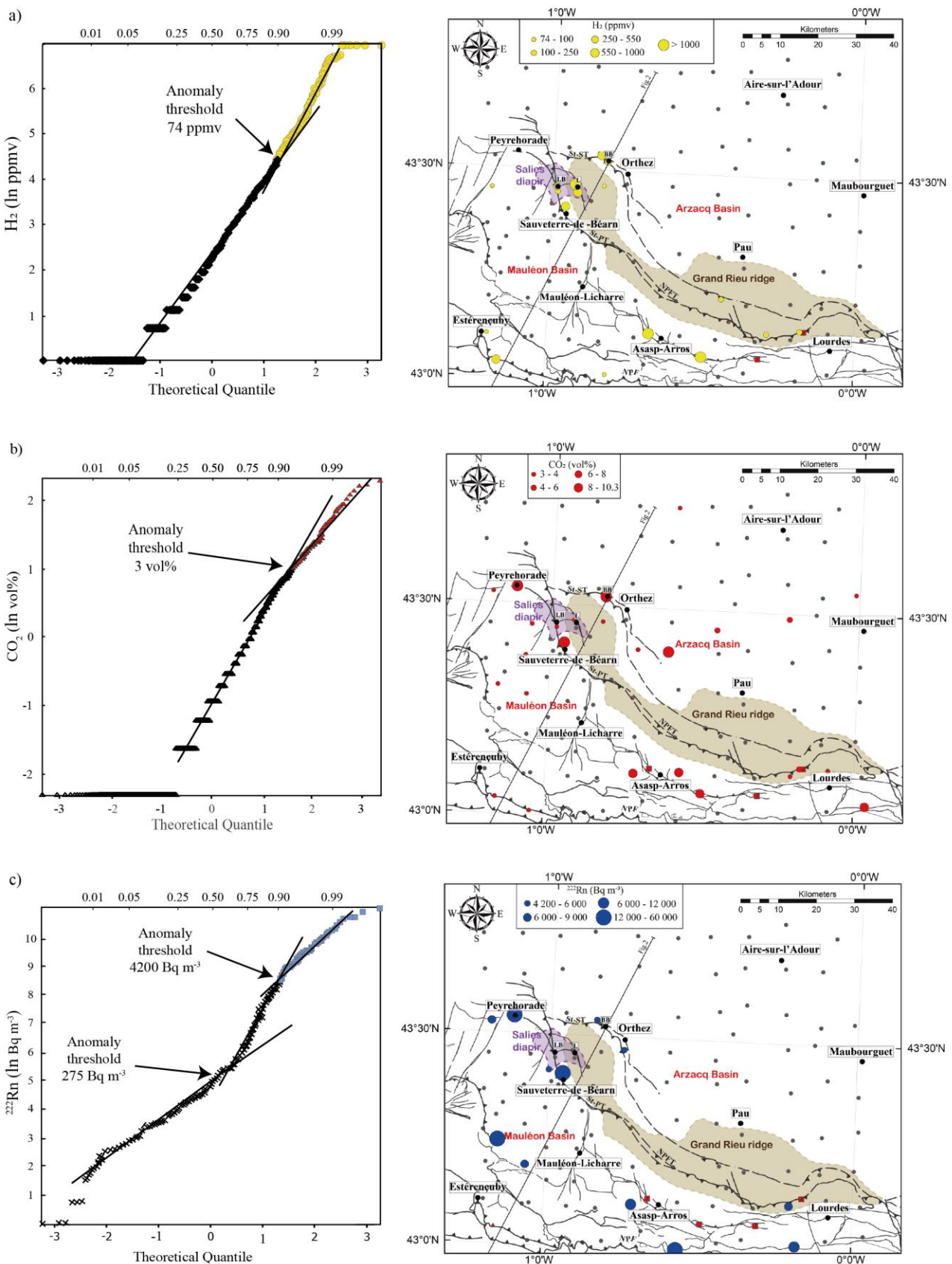
346 **Figure 3.** (a) Geological map of the studied area with the localization of the Mauléon
347 and Arzacq Basins split apart by the Grand Rieu ridge and the NPFT faults networks (St-ST -
348 Saint-Suzanne Thrust; St-PT - Saint-Palais Thrust; Ducoux et al., 2021). Each red cross
349 corresponds to a measurement site. (b, c, and d) Contour maps of the mean concentration of
350 H₂, CO₂ and ²²²Rn soil gas measured at each sampling site, respectively.

351 **5 DISCUSSION**

352 5.1 Soil gas background concentration and identification of gas anomaly
353 thresholds

354 Statistical information about the soil gas survey is reported in Table 2 (min, max,
355 median, standard deviation). All the measurements were acquired under similar
356 meteorological conditions and can be compared to atmospheric gases concentrations of ²²²Rn
357 (0.01 kBq m⁻³), H₂ (531 ppb), and CO₂ (0.039 vol%) (Baubron et al., 2002; Novelli et al.,
358 1999).

359 Given the multiple potential sources of gases and the variability of their concentrations
360 with respect to the atmosphere, the soil gas anomaly thresholds cannot be determined in an
361 absolute way but a statistical approach can provide fruitful information (Ciotoli et al., 2016).
362 Here, the background level of the soil gas was determined from the quantile-quantile plot (Q-
363 Q plot) as described by Sinclair (1991). This procedure requires the identification of both
364 quasi-linear segments on a probability curve and inflection points between the different linear
365 trends (Lombardi et al., 2010; Reimann et al., 2005). The intersection between the different
366 straight lines corresponds to threshold values. It is a graphical method used to identify
367 different gas population above the background level which will be presented and used in the
368 following sections (Fig. 4).



370 **Figure 4.** On the left-hand side is shown the quantile-quantile plots (Q-Q plots)
371 calculated for (a) H₂, (b) ²²²Rn and (c) CO₂ soil gas measurements. The corresponding
372 anomaly threshold values are 74 ppmv, 4,200 Bq m⁻³ and 3 vol%, respectively. The spatial
373 distribution of these anomalies is displayed on the right-hand side of each Q-Q plots. NPFT –
374 North Pyrenean Frontal Thrust; NPF – North Pyrenean Fault; St-ST - Saint-Suzanne Thrust;
375 St-PT - Saint-Palais Thrust.

376 5.1.1 Hydrogen concentration anomalies

377 The Q-Q plot calculated for H₂ concentration highlights a non-linear evolution
378 indicating the presence of at least two origins or sources for this gas (Fig. 4a). The inflection
379 point between these linear trends indicates a soil gas concentration threshold anomaly at 74
380 ppmv.

381 The spatial distribution of H₂ concentrations is not random. Indeed, most of the
382 measurements ranging from 1 to 74 ppmv (i.e. below the threshold) are located within the
383 Arzacq and the Mauléon basins. The higher hydrogen concentrations (> 74 ppmv) are located
384 near the main faults such as NPFT and NPF. The other anomalies, disconnected to these
385 faults, are located close to the Iherzolite bodies.

386 The hydrogen concentration below the threshold anomaly, i.e. the sharp change in
387 concentration, could be linked to a microbial production. Microbial H₂ can be produced from
388 different processes in soils such as fermentation, nitrogen fixation, anaerobic carbon
389 monoxide oxidation or phosphite oxidation (Sipma et al., 2006; Schwartz et al., 2013).
390 Hydrogen-producing microorganisms use metallo-enzymes such as [FeFe], [NiFe] and [Fe]
391 hydrogenase in their metabolisms (Gregory et al., 2019). These enzymes can also be used in
392 the reverse reaction for H₂ uptake and oxidation. These metallo-enzymes are present in
393 anaerobic bacteria and eukaryotes (Peters et al., 2015). Fermentation is the most common
394 process in nature to produce H₂ and may be important where organic matter is abundant.
395 However, H₂ is usually maintained at low concentration in superficial environments because
396 fermentative H₂ producer and respiratory H₂ consumers live in symbiosis or consortia in the
397 microbial mats (Gregory et al., 2019, Kessler et al., 2019; Thauer et al., 1996). Thus, the net
398 H₂ ecosystem flux is mainly controlled by soil uptake except during the leaf senescence in
399 Autumn (Meredith et al., 2016). The optimum uptake temperature is approximately 30 °C
400 (Ehhalt & Rohrer, 2011) and decreased with soil saturation, as water-filled pore spaces that
401 prevent the gas diffusion (Conrad & Seiler, 1985; Popa et al., 2011). The type of soil is an
402 important factor for both H₂ uptake and emission (Ehhalt & Rohrer, 2009). The uptake of H₂
403 is mainly related to the amount of hydrogenase in soil bacteria and to environmental
404 conditions (Meredith et al., 2017). The rate of H₂ uptake is correlated to the abundance of H₂-
405 oxidizing bacteria (Khdhiri et al., 2015). The highest uptake rates are recorded in forest soils
406 while in grasslands the rates are lower (Chen et al 2015; Ehhalt & Rohrer, 2009; Khdhiri et
407 al., 2015). Thus, the H₂ concentration in soils generally remains at low level, with lower
408 values in forest soils than in grassland: 500 and 2500 ppb, respectively (Chen et al 2015). In
409 this study, all H₂ concentration values below 10 ppmv can be the result of biological
410 processes, while the high concentration values (> 74 ppm) reflect the contribution of other
411 sources that may be deep-seated.

412 The hydrogen concentration ranging from 74 to > 1000 ppmv (i.e. above the threshold
413 anomaly) seems to be clustered to the north west of Grand Rieu ridge and above the Salies
414 salt diapir. These high H₂-concentrations may result from different sources than those below
415 the threshold concentration value. They could be linked to mechano-radical reactions
416 occurring along active faults or to a deeper production of H₂ through serpentinization, or
417 water radiolysis. The rock crushing along fault planes results in the formation of fresh surfaces
418 that are extremely reactive. The reaction between these surfaces and water potentially

419 produces H₂ (Hirose et al., 2011; Kita et al., 1982). This mechanism is often invoked as the
420 source of H₂ in active tectonic areas (Dogan et al., 2007). However, several studies have
421 shown that the concentration of H₂ in the soil along active fault rarely exceed 100 ppm
422 (Dogan et al., 2007; Li et al., 2013). Currently, the Pyrenean belt is in a post-orogenic
423 situation, where earthquakes of low-magnitude occur currently. However, no earthquake with
424 magnitude > 2.9 was recorded by the BCSF – RéNaSS seismic network near the surface along
425 the NPFT during the sampling campaign. Thus, we can safely exclude rock comminution and
426 mechano-radical process as major sources of H₂ in the targeted area. Therefore, others deep-
427 seated origins for H₂, such as mantle rocks serpentinization or water radiolysis can be
428 envisioned to explain the high H₂ concentration recorded near Sauveterre-de-Béarn. The role
429 of deeply rooted faults in H₂ drainage is emphasized in the next section.

430 High concentration of H₂, i.e. > 1000 ppmv, are also recorded close to the two
431 Iherzolite bodies of Turon de la Técouère and Urdach (Table A1). The origin of these gas
432 anomalies is probably not deep-sourced, but may correspond to low temperature
433 serpentinization process, and to the release of gases entrapped in the rock as observed at a
434 larger scale in numerous ophiolites worldwide (Etiope et al., 2011).

435 5.1.2 CO₂ concentration anomalies

436 The Q-Q plot calculated for CO₂ exhibits a non-linear evolution with an
437 inflection point at 3 vol% that corresponds to a threshold anomaly (Fig. 4b). The CO₂
438 concentration below this value could be attributed to organic material oxidation, micro-
439 organisms or plants respiration (Romanak et al., 2014; Sugisaki, 1983). The CO₂
440 concentrations above this threshold anomaly could result from a mixing of potential deep
441 sources such as mantle degassing, carbonate metamorphism, or carbonate dissolution with
442 other surface sources as described above (Cooper et al., 1997).

443 The locations for CO₂ anomalies both in the basins and in fault zones are presented in
444 Figure 4c. The anomalies observed in the basins are disconnected from the deep structure,
445 which lead us to suppose that they are mainly the result of biological processes as detailed in
446 the previous section. The other CO₂ anomalies are localized along faults (Fig. 4b) and are
447 particularly clustered near the Salies diapir and to the north west of Grand Rieu ridge. These
448 latter anomalies are also correlated with the H₂ and ²²²Rn anomalies at this location. This
449 clustering strengthens the scenario of an active gas-bearing fault zone where CO₂ acts as a
450 carrier gas for other species (H₂ and ²²²Rn) from deep-seated sources. Note that H₂ can also
451 migrate independently from other gases because of the small size and high diffusivity of the
452 molecule.

453 5.1.3 Radon concentration anomalies

454 The Q-Q plot calculated for ²²²Rn also highlights a non-linear spatial evolution
455 of its concentration with two inflection points indicating at least two possible threshold
456 anomalies, the first at 275 Bq m⁻³ and the second at 4200 Bq m⁻³ (Fig. 4c). Radon
457 concentrations below the first threshold anomaly at 275 Bq m⁻³ correspond to the background
458 level in the area as described by the French Institute for Radioprotection and Nuclear Safety.
459 Radon concentrations between 275 and 4200 Bq m⁻³ are randomly distributed above the
460 sedimentary basins and generally located far from the faults. The radon concentrations above
461 the second threshold anomalies (i.e. 4200 Bq m⁻³) can be as high as 57 kBq m⁻³. These high
462 values are mainly localized along the faults (Fig. 4c) and more particularly to the north
463 western part of Grand Rieu ridge, around the Salies salt diapir, where high H₂ concentrations
464 are also recorded. Note that, the two anomalous values recorded within the core of the
465 Mauléon Basin are the only exceptions to this distribution along faults of the high ²²²Rn
466 concentrations.

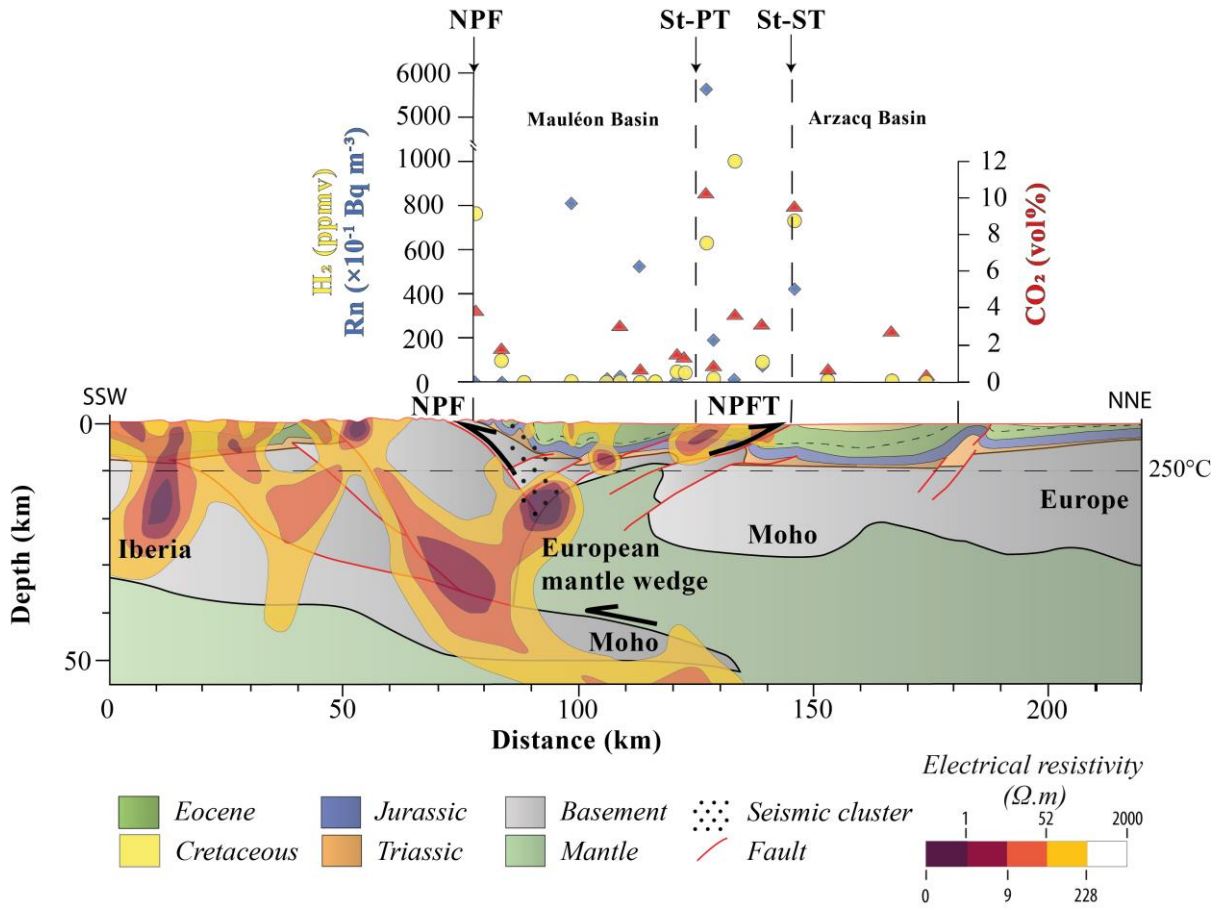
Because of its short half-life (3.82 days), ^{222}Rn must be carried rapidly upwards by ascending fluid to remain at high concentration when escaping into the atmosphere. Its presence at elevated concentration in soils indicates both active fluid circulation and subsurface lithologies enriched in ^{238}U , ^{232}Th and ^{40}K (Baubron et al., 2002). It has been already proven that ^{222}Rn is a useful pathfinder to map hydrothermal systems and active faults (Toutain & Baubron, 1999). Therefore, the high concentration of ^{222}Rn correlated with high H_2 and CO_2 concentrations near the Salies diapir, and along the NPFT near Sauveterre-de-Béarn, is a strong evidence for an active fluid circulation in deep-seated formations. Hydrogen may be at least partly sourced from water radiolysis, because these high ^{222}Rn concentrations testify for the presence of radioactive elements at depth.

5.2 Possible H_2 production system in the Pyrenean foothills

The western part of Pyrenean structure is characterized by a massive mantle body at shallow depth (< 10 km) as inferred from geophysical data (Chevrot et al., 2015, 2018; Garcia-Senz et al., 2019; Lacan, 2008; Wang et al., 2016). Another important observation is the occurrence of quasi-periodic seismic activity located to the south of the NPZ beneath the Mauléon Basin (Fig. 5). Numerous studies interpret these seismicity patterns as the result of stress triggered by fluid flows (Faulkner et al., 2010; Hainzl, 2004; Hardebeck, 2012; Rigo et al., 2008). Souriau et al. (2014) indicate that these earthquake clusters might be related to the convective circulation of fluids along the NPF (Fig. 5). Fluid circulation in deeply rooted faults is confirmed by helium and ^{222}Rn anomalies in soil gas (Baubron et al., 2002). Furthermore, the presence of fluid has been detected by low electrical resistivity at 13 to 15 km depths (Campanya et al., 2012). Such a depth also corresponds to the location of the seismic swarm identified by Souriau et al. (2014) (Fig. 5).

The regional geothermal gradient of $25.0 \pm 2.7 \text{ }^{\circ}\text{C km}^{-1}$ (Bonté et al., 2010) is relatively modest, but the north western part of Mauléon Basin (Fig. 3a) displays anomalously high temperatures above $65 \text{ }^{\circ}\text{C}$ at 1000 to 2000 m depth. An indication of this thermal anomaly is the presence of numerous hydrothermal springs in the western part of Mauléon Basin; such as Combo-les-Bains, or Salies-de-Béarn. Hot fluid circulation may create a convection cell that drives heat upwards from deep thermal anomaly (Bonté et al., 2010). Given the regional geothermal gradient value, one may also expect temperatures at the top of the exhumated mantle at about 10 km depth to be around $250 \text{ }^{\circ}\text{C}$ (Saspiturry et al., 2020). Such a temperature is optimum for efficient serpentinization of the mantle rocks, magnetite formation, and H_2 generation (Malvoisin et al., 2011; Klein et al., 2020).

Therefore, the combined presence of both, a dense mantle body below the Mauléon Basin potentially subject to an active serpentinization, and deeply-rooted faults corresponding to the NPFT and the NPF zones (Fig. 2), represents a favorable geological setting for H_2 generation and drainage. Water radiolysis may also contribute to H_2 production, but to date we cannot discriminate this source from serpentinization. In the present case, we note however, that the importance of water radiolysis may be secondary compare to serpentinization in the global H_2 budget. Indeed, Warr et al. (2019) indicate that the contribution of water radiolysis on H_2 production is higher in felsic environments whereas its production by serpentinization comes mainly from mafic environments. Here, the presence of a large mantle body (i.e. ultra-mafic rocks) at shallow depth seems to provide the most fertile environment for H_2 generation. We therefore assume that H_2 is more likely generated by serpentinization than by radiolysis.



512 **Figure 5.** (bottom) Geological interpretation of the tomographic model (modified
 513 from Wang et al., 2016) superimposed to both a two-dimensional electrical resistivity model
 514 (after Campanyà et al., 2012) and the projection of a deep seismic cluster (after Souriau et al.,
 515 2014). The location of the section is shown on Figure 1. (top) H₂ (circle), ²²²Rn (diamond)
 516 and CO₂ (triangles) max concentrations obtained along this section. NPFT – North Pyrenean
 517 Frontal Thrust; NPF – North Pyrenean Fault; St-ST - Saint-Suzanne Thrust; St-PT - Saint-
 518 Palais Thrust

519 In fact, the high H₂ emission spots obtained from the soil gas measurements carried
 520 out in the western Pyrenees agree well with the presence of this mantle body at shallow depth
 521 and the deep-rooted faults. The gas concentration along the western ECORS-Arzacq profile is
 522 displayed in Figure 5. The highest H₂, CO₂ and ²²²Rn soil gas concentrations were recorded
 523 along the NPFT and the Grand Rieu ridge at >1000 ppmv, 10 vol%, and 57 kBq m⁻³,
 524 respectively. Such deeply rooted faults, described as weakened zones partly composed of
 525 highly connected fracture networks, represent preferential pathways for fluid circulation
 526 carrying H₂ and other gases from deep sources to the surface (Baubron et al., 2002; Donzé et
 527 al., 2020; Gal & Gadalia, 2011). The gas concentration measurements carried out in the
 528 Mauléon and Arzacq Basins display lower values than within the Grand Rieu ridge (Fig 3a)
 529 and show a strong variability in concentration between H₂, CO₂ and ²²²Rn. Hydrogen is nearly
 530 absent from these basins while the ²²²Rn is only present in Mauléon Basin and CO₂ is present

531 in both basins. These basins were never connected during the Cretaceous rifting event,
532 because they were separated by the Grand Rieu. The Arzacq Basin is therefore not
533 connected to the mantle structure well identified below the Mauléon Basin (Masini et al.,
534 2014; Lescoutre et al., 2019). Hence, these major structural features explain very well the
535 contrasted in term of gas concentration patterns observed in-between these two basins.

536 In addition, the main hot spots located between Sauveterre-de-Béarn, Orthez and
537 Peyrehorade are close to or just above the Salies salt diapir whose roof is only at less than 70
538 m below the surface (Berard & Mazurier, 2000). Such a structural configuration may also
539 offer potential traps for deep-seated gases such as H₂. Indeed, salt formation is considered to
540 offer the most promising option for large scale H₂ storage, because of their excellent sealing
541 capacity and the relatively inert nature of salt with respect to H₂ (Sainz-Garcia et al., 2017;
542 Tarkowski, 2019; Zivar et al., 2020). High H₂ concentrations (up to 30 vol%) have already
543 been documented in evaporite formations and in particular in salt deposits (Warren, 2016). In
544 salt formations, H₂ may have several origins like production during early biodegradation of
545 organic matter, and water radiolysis due to elevated concentration of ⁴⁰K and ⁸⁷Rb, but the
546 preponderant contribution of exogenic sources with subsequent migration into the evaporite
547 trap is the most satisfying explanation.

548 6. Conclusions

549 Based on soil gas analysis and mapping we have discovered several hotspots of H₂,
550 CO₂, ²²²Rn where the concentration of these gases exceeds the regional background by two
551 order of magnitude and more. The sampling sites of high H₂ concentration (> 1000 ppmv),
552 together with CO₂ (up to 10 vol%), and ²²²Rn (up to 60 kBq m⁻³) are mostly located close to
553 the North Pyrenean Frontal Thrust. The Crossing the information based on soil gas maps with
554 different geophysical and geological datasets led us to identify a possible fertile environment
555 for H₂ generation and drainage. First, outcrops of serpentinized peridotites in the NPZ are
556 good indicator of the presence of exhumed mantle rocks at depth . Second, the geophysical
557 observations reveal the presence of massive mantle body at shallow depth (< 10 km from
558 tomographic, magnetic and gravimetric investigations) where active serpentinization may
559 occur. Third, the H₂ and ²²²Rn may be carried upward by CO₂ along major faults that connect
560 the mantle body to the surface. The Salies salt diapir whose roof is only at less than 70 m
561 below the surface represents an ideal gas trap for deep-seated gases such as H₂.

562 The discovery of these hotspots paves the way for detailed studies of noble gases and
563 stable isotopes composition, but also for careful microbiological and pedological
564 investigations to better constrain H₂ source(s) and migration path. The targeting approach
565 deployed in our study may be applied elsewhere in the world and more particularly in
566 orogenic belts presenting a geological configuration comparable to the western Pyrenean area.
567 These orogenic areas, rich in ultramafic rocks, could be preferentially targeted for an
568 industrial prospection of native H₂ resources.

569 Acknowledgments, Samples, and Data

570 This work was conducted in the framework of the Convergence project
571 (<https://convergent-margins.com/>), funded by TOTAL S.E.. Magali Pujol, Dominique Duclerc
572 and Isabelle Mitteau are warmly thanks for support during the field investigation and
573 analytical measurements. Supplementary data reported in this study are given in supporting
574 information and all soil gas data are stored in EarthChem repository at **pending (will be**
575 **deposit after the review**

576
577
578
579

Supplementary material

Table A1. All untreated soil gas data

Table A2. Average of soil gas data at each location

580

References

- 581 Abrajano, T. A., Sturchio, N. C., Bohlke, J. K., Lyon, G. L., Poreda, R. J., & Stevens,
582 C. M. (1988). Methane-hydrogen gas seeps, Zambales Ophiolite, Philippines: Deep or
583 shallow origin? *Chemical Geology*, 71(1–3), 211–222. [https://doi.org/10.1016/0009-2541\(88\)90116-7](https://doi.org/10.1016/0009-2541(88)90116-7)
- 585 Azambre, B., & Rossy, M., 1976, Le magmatisme alcalin d'age cretace, dans les
586 Pyrenees occidentales et l'Arc basque; ses relations avec le metamorphisme et la tectonique.
587 Bulletin de la Societe Geologique de France, S7–XVIII, 1725–1728.
588 <https://doi.org/10.2113/gssgbull.S7-XVIII.6.1725>
- 589 Azambre, B., Rossy, M., & Albareda, F., 1992, Petrology of the alkaline magmatism
590 from the Cretaceous North-Pyrenean rift zone (France and Spain). European Journal of
591 Mineralogy, 4, 813–834.
- 592 Baubron, J.-C., Rigo, A., & Toutain, J.-P. (1999). Soil gas profiles as a tool to
593 characterise active tectonic areas: the Jaut Pass example (Pyrenees, France). *Earth and*
594 *Planetary Science Letters*, 13. [https://doi.org/10.1016/S0012-821X\(01\)00596-9](https://doi.org/10.1016/S0012-821X(01)00596-9)
- 595 Berard, P., Mazurier, C. (2000) Ressources en eaux thermales et minérales des stations
596 du département des Pyrénées-Atlantiques. Station thermale de Salies-de-Béarn. *Rapport*
597 *BRGM/RP 50176-FR*
- 598 Bernus-Maury, C., 1984, Etude des paragenèses caractéristiques du métamorphisme
599 mésozoïque dans la partie orientale des Pyrénées (French). Paris 6.
- 600 Bonté, D., Guillou-Frottier, L., Garibaldi, C., Bourgine, B., Lopez, S., Bouchot, V., &
601 Lucaleau, F. (2010). Subsurface temperature maps in French sedimentary basins: new data
602 compilation and interpolation. *Bulletin de La Société Géologique de France*, 181(4), 377–
603 390. <https://doi.org/10.2113/gssgbull.181.4.377>
- 604 Cannat, M., Fontaine, F., & Escartín, J. (2010). Serpentization and associated
605 hydrogen and methane fluxes at slow spreading ridges. In P. A. Rona, C. W. Devey, J.
606 Dymant, & B. J. Murton (Eds.), *Geophysical Monograph Series* (Vol. 188, pp. 241–264).
607 Washington, D. C.: American Geophysical Union. <https://doi.org/10.1029/2008GM000760>
- 608 Casas, A., Kearey, P., Rivero, L., & Adam, C. R. (1997). Gravity anomaly map of the
609 Pyrenean region and a comparison of the deep geological structure of the western and eastern
610 Pyrenees. *Earth and Planetary Science Letters*, 150(1–2), 65–78.
611 [https://doi.org/10.1016/S0012-821X\(97\)00087-3](https://doi.org/10.1016/S0012-821X(97)00087-3)
- 612 Charlou, J. L., Donval, J. P., Konn, C., Ondréas, H., Fouquet, Y., Jean-Baptiste, P., &
613 Fourré, E. (2010). High production and fluxes of H₂ and CH₄ and evidence of abiotic
614 hydrocarbon synthesis by serpentization in ultramafic-hosted hydrothermal systems on the
615 Mid-Atlantic Ridge. In P. A. Rona, C. W. Devey, J. Dymant, & B. J. Murton (Eds.),
616 *Geophysical Monograph Series* (Vol. 188, pp. 265–296). Washington, D. C.: American
617 Geophysical Union. <https://doi.org/10.1029/2008GM000752>
- 618 Chavagnac, V., Monnin, C., Ceuleneer, G., Boulart, C., & Hoareau, G. (2013).
619 Characterization of hyperalkaline fluids produced by low-temperature serpentization of
620 mantle peridotites in the Oman and Ligurian ophiolites: Hyperalkaline Waters in Oman and
621 Liguria. *Geochemistry, Geophysics, Geosystems*, 14(7), 2496–2522.
622 <https://doi.org/10.1002/ggge.20147>
- 623 Chevrot, S., Sylvander, M., Diaz, J., Ruiz, M., Paul, A., & the PYROPE Working
624 Group. (2015). The Pyrenean architecture as revealed by teleseismic P-to-S converted waves

- 625 recorded along two dense transects. *Geophysical Journal International*, 200(2), 1094–1105.
626 <https://doi.org/10.1093/gji/ggu400>
- 627 Chevrot, Sébastien, Sylvander, M., Diaz, J., Martin, R., Moutherau, F., Manatschal,
628 G., et al. (2018). The non-cylindrical crustal architecture of the Pyrenees. *Scientific Reports*,
629 8(1), 9591. <https://doi.org/10.1038/s41598-018-27889-x>
- 630 Choukroune, P. (1989). The Ecors Pyrenean deep seismic profile reflection data and
631 the overall structure of an orogenic belt. *Tectonics*, 8(1), 23–39.
632 <https://doi.org/10.1029/TC008i001p00023>
- 633 Christensen, N. I. (2004). Serpentinites, Peridotites, and Seismology. *International
634 Geology Review*, 46(9), 795–816. <https://doi.org/10.2747/0020-6814.46.9.795>
- 635 Ciotoli, G., Sciarra, A., Annunziatellis, A., & Bigi, S. (2016). Soil gas geochemical
636 behaviour across buried and exposed faults during the 24 August 2016 central Italy
637 earthquake. *ANNALS OF GEOPHYSICS*, 14. <https://doi.org/10.4401/ag-7242>
- 638 Clerc, C., Lagabrielle, Y., Neumaier, M., Reynaud, J. Y., & de Saint Blanquat, M.,
639 2012, Exhumation of subcontinental mantle rocks: evidence from ultramafic-bearing clastic
640 deposits nearby the Lherz peridotite body, French Pyrenees. *Bulletin de la Société géologique
641 de France*, 183(5), 443-459.
- 642 Clerc, C., Boulvais, P., Lagabrielle, Y., & de Saint Blanquat, M., 2013, Ophicalcites
643 from the northern Pyrenean belt: a field, petrographic and stable isotope study. *International
644 Journal of Earth Sciences*, 103(1), 141-163.
- 645 Cooper, B. A., Raven, M. J., & Samuel, L. (1997). Origin and geological controls on
646 subsurface CO₂ distribution with examples from western Indonesia. In *Proceedings of the
647 Petroleum Systems of SE Asia and Australasia Conference*, 877–92
- 648 Dauteuil, O., & Ricou, L. E., 1989, Une circulation de fluides de haute-temperature a
649 l'origine du metamorphisme cretace nord-pyreneen. *Circ. High-Temp. Fluids Orig. North
650 Pyrenean Cretac. Metamorph. Geodinamica Acta*, 3, 237–250.
- 651 Deville, E., & Prinzhofner, A. (2016). The origin of N₂-H₂-CH₄-rich natural gas
652 seepages in ophiolitic context: A major and noble gases study of fluid seepages in New
653 Caledonia. *Chemical Geology*, 440, 139–147. <https://doi.org/10.1016/j.chemgeo.2016.06.011>
- 654 Disnar, J. R., & Gauthier, B. (1988). Exploration for concealed orebodies by the
655 analysis of volatile organic compounds contained in surface rocks: Trèves Zn-Pb deposit
656 (Gard, France), 18. [https://doi.org/10.1016/0375-6742\(88\)90058-1](https://doi.org/10.1016/0375-6742(88)90058-1)
- 657 Dogan, T., Mori, T., Tsunomori, F., & Notsu, K. (2007). Soil H₂ and CO₂ Surveys at
658 Several Active Faults in Japan. *Pure and Applied Geophysics*, 164(12), 2449–2463.
659 <https://doi.org/10.1007/s00024-007-0277-5>
- 660 Donzé, F.-V., Tsopela, A., Guglielmi, Y., Henry, P., & Gout, C. (2020). Fluid
661 migration in faulted shale rocks: channeling below active faulting threshold. *European
662 Journal of Environmental and Civil Engineering*, 1–15.
663 <https://doi.org/10.1080/19648189.2020.1765200>
- 664 Donzé, F.-V., Truche, L., Shekari Namin, P., Lefevre, N., & Bazarkina, E. F. (2020).
665 Migration of Natural Hydrogen from Deep-Seated Sources in the São Francisco Basin, Brazil.
666 *Geosciences*, 10(9), 346. <https://doi.org/10.3390/geosciences10090346>
- 667 Ducoux, M., Jolivet, L., Callot, J. P., Aubourg, C., Masini, E., Lahfid, A., ... &
668 Baudin, T. (2019). The Nappe des Marbres unit of the Basque-Cantabrian Basin: the tectono-
669 thermal evolution of a fossil hyperextended rift basin. *Tectonics*, 38(11), 3881-3915.
- 670 ECORS Team, Daignières, M., Séguret, M., & Specht, M. (1994). The Arzacq-
671 Western Pyrenees ECORS Deep Seismic Profile. In A. Mascle (Ed.), *Hydrocarbon and
672 Petroleum Geology of France* (pp. 199–208). Berlin, Heidelberg: Springer Berlin Heidelberg.
673 https://doi.org/10.1007/978-3-642-78849-9_15

- 674 Ehhalt, D. H., & Rohrer, F. (2009). The tropospheric cycle of H₂: a critical review.
675 Tellus B: Chemical and Physical Meteorology, 61(3), 500-535.
- 676 Ehhalt, D. H., & Rohrer, F. (2011). The dependence of soil H₂ uptake on temperature
677 and moisture: a reanalysis of laboratory data. Tellus B: Chemical and Physical Meteorology,
678 63(5), 1040-1051.
- 679 Etiope, G., Judas, J., & Whiticar, M. J. (2015). Occurrence of abiotic methane in the
680 eastern United Arab Emirates ophiolite aquifer. *Arabian Journal of Geosciences*, 8(12),
681 11345–11348. <https://doi.org/10.1007/s12517-015-1975-4>
- 682 Etiope, Giuseppe, Schoell, M., & Hosgörmez, H. (2011a). Abiotic methane flux from
683 the Chimaera seep and Tekirova ophiolites (Turkey): Understanding gas exhalation from low
684 temperature serpentinization and implications for Mars. *Earth and Planetary Science Letters*,
685 310(1–2), 96–104. <https://doi.org/10.1016/j.epsl.2011.08.001>
- 686 Etiope, Giuseppe, Schoell, M., & Hosgörmez, H. (2011b). Abiotic methane flux from
687 the Chimaera seep and Tekirova ophiolites (Turkey): Understanding gas exhalation from low
688 temperature serpentinization and implications for Mars. *Earth and Planetary Science Letters*,
689 310(1–2), 96–104. <https://doi.org/10.1016/j.epsl.2011.08.001>
- 690 Fabriès, J., Lorand, J.-P., Bodinier, J.-L., & Dupuy, C., 1991, Evolution of the Upper
691 Mantle beneath the Pyrenees: Evidence from Orogenic Spinel Lherzolite Massifs. *Journal of*
692 *Petrology, Special_Volume*, 55–76. https://doi.org/10.1093/petrology/Special_Volume.2.55.
- 693 Fabriès, J., Lorand, J.-P., & Bodinier, J.-L. (1998). Petrogenetic evolution of orogenic
694 lherzolite massifs in the central and western Pyrenees. *Tectonophysics*, 292(1–2), 145–167.
695 [https://doi.org/10.1016/S0040-1951\(98\)00055-9](https://doi.org/10.1016/S0040-1951(98)00055-9)
- 696 Faulkner, D. R., Jackson, C. A. L., Lunn, R. J., Schlische, R. W., Shipton, Z. K.,
697 Wibberley, C. A. J., & Withjack, M. O. (2010). A review of recent developments concerning
698 the structure, mechanics and fluid flow properties of fault zones. *Journal of Structural*
699 *Geology*, 32(11), 1557–1575. <https://doi.org/10.1016/j.jsg.2010.06.009>
- 700 Fiebig, J., Woodland, A. B., Spangenberg, J., & Oschmann, W. (2007). Natural
701 evidence for rapid abiogenic hydrothermal generation of CH₄. *Geochimica et Cosmochimica*
702 *Acta*, 71(12), 3028–3039. <https://doi.org/10.1016/j.gca.2007.04.010>
- 703 Gal, F., & Gadalia, A. (2011). Soil gas measurements around the most recent volcanic
704 system of metropolitan France (Lake Pavin, Massif Central). *Comptes Rendus Geoscience*,
705 343(1), 43–54. <https://doi.org/10.1016/j.crte.2010.11.008>
- 706 Gao, Y., Wang, M., & Zhang, D. (2011). Application of ‘metals-in-soil-gas’
707 techniques to mineral exploration in exotic overburden. *Geochemistry: Exploration,*
708 *Environment, Analysis*, 11(2), 63–70. <https://doi.org/10.1144/1467-7873/09-IAGS-243>
- 709 García-Senz, J., 2002, Cuencas extensivas del Cretacico Inferior en los Pirineos
710 Centrales – formacion y subsecuente inversion. [PhD thesis]. University of Barcelona,
711 Barcelona.
- 712 García-Senz, J., Pedrera, A., Ayala, C., Ruiz-Constán, A., Robador, A., & Rodríguez-
713 Fernández, L. R. (2020). Inversion of the north Iberian hyperextended margin: the role of
714 exhumed mantle indentation during continental collision. *Geological Society, London, Special*
715 *Publications*, 490(1), 177–198. <https://doi.org/10.1144/SP490-2019-112>
- 716 Garrido-Megias, A., & Ríos Aragues, L. M., 1972, Síntesis geologica del Secundario y
717 Terciario entre los ríos Cinca y Segre (Pirineo Central de la vertiente sur pirenaica, provincias
718 de Huesca y Lérida). *Boletín Geológico y Minero*, 83, 1–47.
- 719 Gaucher, E. C. (2020). New Perspectives in the Industrial Exploration for Native
720 Hydrogen. *Elements*, 16(1), 8–9. <https://doi.org/10.2138/gselements.16.1.8>
- 721 Golberg, J. M., & Leyreloup, A. F., 1990, High temperature-low pressure Cretaceous
722 metamorphism related to crustal thinning (Eastern North Pyrenean Zone, France).

- 723 Contributions to Mineralogy and Petrology, 104, 194–207.
724 <https://doi.org/10.1007/BF00306443>
- 725 Gomez-Romeu, J., Kusznir, N., Roberts, A., & Manatschal, G. (2020). Measurements
726 of the extension required for crustal breakup on the magma-poor Iberia-Newfoundland
727 conjugate margins. *Marine and Petroleum Geology*, 118, 104403.
- 728 Grandjean, G. (1994). Etude des structures crustales dans une portion de chaîne et de
729 leur relation avec les bassins sédimentaires. Application aux Pyrénées occidentales. *Bulletin
730 Des Centres de Recherches Exploration-Production Elf-Aquitaine*, 18(2), 391–420.
- 731 Gregory, S., Barnett, M., Field, L., & Milodowski, A. (2019). Subsurface Microbial
732 Hydrogen Cycling: Natural Occurrence and Implications for Industry. *Microorganisms*, 7(2),
733 53. <https://doi.org/10.3390/microorganisms7020053>
- 734 Hainzl, S. (2004). Seismicity patterns of earthquake swarms due to fluid intrusion and
735 stress triggering. *Geophysical Journal International*, 159(3), 1090–1096.
736 <https://doi.org/10.1111/j.1365-246X.2004.02463.x>
- 737 Halas, P., Dupuy, A., Franceschi, M., Bordmann, V., Fleury, J.-M., & Duclerc, D.
738 (2021). Hydrogen gas in circular depressions in South Gironde, France: Flux, stock, or
739 artefact? *Applied Geochemistry*, 127, 104928.
740 <https://doi.org/10.1016/j.apgeochem.2021.104928>
- 741 Hardebeck, J. L. (2012). Fluid-Driven Seismicity Response of the Rinconada Fault
742 near Paso Robles, California, to the 2003 M 6.5 San Simeon Earthquake. *Bulletin of the
743 Seismological Society of America*, 102(1), 377–390. <https://doi.org/10.1785/0120110169>
- 744 Hinkle, M. E., Ryder, J. L., Sutley, S. J., & Botinelly, T. (1990). Production of sulfur
745 gases and carbon dioxide by synthetic weathering of crushed drill cores from the Santa Cruz
746 porphyry copper deposit near Casa Grande, Pinal County, Arizona. *Journal of Geochemical
747 Exploration*, 38(1–2), 43–67. [https://doi.org/10.1016/0375-6742\(90\)90092-O](https://doi.org/10.1016/0375-6742(90)90092-O)
- 748 Hirose, T., Kawagucci, S., & Suzuki, K. (2011). Mechanoradical H₂ generation
749 during simulated faulting: Implications for an earthquake-driven subsurface biosphere: H₂
750 GENERATION DURING EARTHQUAKES. *Geophysical Research Letters*, 38(17), n/a-n/a.
751 <https://doi.org/10.1029/2011GL048850>
- 752 Jammes, S., Manatschal, G., Lavier, L., & Masini, E. (2009). Tectonosedimentary
753 evolution related to extreme crustal thinning ahead of a propagating ocean: Example of the
754 western Pyrenees: EXTREME CRUSTAL THINNING IN THE PYRENEES. *Tectonics*,
755 28(4), n/a-n/a. <https://doi.org/10.1029/2008TC002406>
- 756 Jammes, S., Lavier, L., & Manatschal, G. (2010). Extreme crustal thinning in the Bay
757 of Biscay and the Western Pyrenees: From observations to modeling: MODELIZATION OF
758 EXTREME CRUSTAL THINNING. *Geochemistry, Geophysics, Geosystems*, 11(10), n/a-n/a.
759 <https://doi.org/10.1029/2010GC003218>
- 760 Johnson, J. E., Mienert, J., Plaza-Faverola, A., Vadakkepuliyambatta, S., Knies, J.,
761 Bünz, S., et al. (2015). Abiotic methane from ultraslow-spreading ridges can charge Arctic
762 gas hydrates. *Geology*, 43(5), 371–374. <https://doi.org/10.1130/G36440.1>
- 763 Kessler, A. J., Chen, Y.-J., Waite, D. W., Hutchinson, T., Koh, S., Popa, M. E., et al.
764 (2019). Bacterial fermentation and respiration processes are uncoupled in anoxic permeable
765 sediments. *Nature Microbiology*, 4(6), 1014–1023. <https://doi.org/10.1038/s41564-019-0391-z>
- 766 Kita, I., Matsuo, S., & Wakita, H. (1982). H₂ generation by reaction between H₂O
767 and crushed rock: An experimental study on H₂ degassing from the active fault zone. *Journal
768 of Geophysical Research: Solid Earth*, 87(B13), 10789–10795.
769 <https://doi.org/10.1029/JB087iB13p10789>
- 770 Korotcenkov, G., Han, S. D., & Stetter, J. R. (2009). Review of Electrochemical
771 Hydrogen Sensors. *Chemical Reviews*, 109(3), 1402–1433. <https://doi.org/10.1021/cr800339k>

- 773 Lacan, P. (2008). Activité sismotectonique plio-quaternaire de l'ouest des Pyrénées.
774 <https://tel.archives-ouvertes.fr/tel-01783939>
- 775 Labaume, P., & Teixell, A., 2020, Evolution of salt structures of the Pyrenean rift
776 (Chaînons Béarnais, France): From hyper-extension to tectonic inversion. *Tectonophysics*,
777 228451.
- 778 Lagabrielle, Y., & Bodinier, J.-L. (2008). Submarine reworking of exhumed
779 subcontinental mantle rocks: field evidence from the Lherz peridotites, French Pyrenees:
780 Cretaceous exhumation of pyrenean mantle. *Terra Nova*, 20(1), 11–21.
781 <https://doi.org/10.1111/j.1365-3121.2007.00781.x>
- 782 Lagabrielle, Y., Labaume, P., & de Saint Blanquat, M. (2010). Mantle exhumation,
783 crustal denudation, and gravity tectonics during Cretaceous rifting in the Pyrenean realm (SW
784 Europe): Insights from the geological setting of the lherzolite bodies: PYRENEAN
785 LHERZOLITES, GRAVITY TECTONICS. *Tectonics*, 29(4).
786 <https://doi.org/10.1029/2009TC002588>
- 787 Lagabrielle, Y., Clerc, C., Vauchez, A., Lahfid, A., Labaume, P., Azambre, B.,
788 Fourcade, S., & Dautria, J. M., 2016, Very high geothermal gradient during mantle
789 exhumation recorded in mylonitic marbles and carbonate breccias from a Mesozoic Pyrenean
790 palaeomargin (Lherz area, North Pyrenean Zone, France). *Comptes Rendus Géoscience*,
791 348(3-4), 290-300.
- 792 Larin, N., Zgonnik, V., Rodina, S., Deville, E., Prinzhofer, A., & Larin, V. N. (2015a).
793 Natural Molecular Hydrogen Seepage Associated with Surficial, Rounded Depressions on the
794 European Craton in Russia. *Natural Resources Research*, 24(3), 369–383.
795 <https://doi.org/10.1007/s11053-014-9257-5>
- 796 Le Fur Balouet, S., (1985). Les séquences paléovolcaniques du domaine pyrénéen
797 depuis le Stéphano-permien jusqu'au Crétacé: essai d'identification basé sur l'étude
798 géochimique des éléments en traces (Doctoral dissertation), Thesis 3 ème Cycle, Paris VI, pp.
799 320.
- 800 Lescoutre, R., Tugend, J., Brune, S., Masini, E., & Manatschal, G., 2019, Thermal
801 evolution of asymmetric hyperextended magma-poor rift systems: results from numerical
802 modelling and Pyrenean field observations. *Geochemistry, Geophysics, Geosystems*.
803 doi:10.1029/2019gc008600
- 804 Lescoutre, R., & Manatschal, G. (2020). Role of rift-inheritance and segmentation for
805 orogenic evolution: example from the Pyrenean-Cantabrian systemRôle de l'héritage associé
806 au rift et à sa segmentation pour l'évolution orogénique: exemple du système pyrénéo-
807 cantabrique. *Bulletin de la Société Géologique de France*, 191(1).
- 808 Lewan, M. D. (1997). Experiments on the role of water in petroleum formation.
809 *Geochimica et Cosmochimica Acta*, 61(17), 3691–3723. [https://doi.org/10.1016/S0016-7037\(97\)00176-2](https://doi.org/10.1016/S0016-7037(97)00176-2)
- 810 Li, X., Krooss, B. M., Weniger, P., & Littke, R. (2017). Molecular hydrogen (H₂) and
811 light hydrocarbon gases generation from marine and lacustrine source rocks during closed-
812 system laboratory pyrolysis experiments. *Journal of Analytical and Applied Pyrolysis*, 126,
813 275–287. <https://doi.org/10.1016/j.jaat.2017.05.019>
- 814 Li, Y., Du, J., Wang, X., Zhou, X., Xie, C., & Cui, Y. (2013). Spatial Variations of
815 Soil Gas Geochemistry in the Tangshan Area of Northern China. *Terrestrial, Atmospheric
816 and Oceanic Sciences*, 24(3), 323. [https://doi.org/10.3319/TAO.2012.11.26.01\(TT\)](https://doi.org/10.3319/TAO.2012.11.26.01(TT))
- 817 Lin, L.-H., Slater, G. F., Sherwood Lollar, B., Lacrampe-Couloume, G., & Onstott, T.
818 C. (2005a). The yield and isotopic composition of radiolytic H₂, a potential energy source for
819 the deep subsurface biosphere. *Geochimica et Cosmochimica Acta*, 69(4), 893–903.
820 <https://doi.org/10.1016/j.gca.2004.07.032>

- 822 Lin, L.-H., Hall, J., Lippmann-Pipke, J., Ward, J. A., Sherwood Lollar, B., DeFlaun,
823 M., et al. (2005b). Radiolytic H₂ in continental crust: Nuclear power for deep subsurface
824 microbial communities: radiolytic H₂ in continental crust. *Geochemistry, Geophysics,
825 Geosystems*, 6(7), n/a-n/a. <https://doi.org/10.1029/2004GC000907>
- 826 Lombardi, S., & Voltattorni, N. (2010). Rn, He and CO₂ soil gas geochemistry for the
827 study of active and inactive faults. *Applied Geochemistry*, 25(8), 1206–1220.
828 <https://doi.org/10.1016/j.apgeochem.2010.05.006>
- 829 Lorant, F., & Behar, F. (2002). Late Generation of Methane from Mature Kerogens.
830 *Energy & Fuels*, 16(2), 412–427. <https://doi.org/10.1021/ef010126x>
- 831 Malvoisin, B., Carlut, J., & Brunet, F. (2012). Serpentization of oceanic peridotites:
832 1. A high-sensitivity method to monitor magnetite production in hydrothermal experiments.
833 *Journal of Geophysical Research: Solid Earth*, 117(B1).
834 <https://doi.org/10.1029/2011JB008612>
- 835 Marcaillou, C., Muñoz, M., Vidal, O., Parra, T., & Harfouche, M. (2011).
836 Mineralogical evidence for H₂ degassing during serpentization at 300°C/300bar. *Earth and
837 Planetary Science Letters*, 303(3–4), 281–290. <https://doi.org/10.1016/j.epsl.2011.01.006>
- 838 Masini, E., Manatschal, G., Tugend, J., Mohn, G., & Flament, J.-M. (2014). The
839 tectono-sedimentary evolution of a hyper-extended rift basin: the example of the Arzacq–
840 Mauléon rift system (Western Pyrenees, SW France). *International Journal of Earth Sciences*,
841 103(6), 1569–1596. <https://doi.org/10.1007/s00531-014-1023-8>
- 842 Mayhew, L. E., Ellison, E. T., McCollom, T. M., Trainor, T. P., & Templeton, A. S.
843 (2013). Hydrogen generation from low-temperature water–rock reactions. *Nature Geoscience*,
844 6(6), 478–484. <https://doi.org/10.1038/ngeo1825>
- 845 McCarthy, J. H., & Reimer, G. M. (1986). Advances in soil gas geochemical
846 exploration for natural resources: Some current examples and practices. *Journal of
847 Geophysical Research: Solid Earth*, 91(B12), 12327–12338.
848 <https://doi.org/10.1029/JB091iB12p12327>
- 849 McCollom, T. M. (2013). Laboratory Simulations of Abiotic Hydrocarbon Formation
850 in Earth’s Deep Subsurface. *Reviews in Mineralogy and Geochemistry*, 75(1), 467–494.
851 <https://doi.org/10.2138/rmg.2013.75.15>
- 852 McCollom, T. M., Klein, F., Robbins, M., Moskowitz, B., Berqué, T. S., Jöns, N., et
853 al. (2016). Temperature trends for reaction rates, hydrogen generation, and partitioning of iron
854 during experimental serpentization of olivine. *Geochimica et Cosmochimica Acta*, 181,
855 175–200. <https://doi.org/10.1016/j.gca.2016.03.002>
- 856 Meredith, L. K., Commane, R., Keenan, T. F., Klosterman, S. T., Munger, J. W.,
857 Templer, P. H., ... & Prinn, R. G. (2017). Ecosystem fluxes of hydrogen in a mid-latitude
858 forest driven by soil microorganisms and plants. *Global change biology*, 23(2), 906–919.
- 859 Monnin, C., Chavagnac, V., Boulart, C., Ménez, B., Gérard, M., Gérard, E., et al.
860 (2014). Fluid chemistry of the low temperature hyperalkaline hydrothermal system of Prony
861 Bay (New Caledonia). *Biogeosciences*, 11(20), 5687–5706. [https://doi.org/10.5194/bg-11-5687-2014](https://doi.org/10.5194/bg-11-
862 5687-2014)
- 863 Moretti, I., Prinzhofer, A., Françolin, J., Pacheco, C., Rosanne, M., Rupin, F., &
864 Mertens, J. (2021). Long-term monitoring of natural hydrogen superficial emissions in a
865 brazilian cratonic environment. Sporadic large pulses versus daily periodic emissions.
866 *International Journal of Hydrogen Energy*, 46(5), 3615–3628.
867 <https://doi.org/10.1016/j.ijhydene.2020.11.026>
- 868 Mouthereau, F., Filleaudeau, P.-Y., Vacherat, A., Pik, R., Lacombe, O., Fellin, M. G.,
869 et al. (2014). Placing limits to shortening evolution in the Pyrenees: Role of margin
870 architecture and implications for the Iberia/Europe convergence: Plate convergence in the
871 Pyrenees. *Tectonics*, 33(12), 2283–2314. <https://doi.org/10.1002/2014TC003663>

- 872 Muñoz, J. A., 1992, Evolution of a continental collision belt; ECORS-Pyrenees crustal
873 balanced cross-section. In K. R. Mcclay (Ed.), Thrust tectonics, (pp. 235–246). London,
874 United Kingdom: Chapman & Hall
- 875 Muñoz, J.A., 2002, The Pyrenees. In: Gibbons, W., Moreno, T. (eds.). The Geology of
876 Spain. The Geological Society of London, 370-385
- 877 Murray, J., Clément, A., Fritz, B., Schmittbuhl, J., Bordmann, V., & Fleury, J. M.
878 (2020). Abiotic hydrogen generation from biotite-rich granite: A case study of the Soultz-
879 sous-Forêts geothermal site, France. *Applied Geochemistry*, 119, 104631.
880 <https://doi.org/10.1016/j.apgeochem.2020.104631>
- 881 Neal, C., & Stanger, G. (1983). Hydrogen generation from mantle source rocks in
882 Oman. *Earth and Planetary Science Letters*, 66, 315–320. [https://doi.org/10.1016/0012-821X\(83\)90144-9](https://doi.org/10.1016/0012-821X(83)90144-9)
- 884 Noble, R. R. P., Lintern, M. J., Townley, B., Anand, R. R., Gray, D. G., & Reid, N.
885 (2013). Metal migration at the North Miitel Ni sulphide deposit in the southern Yilgarn
886 Craton: Part 3, gas and overview. *Geochemistry: Exploration, Environment, Analysis*, 13(2),
887 99–113. <https://doi.org/10.1144/geochem2012-131>
- 888 Novelli, P. C., Lang, P. M., Masarie, K. A., Hurst, D. F., Myers, R., & Elkins, J. W.
889 (1999). Molecular hydrogen in the troposphere: Global distribution and budget. *Journal of*
890 *Geophysical Research: Atmospheres*, 104(D23), 30427–30444.
891 <https://doi.org/10.1029/1999JD900788>
- 892 Ortiz, A., Guillocheau, F., Lasseur, E., Briais, J., Robin, C., Serrano, O., & Fillon, C.,
893 2020, Sediment routing system and sink preservation during the post-orogenic evolution of a
894 retro-foreland basin: The case example of the North Pyrenean (Aquitaine, Bay of Biscay)
895 Basins. *Marine and Petroleum Geology*, 112, 104085.
- 896 Oufi, O. (2002). Magnetic properties of variably serpentinitized abyssal peridotites.
897 *Journal of Geophysical Research*, 107(B5), 2095. <https://doi.org/10.1029/2001JB000549>
- 898 Pedreira, D., Pulgar, J., Gallart, J., & Torné, M. (2007). Three-dimensional gravity and
899 magnetic modeling of crustal indentation and wedging in the western Pyrenees-Cantabrian
900 Mountains. *Journal of Geophysical Research: Solid Earth*, 112(B12).
901 <https://doi.org/10.1029/2007JB005021>
- 902 Pedrera, A., García-Senz, J., Ayala, C., Ruiz-Constán, A., Rodríguez-
903 Fernández, L. R., Robador, A., & González Menéndez, L. (2017). Reconstruction of the
904 Exhumed Mantle Across the North Iberian Margin by Crustal-Scale 3-D Gravity Inversion
905 and Geological Cross Section: Mantle Along the Basque-Cantabrian Basin. *Tectonics*, 36(12),
906 3155–3177. <https://doi.org/10.1002/2017TC004716>
- 907 Pereira, A. J. S. C., Godinho, M. M., & Neves, L. J. P. F. (2010). On the influence of
908 faulting on small-scale soil-gas radon variability: a case study in the Iberian Uranium
909 Province. *Journal of Environmental Radioactivity*, 101(10), 875–882.
910 <https://doi.org/10.1016/j.jenvrad.2010.05.014>
- 911 Peters, J. W., Schut, G. J., Boyd, E. S., Mulder, D. W., Shepard, E. M., Broderick, J.
912 B., et al. (2015). [FeFe]- and [NiFe]-hydrogenase diversity, mechanism, and maturation.
913 *Biochimica et Biophysica Acta (BBA) - Molecular Cell Research*, 1853(6), 1350–1369.
914 <https://doi.org/10.1016/j.bbamcr.2014.11.021>
- 915 Polito, P. A., Clarke, J. D. A., Bone, Y., & Viellenave, J. (2002). A CO₂–O₂–light
916 hydrocarbon–soil-gas anomaly above the Junction orogenic gold deposit: a potential,
917 alternative exploration technique. *Geochemistry: Exploration, Environment, Analysis*, 2(4),
918 333–344. <https://doi.org/10.1144/1467-787302-035>
- 919 Potter, J., & Konnerup-Madsen, J. (2003). A review of the occurrence and origin of
920 abiogenic hydrocarbons in igneous rocks. *Geological Society, London, Special Publications*,
921 214(1), 151–173. <https://doi.org/10.1144/GSL.SP.2003.214.01.10>

- 922 Prinzhöfer, A., Tahara Cissé, C. S., & Diallo, A. B. (2018). Discovery of a large
923 accumulation of natural hydrogen in Bourakebougou (Mali). *International Journal of*
924 *Hydrogen Energy*, 43(42), 19315–19326. <https://doi.org/10.1016/j.ijhydene.2018.08.193>
- 925 Prinzhöfer, A., Moretti, I., Françolin, J., Pacheco, C., D'Agostino, A., Werly, J., &
926 Rupin, F. (2019). Natural hydrogen continuous emission from sedimentary basins: The
927 example of a Brazilian H₂-emitting structure. *International Journal of Hydrogen Energy*,
928 44(12), 5676–5685. <https://doi.org/10.1016/j.ijhydene.2019.01.119>
- 929 Qureshi, A. A., Samad Beg, M. A., Ahmed, F., & Khan, H. A. (1988). Uranium
930 exploration in Pakistan using alpha sensitive plastic films (ASPF). *International Journal of*
931 *Radiation Applications and Instrumentation. Part D. Nuclear Tracks and Radiation*
932 *Measurements*, 15(1–4), 735–739. [https://doi.org/10.1016/1359-0189\(88\)90240-3](https://doi.org/10.1016/1359-0189(88)90240-3)
- 933 Ravier, J., 1959, Le metamorphisme des terrains secondaires des Pyrénées, Mémoires
934 Soc. Geol. Fr. Nouv. Ser., (Vol. 38). Paris: Société géologique de France.
- 935 Reimann, C., Filzmoser, P., & Garrett, R. G. (2005). Background and threshold:
936 critical comparison of methods of determination. *Science of The Total Environment*, 346(1–
937 3), 1–16. <https://doi.org/10.1016/j.scitotenv.2004.11.023>
- 938 Rigo, A., Béthoux, N., Masson, F., & Ritz, J.-F. (2008). Seismicity rate and wave-
939 velocity variations as consequences of rainfall: the case of the catastrophic storm of
940 September 2002 in the Nîmes Fault region (Gard, France). *Geophysical Journal International*,
941 173(2), 473–482. <https://doi.org/10.1111/j.1365-246X.2008.03718.x>
- 942 Romanak, K. D., Bennett, P. C., Yang, C., & Hovorka, S. D. (2012). Process-based
943 approach to CO₂ leakage detection by vadose zone gas monitoring at geologic CO₂ storage
944 sites: process-based leakage detection. *Geophysical Research Letters*, 39(15).
945 <https://doi.org/10.1029/2012GL052426>
- 946 Rossy, M., Azambre, B., & Albarède, F., 1992, REE and Sr/1bNd isotope
947 geochemistry of the alkaline magmatism from the Cretaceous North Pyrenean Rift Zone
948 (France-Spain). *Chemical Geology*, 97, 33–46. [https://doi.org/10.1016/0009-2541\(92\)90134-Q](https://doi.org/10.1016/0009-2541(92)90134-Q)
- 949 Roure, F., Choukroune, P., Berastegui, X., Muñoz, J. A., Villien, A., Matheron, P., ...
950 & Deramond, J. (1989). ECORS deep seismic data and balanced cross sections: Geometric
951 constraints on the evolution of the Pyrenees. *Tectonics*, 8(1), 41–50.
- 952 Sahu, P., Mishra, D. P., Panigrahi, D. C., Jha, V., & Patnaik, R. L. (2013). Radon
953 emanation from low-grade uranium ore. *Journal of Environmental Radioactivity*, 126, 104–
954 114. <https://doi.org/10.1016/j.jenvrad.2013.07.014>
- 955 Sainz-García, A., Abarca, E., Rubí, V., & Grandia, F. (2017). Assessment of feasible
956 strategies for seasonal underground hydrogen storage in a saline aquifer. *International*
957 *Journal of Hydrogen Energy*, 42(26), 16657–16666.
958 <https://doi.org/10.1016/j.ijhydene.2017.05.076>
- 959 Sasiputry, N., Lahfid, A., Baudin, T., Guillou-Frottier, L., Razin, P., Issautier, B., et
960 al. (2020). Paleogeothermal Gradients Across an Inverted Hyperextended Rift System:
961 Example of the Mauléon Fossil Rift (Western Pyrenees). *Tectonics*, 39(10).
962 <https://doi.org/10.1029/2020TC006206>
- 963 Sato, M., Sutton, A. J., & McGee, K. A. (1985). Anomalous hydrogen emissions from
964 the San Andreas fault observed at the Cienega Winery, central California. *Pure and Applied*
965 *Geophysics PAGEOPH*, 122(2–4), 376–391. <https://doi.org/10.1007/BF00874606>
- 966 Sauvage, J. F., Flinders, A., Spivack, A. J., Pockalny, R., Dunlea, A. G., Anderson, C.
967 H., et al. (2021). The contribution of water radiolysis to marine sedimentary life. *Nature*
968 *Communications*, 12(1), 1297. <https://doi.org/10.1038/s41467-021-21218-z>

- 970 Schrenk, M. O., Brazelton, W. J., & Lang, S. Q. (2013). Serpentinitization, Carbon, and
971 Deep Life. *Reviews in Mineralogy and Geochemistry*, 75(1), 575–606.
972 <https://doi.org/10.2138/rmg.2013.75.18>
- 973 Schwartz, E., & Friedrich, B. (2006). The H₂-metabolizing prokaryotes. *The*
974 *Prokaryotes*, 7, 496–563. https://doi.org/10.1007/0-387-30742-7_17
- 975 Sherwood Lollar, B. S., Heuer, V. B., McDermott, J., Tille, S., Warr, O., Moran, J. J.,
976 ... & Hinrichs, K. U. (2021). A window into the abiotic carbon cycle—Acetate and formate in
977 fracture waters in 2.7 billion year-old host rocks of the Canadian Shield. *Geochimica et*
978 *Cosmochimica Acta*, 294, 295–314.
- 979 Sherwood Lollar, B. S., Lacrampe-Couloume, G., Slater, G. F., Ward, J., Moser, D. P.,
980 & Gihring, T. M. (2006). Unravelling abiogenic and biogenic sources of methane in the
981 Earth's deep subsurface. *Chemical Geology*, 12.
982 <https://doi.org/10.1016/j.chemgeo.2005.09.027>
- 983 Sherwood Lollar, B. S., Onstott, T. C., Lacrampe-Couloume, G., & Ballentine, C. J.
984 (2014). The contribution of the Precambrian continental lithosphere to global H₂ production.
985 *Nature*, 516(7531), 379–382. <https://doi.org/10.1038/nature14017>
- 986 Sibson, R. (1981). A brief description of natural neighbour interpolation. *Interpreting*
987 *Multivariate Data*.
- 988 Sinclair, A. J. (1991). A fundamental approach to threshold estimation in exploration
989 geochemistry: probability plots revisited. *Journal of Geochemical Exploration*, 41(1–2), 1–
990 22. [https://doi.org/10.1016/0375-6742\(91\)90071-2](https://doi.org/10.1016/0375-6742(91)90071-2)
- 991 Sipma, J., Henstra, A. M., Parshina, S. N., Lens, P. N. L., Lettinga, G., & Stams, A. J.
992 M. (2006). Microbial CO Conversions with Applications in Synthesis Gas Purification and
993 Bio-Desulfurization. *Critical Reviews in Biotechnology*, 26(1), 41–65.
994 <https://doi.org/10.1080/07388550500513974>
- 995 Smith, N. J. P., Shepherd, T. J., Styles, M. T., & Williams, G. M. (2005). Hydrogen
996 exploration: a review of global hydrogen accumulations and implications for prospective
997 areas in NW Europe. *Geological Society, London, Petroleum Geology Conference Series*,
998 6(1), 349–358. <https://doi.org/10.1144/0060349>
- 999 Souriau, A., Rigo, A., Sylvander, M., Benahmed, S., & Grimaud, F. (2014). Seismicity
1000 in central-western Pyrenees (France): A consequence of the subsidence of dense exhumed
1001 bodies. *Tectonophysics*, 621, 123–131. <https://doi.org/10.1016/j.tecto.2014.02.008>
- 1002 Sugisaki, R., Ido, M., Takeda, H., Isobe, Y., Hayashi, Y., Nakamura, N., et al. (1983).
1003 Origin of Hydrogen and Carbon Dioxide in Fault Gases and Its Relation to Fault Activity. *The*
1004 *Journal of Geology*, 91(3), 239–258. <https://doi.org/10.1086/628769>
- 1005 Tarkowski, R. (2019). Underground hydrogen storage: Characteristics and prospects.
1006 *Renewable and Sustainable Energy Reviews*, 105, 86–94.
1007 <https://doi.org/10.1016/j.rser.2019.01.051>
- 1008 Teixell, A., 1998, Crustal structure and orogenic material budget in the west central
1009 Pyrenees. *Tectonics*, 17(3), 395–406.
- 1010 Teixell, A., Labaume, P., & Lagabrielle, Y. (2016). The crustal evolution of the west-
1011 central Pyrenees revisited: Inferences from a new kinematic scenario. *Comptes Rendus*
1012 *Geoscience*, 348(3–4), 257–267. <https://doi.org/10.1016/j.crte.2015.10.010>
- 1013 Teixell, A., Labaume, P., Ayarza, P., Espurt, N., de Saint Blanquat, M., & Lagabrielle,
1014 Y., 2018, Crustal structure and evolution of the Pyrenean-Cantabrian belt: A review and new
1015 interpretations from recent concepts and data. *Tectonophysics*, 724–725, 146–170.
1016 <https://doi.org/10.1016/j.tecto.2018.01.009>
- 1017 Thauer, R. K., Klein, A. R., & Hartmann, G. C. (1996). Reactions with Molecular
1018 Hydrogen in Microorganisms: Evidence for a Purely Organic Hydrogenation Catalyst.
1019 *Chemical Reviews*, 96(7), 3031–3042. <https://doi.org/10.1021/cr9500601>

- 1020 Toft, P. B., Arkani-Hamed, J., & Haggerty, S. E. (1990). The effects of
1021 serpentinization on density and magnetic susceptibility: a petrophysical model. *Physics of the*
1022 *Earth and Planetary Interiors*, 65(1–2), 137–157. [https://doi.org/10.1016/0031-9201\(90\)90082-9](https://doi.org/10.1016/0031-9201(90)90082-9)
- 1024 Toutain, J.-P., & Baubron, J.-C. (1999). Gas geochemistry and seismotectonics: a
1025 review. *Tectonophysics*, 304(1–2), 1–27. [https://doi.org/10.1016/S0040-1951\(98\)00295-9](https://doi.org/10.1016/S0040-1951(98)00295-9)
- 1026 Truche, L., & Bazarkina, E. F. (2019). Natural hydrogen the fuel of the 21st century.
1027 *E3S Web of Conferences*, 98, 03006. <https://doi.org/10.1051/e3sconf/20199803006>
- 1028 Truche, L., Joubert, G., Dargent, M., Martz, P., Cathelineau, M., Rigaudier, T., &
1029 Quirt, D. (2018). Clay minerals trap hydrogen in the Earth's crust: Evidence from the Cigar
1030 Lake uranium deposit, Athabasca. *Earth and Planetary Science Letters*, 493, 186–197.
1031 <https://doi.org/10.1016/j.epsl.2018.04.038>
- 1032 Truche, L., McCollom, T. M., & Martinez, I. (2020). Hydrogen and abiotic
1033 hydrocarbons: molecules that change the world. *Elements: An International Magazine of*
1034 *Mineralogy, Geochemistry, and Petrology*, 16(1), 13–18.
- 1035 Tugend, J., Manatschal, G., Kusznir, N. J., Masini, E., Mohn, G., & Thinon, I. (2014).
1036 Formation and deformation of hyperextended rift systems: Insights from rift domain mapping
1037 in the Bay of Biscay-Pyrenees. *Tectonics*, 33(7), 1239–1276.
1038 <https://doi.org/10.1002/2014TC003529>
- 1039 Tugend, J., Manatschal, G., & Kusznir, N. J., 2015b, Spatial and temporal evolution of
1040 hyperextended rift systems: Implication for the nature, kinematics, and timing of the Iberian-
1041 European plate boundary. *Geology*, 43(1), 15–18. <https://doi.org/10.1130/G36072.1>
- 1042 Vacher, P., & Souriau, A. (2001). A three-dimensional model of the Pyrenean deep
1043 structure based on gravity modelling, seismic images and petrological constraints.
1044 *Geophysical Journal International*, 145(2), 460–470. <https://doi.org/10.1046/j.0956-540x.2001.01393.x>
- 1045 Vacquand, C., Deville, E., Beaumont, V., Guyot, F., Sissmann, O., Pillot, D., et al.
1046 (2018). Reduced gas seepages in ophiolitic complexes: Evidences for multiple origins of the
1047 H₂-CH₄-N₂ gas mixtures. *Geochimica et Cosmochimica Acta*, 223, 437–461.
1048 <https://doi.org/10.1016/j.gca.2017.12.018>
- 1049 Vandenborre, J., Truche, L., Costagliola, A., Craff, E., Blain, G., Baty, V., Haddad, F.
1050 and Fattahi, M., 2021. Carboxylate anion generation in aqueous solution from carbonate
1051 radiolysis, a potential route for abiotic organic acid synthesis on Earth and beyond. *Earth and*
1052 *Planetary Science Letters*, 564, p.116892.
- 1053 Vergés, J., Millán, H., Roca, E., Muñoz, J. A., Marzo, M., Cirés, J., et al., 1995,
1054 Eastern Pyrenees and related foreland basins: pre-, syn- and post-collisional crustal-scale
1055 cross-sections. *Marine and Petroleum Geology*, 12, 903–915. [https://doi.org/10.1016/0264-8172\(95\)98854-X](https://doi.org/10.1016/0264-8172(95)98854-X)
- 1056 Vergés, J., & García-Senz, J., 2001, Mesozoic evolution and Cainozoic inversion of
1057 the Pyrenean rift. In P. A. Ziegler, et al. (Eds.), *Peri-Tethyan Rift/Wrench Basins and Passive*
1058 *Margins*, mémoire, (pp. 187–212).
- 1059 Vergés, J., Fernández, M., & Martínez, A. (2002). The Pyrenean orogen: pre-, syn-,
1060 and post-collisional evolution. *Journal of the Virtual Explorer*, 08.
1061 <https://doi.org/10.3809/jvirtex.2002.00058>
- 1062 Wang, Y., Chevrot, S., Monteiller, V., Komatitsch, D., Moutherneau, F., Manatschal,
1063 G., et al. (2016). The deep roots of the western Pyrenees revealed by full waveform inversion
1064 of teleseismic P waves. *Geology*, 44(6), 475–478. <https://doi.org/10.1130/G37812.1>
- 1065 Warren, J., 2016. Gases in evaporites: part 2 of 3: nature, distribution and sources.
1066 Salty Matters reports.
- 1067
- 1068

- 1069 Worman, S. L., Pratson, L. F., Karson, J. A., & Klein, E. M. (2016). Global rate and
1070 distribution of H₂ gas produced by serpentinization within oceanic lithosphere: H₂ formation
1071 in ocean lithosphere. *Geophysical Research Letters*, 43(12), 6435–6443.
1072 <https://doi.org/10.1002/2016GL069066>
- 1073 Worman, S. L., Pratson, L. F., Karson, J. A., & Schlesinger, W. H. (2020). Abiotic
1074 hydrogen (H₂) sources and sinks near the Mid-Ocean Ridge (MOR) with implications for the
1075 subseafloor biosphere. *Proceedings of the National Academy of Sciences*, 117(24), 13283–
1076 13293. <https://doi.org/10.1073/pnas.2002619117>
- 1077 Xiang, Y., Sun, X., Liu, D., Yan, L., Wang, B., & Gao, X. (2020). Spatial Distribution
1078 of Rn, CO₂, Hg, and H₂ Concentrations in Soil Gas Across a Thrust Fault in Xinjiang, China.
1079 *Frontiers in Earth Science*, 8, 554924. <https://doi.org/10.3389/feart.2020.554924>
- 1080 Zgonnik, V., Beaumont, V., Deville, E., Larin, N., Pillot, D., & Farrell, K. M. (2015).
1081 Evidence for natural molecular hydrogen seepage associated with Carolina bays (surficial,
1082 ovoid depressions on the Atlantic Coastal Plain, Province of the USA). *Progress in Earth and
1083 Planetary Science*, 2(1), 31. <https://doi.org/10.1186/s40645-015-0062-5>
- 1084 Zivar, D., Kumar, S., & Foroozesh, J. (2020). Underground hydrogen storage: A
1085 comprehensive review. *International Journal of Hydrogen Energy*, S0360319920331426.
1086 <https://doi.org/10.1016/j.ijhydene.2020.08.138>

Location	X	Y	CH ₄ (vol%)	CO ₂ (vol%)	O ₂ (vol%)	H ₂ ppmv	CO ppmv	H ₂ S ppmv	ppmv	Balance (vol%)	Radon (bq m ⁻³)	Atmospheric pressure (mbar)	Humidity (%)	Temperature (°C)	soil type
Peyroraide	-1.110608	43.53165	0	3.1	18.8	31	4	0	78.8	13260	101.5	83.8	23	Grassland	
La Bourgade	-1.186809	43.519494	0	0.1	3.8	0	0	0	15.8	7444	101.6	77.7	24	Forest	
Sud Bardos	-1.1929778	43.455451	0	0.9	20.3	34	2	0	79.2	72	101.2	91.9	25	Grassland	
Isturitz	-1.2023857	43.358344	0	1.0	19.9	16	2	0	79.3	199	1004	68.8	27	Grassland	
Iholdy	-1.197617	43.267475	0	1.1	19.7	1	1	0	79.4	177	987	85.7	27	Grassland	
Bois d'Ostabat	-1.063698	43.282326	0	1.0	20.2	3	1	0	79.5	283	993	79.1	29	Meadow	
Gabat	-1.0722578	43.37346	0	1.1	20.4	2	1	0	79.5	76	1000	85.6	33	Grassland	
Arancou	-1.0562003	43.45526	0	0.9	19.0	18	4	0	79.6	66	1006	70.2	36	Grassland	
Puyo	-0.9448968	43.546198	0	0.5	19.9	14	1	0	79.5	29	1007	71.6	35	Grassland	
Salies de Bearn	-0.918758	43.460145	0	1.7	19.7	52	3	0	79.6	132	1007	54.7	35	Grassland	
Saint Laurent Bretagne	-0.1969404	43.382274	0	0.4	16.3	3	1	0	79.2	799	984	72.9	21	Grassland	
Lammeaube	-0.2109628	43.482495	0	1.5	19.8	26	3	0	79.2	309	1002	74.7	23	Grassland	
Castetpugon	-0.2208758	43.503465	0	0.2	20.8	6	2	0	79.0	173	1004	78.4	24	Grassland	
Sensacq	-0.3496236	43.581854	0.18	1.3	20.6	26	3	0	78.9	70	1007	87.2	23	Grassland	
Méracq	-0.3937847	43.512739	0	0.7	20.7	9	2	0	79.0	147	376	213.9	172	Grassland	
Navailles-Angos	-0.3458781	43.405046	0	0.1	20.6	6	1	0	79.3	229	995	76.4	27	Grassland	
Uzein	-0.4410873	43.39658	0	0.7	20.6	4	1	0	79.1	189	1003	76.2	27	Grassland	
Esterenecuby	-1.186799	43.105215	0	1.2	21.0	38	1	0	78.5	29	991	72.3	21	Meadow	
Errozate	-1.15105656	43.042125	0.08	1.3	21.4	18	1	0.2	78.3	5	887	66.3	18	Meadow	
Zazpigain	-1.0379461	43.010372	0	2.2	20.9	27	1	0	78.1	181	861	73.4	17	Meadow	
Pic d'Apanice	-1.0379461	43.100868	0	0.1	20.9	0	1	0.8	78.7	148	901	87.5	20	Meadow	
Alecy	-0.9149188	43.056668	0	1.6	20.7	5	0	1	79.1	63	986	96.3	25	Meadow	
Logibaria	-0.9260405	43.020038	0	0.5	20.8	8	1	1	78.9	35	972	75.1	27	Meadow	
Pic d'issarbe	-0.7955353	43.018106	0	2.0	21.0	66	3	1	78.5	705	864	58.1	23	Meadow	
Montorry	-0.82029	43.066886	0	0.5	21.1	0	0	1	78.7	59	985	97.9	22	Grassland	
Arette	-0.7073994	43.108241	0	1.5	19.9	0	0	1.4	78.9	10978	974	96.7	25	Grassland	
Lourdios Ichère	-0.6689824	43.047011	0	0.2	20.9	0	0	1.2	78.9	1003	964	75.7	27	Meadow	
Bustince Iribéry	-1.1850354	43.19192	0.02	0.2	21.2	17	1	1	78.6	827	993	72.8	22	Grassland	
Saint Juste Ibarré	-1.0561151	43.189128	0	0.5	20.8	0	0	1	78.7	8152	996	90.7	25	Grassland	
Ordiarp	-0.9424667	43.184364	0	0.6	20.7	5	0	1	79.0	43	993	76.6	27	Grassland	
Barcus	-0.7867208	43.188848	0	0.6	20.6	23	3	1	79.0	20	981	72.9	28	Grassland	
Esquile	-0.7048902	43.194938	0	0.4	20.9	0	0	1	78.7	1811	986	64.4	28	Grassland	
Lamidou	-0.7168551	43.285576	0.02	0.9	20.5	15	1	1	79.0	32	999	67.6	27	Grassland	
Moncayolle	-0.8434068	43.264186	0	0.6	20.8	0	0	1.4	79.1	43	988	61.6	29	Grassland	
Ainharp	-0.927231	43.268024	0	0.7	20.1	0	0	1.6	79.3	5296	981	64.8	32	Grassland	
Osseraïn	-0.9605008	43.377704	0	0.4	20.2	1	0	1.8	79.3	252	1007	46.8	36	Grassland	
Laas	-0.8470193	43.379819	0	0.3	20.5	7	0	1.4	79.1	1909	1005	55.6	37	Grassland	
Lameplaa	-0.8235575	43.400734	0	0.8	20.7	46	1	1	78.6	851	1002	69.4	27	Grassland	
Hourquebie	-0.841744	43.534271	0	0.6	20.8	1	1	1	78.6	4280	999	77.2	26	Grassland	
Pibole	-0.7324298	43.503738	0	0.1	21.1	4	1	1	78.7	388	1007	82.4	26	Grassland	
Biron	-0.7487931	43.46425	0	0.0	20.9	0	0	1	79.1	4364	101.0	80.8	28	Grassland	
Sauvelade	-0.7051026	43.396065	0	1.9	20.2	4	2	1	78.8	2456	1005	60.2	31	Grassland	
Abidos	-0.6055312	43.394956	0	2.1	20.8	0	0	1	79.0	88	1006	68.3	30	Grassland	
Arthez de Bearn	-0.5979083	43.463609	0	1.0	20.8	25	1	1.52	79.0	95	998	66.3	32	Grassland	
Castelner	-0.5769138	43.546863	0	0.2	20.9	2	1	1.6	78.9	42	997	53.5	34	Grassland	
Philondenz	-0.440628	43.564529	0	1.0	20.5	4	2	1	79.1	74	996	59.5	33	Grassland	
Monas	-0.4497019	43.450535	0.22	2.5	19.8	24	3	1.8	79.0	45	999	59.6	34	Grassland	
Col de Jaut	-0.3395519	43.056691	0	0.3	19.7	2	1	0	80.2	896	998	58.2	33	Meadow	
Mifaget	-0.3079806	43.110394	0	0.2	19.7	0	0	0	79.3	225	985	75.5	22	Grassland	
Montaut	-0.1910826	43.119642	0	1.6	19.7	5	1	0	79.1	8313	983	76.6	22	Forest	

Location	X	Y	CH ₄ (vol%)	CO ₂ (vol%)	O ₂ (vol%)	H ₂ ppmv	CO ppmv	H ₂ S ppmv	Balance (vol%)	Radon (bq m ⁻³)	Atmospheric pressure (mbar)	Humidity (%)	Temperature (°C)	soil type
Soum de las escures	-0.1717739	43.02286	0	0.4	20.3	3	0	0	79.4	9037	907	65.4	22	Meadow
Agos Vidalos	-0.0679288	43.058751	0	1.4	19.9	2	1	0	79.0	2168	976	89.5	21	Grassland
Gerns-sur-l'Oussonet	0.0547857	43.054632	0	3.8	18.4	18	0	0	79.5	568	933	73.1	22	Meadow
Orincles	0.0411323	43.122241	0	1.3	19.8	8	1	0	79.5	3429	979	89.9	23	Grassland
Juillian	0.0178934	43.20517	0	0.6	20.1	3	0	0	79.4	510	984	79.3	24	Grassland
Pontacq	-0.0917404	43.193646	0	1.0	20.1	11	1	0	79.5	1033	970	73.9	26	Grassland
Loubajac	-0.0703127	43.135432	0	1.6	20.1	22	2	0	79.2	39	965	69.3	25	Grassland
Bénjéac	-0.1968502	43.199635	0	0.6	20.4	6	1	0	79.2	62	990	74.7	24	Grassland
Limendous	-0.184808	43.273269	0	1.1	20.3	13	1	0	79.1	94	979	71.6	21	Grassland
AAST	-0.0906578	43.281296	0	0.5	20.6	4	1	0	78.9	57	976	82.2	20	Grassland
Lagarde	0.0288394	43.297155	0.02	0.4	20.5	4	1	0	79.2	61	989	96.3	20	Grassland
Saint Lézer	0.0255637	43.37813	0	0.5	20.3	2	1	0	79.3	140	994	89.8	22	Grassland
Maubourget	0.0251827	43.480074	0	0.3	20.1	2	0	0	79.5	37	1003	93.1	24	Grassland
Hères	0.0047965	43.543761	0	1.3	19.5	2	0	0	79.6	103	1004	84.5	26	Grassland
Arrosès	-0.1043122	43.536611	0	0.3	20.1	1	0	0	79.6	9109	994	88.1	28	Grassland
Sémécq Blachon	-0.1235543	43.494603	0	0.3	20.1	4	1	0	79.7	482	987	60.8	29	Grassland
Lucaré	-0.078001	43.414286	0	0.8	19.8	0	1	0	79.7	5863	990	63.9	29	Grassland
Bedous	-0.558885	42.966271	0	0.5	20.4	5	0	0	79.2	14754	954	63.8	25	Meadow
Gère Belestin	-0.421927	43.024804	0	0.9	20.0	3	1	0	79.5	125	966	94.5	25	Meadow
Arudy	-0.4376092	43.11053	0	1.4	19.4	1	1	0	79.6	73	974	72.9	28	Grassland
Misériou	-0.5533392	43.115528	0	2.9	19.0	3	0	0	79.0	226	979	69.9	28	Meadow
Précilhon	-0.573282	43.197708	0	0.2	20.1	5	1	0	79.7	60	989	82.2	29	Grassland
Labarcat	-0.4235382	43.205561	0	0.4	19.9	4	1	0	79.7	164	976	62.6	32	Grassland
Lesquerré	-0.3421668	43.193199	0	0.5	20.5	12	3	0	79.1	101	990	79.6	23	Grassland
Bizanos	-0.352381	43.28088	0	0.7	19.5	4	1	0	80.0	181	995	76.7	33	Grassland
Laroïn	-0.4377835	43.304135	0	0.1	19.6	4	1	0	80.2	40	997	60.4	37	Grassland
Haurrot	-0.5678612	43.308278	0	0.3	20.0	3	1	0	79.7	79	1000	49.6	37	Grassland
Gaujacq	-0.711198	43.66121	0	0.9	20.1	7	1	0	79.3	95	1005	66.4	27	Grassland
Peyredière	-0.7198242	43.752812	0	0.3	20.6	1	0	0	79.2	103	1006	85.2	25	Grassland
Gamarde-les-Bains	-0.8611776	43.759642	0	0.6	20.7	19	0	0	79.1	286	1009	89.8	25	Grassland
Candresse	-0.9759565	43.723164	0.02	0.6	20.4	1	0	0	79.1	335	1012	93.7	25	Grassland
Eyrasse	-1.1008223	43.725272	0.02	0.9	19.9	7	2	0	79.3	108	1008	93.9	26	Grassland
Balenton	-1.228461	43.722216	0	0.4	20.2	6	0	0	79.4	123	1006	94.9	26	Grassland
Josse	-1.2201363	43.658525	0	0.2	20.3	7	0	0	79.4	93	1011	90.6	27	Grassland
Heugas	-1.090996	43.631865	0	0.3	20.0	5	1	0	79.8	99	1007	77.8	31	Grassland
Mimbaste	-0.9652388	43.64693	0	0.3	19.9	4	1	0	79.9	149	1009	75.3	32	Grassland
Romarez	-0.838045	43.632978	0	0.2	19.9	5	0	0	80.0	125	1007	63.0	35	Grassland
Bahus soubiran	-0.362971	43.666469	0	0.4	20.5	3	1	0	79.3	88	99	67.2	24	Grassland
Bernède	-0.228397	43.669555	0	0.3	20.6	4	0	0	79.1	85	1007	81.7	22	Grassland
Tarsac	-0.1046477	43.66704	0	0.2	20.5	4	0	0	79.2	157	1005	90.2	22	Grassland
Arblade le haut	-0.0639412	43.743675	0	0.2	20.6	3	0	0	79.3	120	1001	93.8	23	Grassland
Lussagnet	-0.231062	43.774972	0	0.2	20.6	2	0	0	79.3	115	1006	93.0	24	Grassland
Renung	-0.3554283	43.74046	0	0.7	20.2	5	0	0	79.7	36	1002	89.7	27	Grassland
Montgaillard	-0.4818938	43.737794	0	1.0	19.9	20	2	0	79.4	102	1005	79.2	28	Grassland
Audignon	-0.5882988	43.729789	0	1.4	20.2	7	0	0	79.2	51	1010	85.4	27	Grassland
Magetmau	-0.6097428	43.6519	0	1.1	19.7	17	1	0	79.4	45	1004	83.2	28	Grassland
Bats	-0.4601553	43.651404	0	0.6	20.2	5	1	0	79.3	105	1000	70.5	28	Grassland
Lecumberry	-1.1393502	43.143978	0	0.5	20.1	0	0	0	79.3	249	970	81.1	23	Meadow
Pierraene. col de Napole	-0.9862993	43.154179	0	0.1	20.3	0	0	0	79.6	108	983	83.9	25	Meadow
Sauquis saint Etienne	-0.8939265	43.153775	0	0.4	19.9	3	1	0	79.8	99	992	87.5	28	Grassland

Location	X	Y	CH ₄ (vol%)	CO ₂ (vol%)	O ₂ (vol%)	H ₂ ppmv	CO ppmv	H ₂ S ppmv	Balance (vol%)	Radon (bq m ⁻³)	Atmospheric pressure (mbar)	Humidity (%)	Temperature (°C)	soil type
Mauléon Licharre	-0.89056	43.2317	0	0.1	19.9	1	0	0	79.9	63	990	70.0	30	Soil
Charre	-0.87881	43.3195	0	0.6	19.7	13	2	0	79.7	36	1001	62.4	31	Soil
Béhasque Lapiste	-1.00086	43.3238	0	0.1	20.2	2	1	0	79.7	65	1004	61.6	32	Soil
Pagolle	-0.98865	43.2314	0	0.0	20.1	2	0	0	79.7	73	996	56.5	35	Soil
Saint Etienne Lantabat	-1.14774	43.2461	0	0.3	20.5	2	0	0	79.3	12835	994	63.3	33	Soil
Méharin	-1.13918	43.3302	0	0.1	20.5	1	0	0	79.4	61	997	64.6	32	Soil
Orègue	-1.13547	43.3961	0	0.3	20.1	1	0	0	79.6	115	999	62.2	33	Soil
Abitain	-0.99522	43.4123	0	0.3	20.5	1	0	0	79.2	5365	999	70.4	25	Soil
Orion	-0.86208	43.4185	0	0.4	20.1	1	0	0	79.4	86	981	91.8	24	Soil

Location	Date	X	Y	CH ₄ (vol%)	CO ₂ (vol%)	O ₂ (vol%)	H ₂ ppmv	CO ppmv	H ₂ S ppmv	Balance (vol%)	soil type
Montaut	15/02/2018	-0.1645	43.1376944	0	0.2	20.3	8	1	0	79.3	Forest
Montaut	15/02/2018	-0.1647222	43.1376944	0	0.6	19.5	16	6	0	79.7	Forest
Montaut	15/02/2018	-0.1647222	43.1376944	0	0.6	19.5	20	2	0	79.7	Forest
Montaut	15/02/2018	-0.1647778	43.1376944	0	1	19.5	9	1	0	79.3	Forest
Montaut	15/02/2018	-0.1647778	43.1376944	0	1.8	19.1	7	1	0	78.9	Forest
Montaut	15/02/2018	-0.1648611	43.1377222	0	1.2	19.3	13	0	0	79.3	Forest
Montaut	15/02/2018	-0.165	43.1379444	0.5	0.3	20.1	17	2	4	78.9	Forest
Montaut	15/02/2018	-0.1651111	43.1380278	0.8	1.1	18.8	28	15	4	79.1	Forest
Montaut	15/02/2018	-0.1651111	43.1380278	1	0.6	19.8	36	5	8	78.4	Forest
Montaut	15/02/2018	-0.1654722	43.1380833	0	0.7	20	28	1	3	79.1	Forest
Montaut	15/02/2018	-0.1656389	43.1382222	0	0.8	19.9	25	0	2	79.1	Forest
Montaut	15/02/2018	-0.16575	43.1381944	0	0.2	20.4	88	6	1	79.2	Forest
Montaut	15/02/2018	-0.1658333	43.1383056	0	0.1	20.6	28	2	0	79.1	Forest
Montaut	15/02/2018	-0.1658611	43.1383889	0	0.3	20.3	56	7	1	79.2	Forest
Montaut	15/02/2018	-0.1658611	43.1383889	0	1	20	47	16	1	78.8	Forest
Montaut	15/02/2018	-0.1658889	43.1384167	0	0.2	20.5	39	2	0	79.1	Forest
Montaut	15/02/2018	-0.1659444	43.1385278	0.2	0.6	19.6	87	33	1	79.4	Forest
Montaut	15/02/2018	-0.1659444	43.1385278	0.2	0.3	20.4	94	12	1	78.9	Forest
Montaut	15/02/2018	-0.1658889	43.1386944	0	0.4	20.3	43	7	1	79.1	Forest
Montaut	15/02/2018	-0.1662778	43.1386111	0	0.1	20.8	40	1	0	78.9	Forest
Montaut	15/02/2018	-0.1662222	43.1391111	0	0.5	20.4	25	7	0	78.9	Forest
Lasseube	22/02/2018	-0.475571	43.225542	0	0.4	19.8	19	1	0	79	Forest
Lasseube	22/02/2018	-0.4745933	43.2234727	0	1.2	19.6	11	3	0	78.7	Forest
Lasseube	22/02/2018	-0.4745232	43.2234382	0	0.8	19.4	20	3	0	79	Forest
Lasseube	22/02/2018	-0.4743337	43.2235308	0	0.4	20.1	14	1	0	78.9	Forest
Lasseube	22/02/2018	-0.4748103	43.2235812	0	0.2	20.3	49	0	0	78.9	Forest
Lasseube	22/02/2018	-0.474962	43.2235558	0	1.5	19.1	29	1	0	78.7	Forest
Lasseube	22/02/2018	-0.4749757	43.223641	0	0.4	19.8	49	2	0	78.9	Forest
Lasseube	22/02/2018	-0.475238	43.2236543	0	0.4	20.3	42	2	0	78.7	Forest
Lasseube	22/02/2018	-0.4750615	43.2233492	0	1.7	15.6	64	4	0	79.3	Forest
Rébénacq	22/02/2018	-0.3957728	43.1533967	0	0.7	19.8	37	0	0	78.9	Forest
Rébénacq	22/02/2018	-0.3959203	43.1531877	0	0.2	20.3	23	0	0	78.8	Forest
Rébénacq	22/02/2018	-0.3962142	43.1531203	0	0.2	20.7	12	0	0	78.9	Grassland
Rébénacq	22/02/2018	-0.3963295	43.1530043	0	0.2	20.6	5	0	0	78.9	Grassland
Rébénacq	22/02/2018	-0.3965502	43.1526615	0	0.2	20.6	1	0	0	78.9	Grassland
Rébénacq	22/02/2018	-0.3957263	43.1522712	0	0.1	20.7	0	0	0	78.9	Grassland
Rébénacq	22/02/2018	-0.3957627	43.152633	0	0.1	20.8	0	0	0	78.9	Grassland
Col d'urdach	22/02/2018	-0.6641538	43.1180562	0.1	0.4	18.1	1000	79	2	80.5	Meadow
Col d'urdach	22/02/2018	-0.664306	43.1180788	0	0.3	19.2	1000	61	2	80.1	Meadow
Col d'urdach	22/02/2018	-0.664412	43.118094	0	0.2	19.4	323	17	0	79.6	Meadow
Col d'urdach	22/02/2018	-0.6644703	43.1180537	0	0.2	19.9	475	3	0	79.5	Meadow
Col d'urdach	22/02/2018	-0.6644968	43.1181472	0	0.3	20.1	105	4	0	79.5	Meadow
Col d'urdach	22/02/2018	-0.6646515	43.1181627	0.1	0.3	20.4	66	4	0	79.2	Meadow
Col d'urdach	22/02/2018	-0.664736	43.1177692	0.1	0.1	19.8	413	7	0	79.2	Meadow
Montaut	01/03/2018	-0.1643212	43.1380202	0	0.1	20.4	20	0	0	79.5	Forest
Montaut	01/03/2018	-0.1644252	43.1379812	0	0.1	19.6	7	2	0	79.5	Forest
Montaut	01/03/2018	-0.1640965	43.1379307	0	0.1	19.7	4	4	0	79.6	Forest
Montaut	01/03/2018	-0.1643232	43.138064	0	0.1	19.9	6	6	0	79.5	Forest
Montaut	01/03/2018	-0.1642893	43.1381833	0	0.2	19.9	12	2	0	79.4	Forest
Montaut	01/03/2018	-0.1641413	43.1382297	0	0.4	19.6	6	2	0	79.4	Forest
Montaut	01/03/2018	-0.1640383	43.1382155	0	0.1	19.6	14	2	0	79.5	Forest
Montaut	01/03/2018	-0.1637747	43.1383822	0	1.2	19.9	1	0	0	78.8	Forest
Montaut	01/03/2018	-0.1636903	43.1383243	0	0.3	19.4	2	1	0	79.4	Forest
Montaut	01/03/2018	-0.1637943	43.138295	0	0.1	19.7	4	4	0	79.4	Forest
Montaut	01/03/2018	-0.1636315	43.1383545	0	0.1	19.6	7	2	0	79.4	Forest
Montaut	01/03/2018	-0.163641	43.1381857	0	0.1	19.7	3	0	0	79.3	Forest
La Saline	14/03/2018	-0.9750965	43.442167	0.1	0.1	20.5	1	0	0	79.1	Forest
La Saline	14/03/2018	-0.975058	43.4420828	0.1	1.6	20.2	10	1	0	78.8	Forest
La Saline	14/03/2018	-0.9751335	43.4419952	0	2.6	19.5	31	2	0	79	Forest
La Saline	14/03/2018	-0.9751945	43.4421347	0	1.7	20	50	4	0	79.2	Forest
La Saline	14/03/2018	-0.9751592	43.4420173	0	0.4	20.2	53	2	0	79.2	Forest
La Saline	14/03/2018	-0.9748788	43.4421095	0	0.5	20.1	41	4	0	79.2	Forest
La Saline	14/03/2018	-0.9748665	43.4422035	0	0.2	20.6	14	1	0	79.1	Forest
La Saline	14/03/2018	-0.9747237	43.4421727	0	0.4	20.4	9	2	0	79.2	Forest

La Saline	14/03/2018	-0.9744672	43.4421662	0	1	20.1	12	1	0	79.1	Forest
La Saline	14/03/2018	-0.9740355	43.4418158	0	3.1	17.7	9	1	0	79.5	Forest
La Saline	14/03/2018	-0.9729313	43.4416493	0	2.7	19.6	4	1	0	79.3	Forest
La Saline	14/03/2018	-0.9762373	43.4418903	0	1.4	20.6	0	0	0	79	Forest
La Saline	14/03/2018	-0.9762167	43.4416758	0	0.3	20.6	3	0	0	78.9	Forest
La Saline	14/03/2018	-0.9762115	43.441722	0	0.5	20.3	15	1	0	79	Forest
La Saline	14/03/2018	-0.9760372	43.4419772	0	0.7	19.9	3	0	0	79.1	Forest
La Saline	14/03/2018	-0.9754932	43.4420153	0	0.5	20.4	5	1	0	79.1	Forest
La Saline	14/03/2018	-0.9751193	43.4416655	0	4.1	16.6	5	1	0	79.8	Forest
La Saline	14/03/2018	-0.9750193	43.4416693	0	2.6	17.5	1	0	0	79.7	Forest
La Saline	14/03/2018	-0.9752113	43.4416175	0	2.1	18.1	8	0	0	79.3	Forest
La Saline	14/03/2018	-0.9751687	43.441696	0	0.1	20.5	12	2	0	79.2	Forest
La Saline	14/03/2018	-0.9749573	43.4417077	0	0.3	20.3	11	1	0	79.3	Forest
La Saline	14/03/2018	-0.9749468	43.4416613	0	1	20.2	12	0	0	79.1	Forest
La Saline	14/03/2018	-0.974798	43.4412693	0	1.4	17.3	12	1	0	79.7	Forest
La Saline	14/03/2018	-0.9748048	43.4413007	0	0.8	20	4	1	0	79.4	Forest
La Saline	14/03/2018	-0.974995	43.4418665	0	0.3	20.1	13	1	0	79.6	Forest
La Saline	14/03/2018	-0.9751057	43.4420958	0	0.1	20.1	9	0	0	79.6	Forest
La Saline	14/03/2018	-0.9751592	43.4421248	0	0.6	19.8	34	1	0	79.5	Forest
La Saline	14/03/2018	-0.9751247	43.442053	0	0.4	20	7	1	0	79.6	Forest
La Saline	14/03/2018	-0.9750288	43.4421793	0	0.8	19.7	16	0	0	79.6	Forest
La Saline	14/03/2018	-0.9752068	43.4420912	0	0.3	20.1	2	0	0	79.6	Forest
La Saline	14/03/2018	-0.9752217	43.4419373	0	1.1	19.2	5	1	0	79.6	Forest
La Saline	14/03/2018	-0.9747533	43.442334	0	1.1	19.1	18	2	0	79.3	Forest
La Saline	14/03/2018	-0.9748752	43.442813	0	2.8	17.4	31	3	0	80.2	Forest
La Saline	14/03/2018	-0.975023	43.4428177	0	1.4	18.1	157	5	0	79.3	Forest
La Saline	14/03/2018	-0.9752322	43.4429002	0	0.3	20.3	28	1	0	79.4	Forest
La Saline	14/03/2018	-0.9755785	43.4429695	0	2	16.7	63	2	0	79.5	Forest
La Saline	14/03/2018	-0.9757913	43.443018	0	0.3	20.3	7	0	0	79.3	Forest
La Saline	14/03/2018	-0.9758867	43.4430132	0	0.3	20.3	11	1	0	79.3	Forest
La Saline	14/03/2018	-0.9734632	43.4442082	0	2.4	19.7	12	1	0	79.1	Forest
La Saline	14/03/2018	-0.9736822	43.4442152	0	2.1	19.6	77	5	0	79.2	Forest
La Saline	14/03/2018	-0.9735583	43.4441808	0	2.4	19	53	1	0	79.2	Forest
La Saline	14/03/2018	-0.9734462	43.4447463	0	0.3	20.5	6	2	0	79.6	Forest
La Saline	14/03/2018	-0.9734595	43.4446983	0	2.3	18.2	4	2	0	80.3	Forest
La Saline	14/03/2018	-0.9734997	43.444886	0	2.8	17.1	7	0	0	79	Forest
La Saline	14/03/2018	-0.9734445	43.4451275	0	2	19.7	8	4	0	79.1	Forest
La Saline	14/03/2018	-0.9732677	43.4454033	0	0.8	20	3	1	0	79	Forest
La Saline	14/03/2018	-0.9732893	43.4457868	0	0.6	20.4	6	2	0	79	Forest
La Saline	14/03/2018	-0.9734505	43.4466582	0	0.7	20.7	21	2	0	79.1	Forest
La Saline	14/03/2018	-0.9733277	43.4465763	0	0.7	20.3	19	3	0	79	Forest
La Saline	14/03/2018	-0.9735527	43.4448362	0	3.2	17.2	11	4	0	79.6	Forest
La Saline	14/03/2018	-0.9735215	43.444711	0	2.3	18.2	9	2	0	79.4	Forest
Sud Le Bourguet	14/03/2018	-0.9777712	43.4509313	0	0.2	20	67	2	0	79.1	Forest
Sud Le Bourguet	14/03/2018	-0.9773423	43.4512025	0	2.9	18	17	4	0	79	Forest
Sud Le Bourguet	14/03/2018	-0.9776297	43.4513497	0	2.7	18.2	21	0	0	79.2	Forest
Sud Le Bourguet	14/03/2018	-0.9776645	43.451482	0	1.7	19.9	59	5	0	79.2	Forest
Sud Le Bourguet	14/03/2018	-0.9775612	43.451605	0	0.6	20	45	2	0	79.2	Forest
Sud Le Bourguet	14/03/2018	-0.9776637	43.4516368	0	0.7	19.9	41	3	0	79.2	Forest
Sud Le Bourguet	14/03/2018	-0.9781478	43.4539367	0	0.2	20.5	408	3	0	79.4	Forest
Sud Le Bourguet	14/03/2018	-0.9778852	43.4538962	0	2.4	18.6	547	12	0	79.2	Forest
Sud Le Bourguet	14/03/2018	-0.9777805	43.4539298	0	0.3	20.4	145	3	0	79.3	Forest
Sud Le Bourguet	14/03/2018	-0.977751	43.4538078	0	0.5	19.2	45	1	0	79.1	Forest
Sud Le Bourguet	14/03/2018	-0.977703	43.4537505	0	0.5	19.9	54	3	0	79.1	Forest
Sud Le Bourguet	14/03/2018	-0.9778852	43.4536867	0	1.5	19.9	38	3	0	79.2	Forest
Sud Le Bourguet	14/03/2018	-0.9780985	43.4536047	0	2.5	18.1	21	1	0	79.1	Forest
Sud Le Bourguet	14/03/2018	-0.9775505	43.4534532	0	0.9	19.3	1	0	0	78.9	Forest
Sud Le Bourguet	14/03/2018	-0.9775568	43.4531925	0	1.7	19.6	10	2	0	78.9	Forest
Sud Le Bourguet	14/03/2018	-0.9773038	43.4529652	0	4.1	16.5	7	2	0	79.4	Forest
Sud Le Bourguet	14/03/2018	-0.977322	43.4529423	0	3.9	16.6	12	1	0	79.4	Forest
Sud Le Bourguet	14/03/2018	-0.9772428	43.4528433	0	3.8	16.8	19	1	0	78.8	Forest
Sud Le Bourguet	14/03/2018	-0.9772082	43.4529033	0	2.4	19.3	13	3	0	78.2	Forest
Armendarits	15/03/2018	-1.169328	43.287837	0	0.1	20.1	7	1	0	79.7	Grassland
Armendarits	15/03/2018	-1.169328	43.287837	0	0.7	19.7	22	0	0	79.7	Grassland
Armendarits	15/03/2018	-1.1694012	43.2877785	0	0.2	19.8	36	1	0	79.8	Grassland
Armendarits	15/03/2018	-1.169179	43.2880077	0	0.2	19.5	5	1	0	79.7	Grassland
Armendarits	15/03/2018	-1.1689343	43.2881155	0	0.2	19.5	3	1	0	79.9	Grassland

Armendarits	15/03/2018	-1.1689288	43.2882802	0	0.2	19.1	5	0	0	79.9	Grassland
Armendarits	15/03/2018	-1.168786	43.288348	0	0.3	19.3	6	1	0	79.9	Grassland
Armendarits	15/03/2018	-1.1685127	43.2885522	0	0.2	19.9	24	2	0	79.8	Grassland
Armendarits	15/03/2018	-1.1579942	43.3016815	0	0.2	19.6	0	0	0	79.7	Grassland
Armendarits	15/03/2018	-1.1579148	43.3012453	0	0.8	19.7	6	8	0	79.5	Grassland
Armendarits	15/03/2018	-1.1579098	43.3013702	0	0.9	19.5	20	5	0	79.7	Grassland
Armendarits	15/03/2018	-1.1579847	43.3012603	0.1	1.1	19	16	7	0	79.6	Grassland
Armendarits	15/03/2018	-1.1579348	43.3012288	0	0.5	19.9	15	5	0	79.7	Grassland
Armendarits	15/03/2018	-1.1579563	43.3010107	0	0.3	19.6	25	6	0	79.6	Grassland
Armendarits	15/03/2018	-1.1579305	43.3009972	0	0.7	19.5	9	7	0	79.6	Grassland
Armendarits	15/03/2018	-1.1579958	43.300808	0	1.3	19.6	4	2	0	79.7	Grassland
Armendarits	15/03/2018	-1.1580453	43.3006523	0	1.5	19.8	17	5	0	79.1	Grassland
Armendarits	15/03/2018	-1.157992	43.3007188	0	0.6	20.1	9	3	0	80.1	Grassland
Armendarits	15/03/2018	-1.1575958	43.3008153	0	0.5	16.5	6	4	0	79.6	Grassland
Armendarits	15/03/2018	-1.1576383	43.300734	0	0.3	19.9	5	2	0	79.6	Grassland
Armendarits	15/03/2018	-1.1581723	43.301136	0	0.1	20	5	5	0	79.5	Grassland
Armendarits	15/03/2018	-1.1581228	43.3011803	0	3.2	16.5	2	1	0	80.3	Grassland
Armendarits	15/03/2018	-1.1582988	43.3011328	0	2.9	17.1	3	3	0	79.5	Grassland
Armendarits	15/03/2018	-1.1578728	43.3021435	0	0.3	20.3	1	1	0	79.4	Grassland
Armendarits	15/03/2018	-1.1578663	43.3021457	0	0.5	19.9	18	2	0	79.4	Grassland
Armendarits	15/03/2018	-1.1536783	43.3276302	0	0.1	20.3	24	4	0	79.6	Grassland
Armendarits	15/03/2018	-1.1364785	43.3215688	0	0.2	19.9	7	2	0	79.8	Grassland
Armendarits	15/03/2018	-1.1363037	43.3215793	0	0.9	19.4	37	7	0	79.6	Grassland
Armendarits	15/03/2018	-1.1361185	43.3216047	0	0.1	20.2	8	3	0	80	Grassland
Armendarits	15/03/2018	-1.1355955	43.3217743	0	2.4	17.5	17	6	0	79.7	Grassland
Armendarits	15/03/2018	-1.135432	43.3217505	0	0.5	19.9	4	2	0	79.6	Grassland
Armendarits	15/03/2018	-1.1351168	43.3217147	0	0.4	20	13	3	0	79.6	Grassland
Armendarits	15/03/2018	-1.1352648	43.3202693	0	2.6	18.5	11	3	0	79.9	Grassland
Armendarits	15/03/2018	-1.1353303	43.3202363	0	0.8	19.6	47	6	0	79.7	Grassland
Armendarits	15/03/2018	-1.1354513	43.3202388	0	0.1	19.9	15	2	0	79.6	Grassland
Mauléon Nord	22/03/2018	-0.8712205	43.2516035	0	0.2	20.4	7	0	0	79.2	Grassland
Sauveterre	29/03/2018	-0.9467363	43.1756103	0	0.1	20.2	33	3	0	79.7	Grassland
Sauveterre	29/03/2018	-0.9468712	43.4076148	0	0.4	19.9	5	0	0	79.8	Grassland
Sauveterre	29/03/2018	-0.9470058	43.4073415	0	0.2	19.9	3	0	0	79.9	Grassland
Sauveterre	29/03/2018	-0.9472095	43.4070228	0	1.5	18.7	6	0	0	79.8	Grassland
Sauveterre	29/03/2018	-0.9471935	43.4067808	0.4	2.2	16.7	8	1	0	80.7	Grassland
Sauveterre	29/03/2018	-0.9473323	43.4065395	0	1.7	17.5	7	1	0	80	Grassland
Sauveterre	29/03/2018	-0.9475332	43.4062885	0	0.6	19	2	1	0	80.3	Grassland
Sauveterre	29/03/2018	-0.947621	43.406076	0	0.3	19.5	0	0	0	80	Grassland
Sauveterre	29/03/2018	-0.947674	43.4054703	0	0.1	19.9	1	0	0	80	Grassland
Sauveterre	29/03/2018	-0.9478187	43.4054413	0	0.1	19.9	3	0	0	80	Grassland
Sauveterre	29/03/2018	-0.9479578	43.405017	0	0.3	19.8	7	3	0	79.9	Grassland
Sauveterre	29/03/2018	-0.9480075	43.4047863	0	0.3	19.7	2	1	0	80	Grassland
Sauveterre	29/03/2018	-0.9479553	43.4047912	0	0.1	19.8	1	0	0	80.1	Grassland
Sauveterre	29/03/2018	-0.9479248	43.404535	0	0.1	19.8	1	0	0	80	Grassland
Sauveterre	29/03/2018	-0.9479597	43.4043507	0	0.1	19.8	2	1	1	80.1	Grassland
Sauveterre	29/03/2018	-0.9479688	43.4041508	0	0.1	19.8	0	0	0	80	Grassland
Sauveterre	29/03/2018	-0.947961	43.404027	0	0.1	19.8	1	1	1	80	Grassland
Sauveterre	29/03/2018	-0.9482058	43.4038793	0.4	0.7	18.6	4	2	1	80.4	Grassland
Sauveterre	29/03/2018	-0.9481645	43.4038767	0.2	0.4	18.9	7	2	1	80.2	Grassland
Sauveterre	29/03/2018	-0.9489128	43.4036628	0	0.2	19.5	5	1	0	79.9	Grassland
Sauveterre	29/03/2018	-0.9493665	43.4033277	0	0.1	20	2	2	0	79.9	Grassland
Sauveterre	29/03/2018	-0.9497722	43.4040078	0	0.1	20	25	2	0	79.8	Grassland
Sauveterre	29/03/2018	-0.949797	43.4040568	0	0.1	20.1	4	0	0	79.7	Grassland
Sauveterre	29/03/2018	-0.9505142	43.4040775	0	0.8	19.8	9	3	0	79.5	Grassland
Sauveterre	29/03/2018	-0.9506103	43.4040895	0	0.3	19.9	16	1	0	79.8	Grassland
Sauveterre	29/03/2018	-0.950835	43.4040013	0	0.2	20.1	1	0	0	79.5	Grassland
Sauveterre	29/03/2018	-0.950817	43.4042597	0	0.1	20.4	4	1	0	79.5	Grassland
Sauveterre	29/03/2018	-0.9513202	43.4045563	0	0.1	20.4	6	1	0	79.5	Grassland
Sauveterre	29/03/2018	-0.9514618	43.4048278	0	0.1	20.1	11	2	0	79.5	Grassland
Sauveterre	29/03/2018	-0.9518605	43.4055925	0	0.1	20.4	49	2	0	79.3	Grassland
Sauveterre	29/03/2018	-0.9517122	43.4057213	0	1.3	18.9	31	11	0	79.7	Grassland
Sauveterre	29/03/2018	-0.95209	43.4059285	0	2.8	18.1	34	3	0	79.3	Grassland
Sauveterre	29/03/2018	-0.9523202	43.4058108	0	2.6	18	52	4	0	79.3	Grassland
Sauveterre	29/03/2018	-0.9525893	43.4061757	0	2.4	18.3	11	1	0	79.1	Grassland
Sauveterre	29/03/2018	-0.9526067	43.4064645	0	7.2	13.3	148	34	0	80.9	Grassland
Sauveterre	29/03/2018	-0.9527935	43.4065913	0	7.2	13.2	173	24	0	79.7	Grassland

Sauveterre	29/03/2018	-0.9531197	43.4066168	0	5.7	9.2	632	11	1	81.3	Grassland
Sauveterre	29/03/2018	-0.9532543	43.4068952	0	3	15.4	104	6	0	79	Grassland
Sauveterre	29/03/2018	-0.9525438	43.4071193	0	0.6	20.4	187	11	0	78.9	Grassland
Sauveterre	29/03/2018	-0.9525917	43.4073667	0	0.7	20.6	28	3	0	78.9	Grassland
Sauveterre	29/03/2018	-0.9508853	43.4066657	0	0.4	20.7	121	5	0	78.9	Grassland
Sauveterre	29/03/2018	-0.9502885	43.4066168	0	1	19.6	198	7	0	79.4	Grassland
Sauveterre	29/03/2018	-0.9501203	43.4055437	0	1.1	19.4	6	1	0	78.7	Grassland
Sauveterre	29/03/2018	-0.9495548	43.4054707	0	0.1	21.2	6	2	0	78.7	Grassland
Sauveterre	29/03/2018	-0.9490133	43.4054767	0	0.1	21.2	4	1	0	78.7	Grassland
Sauveterre	29/03/2018	-0.949013	43.4054853	0	0.5	20.3	29	3	0	78.8	Grassland
Sauveterre	29/03/2018	-0.9491333	43.4054662	0	2.5	17.4	81	18	0	80.4	Grassland
Sauveterre	29/03/2018	-0.9486832	43.4054683	0	1.8	18.3	177	7	0	79.3	Grassland
Sauveterre	29/03/2018	-0.9480718	43.4052173	0	1.1	19.5	7	0	0	78.5	Grassland
Sauveterre	29/03/2018	-0.9480718	43.4054475	0	0.1	21.1	3	1	0	78.8	Grassland
Sauveterre	29/03/2018	-0.9480718	43.4054633	0	0.6	19.9	3	1	0	78.6	Grassland
Col d'Urdach	18/04/2018	-0.6646265	43.1177437	0.1	0.1	20.1	15	2	0	79.9	Meadow
Col d'Urdach	18/04/2018	-0.66426	43.1180943	0.1	0.4	19.7	2	0	0	79.9	Meadow
Montaut	25/04/2018	-0.168492	43.138661	0	0.7	20.5	27	3	0	79.1	Forest
Montaut	25/04/2018	-0.168492	43.138661	0	0.5	19.9	35	3	0	78.5	Forest
Montaut	25/04/2018	-0.1686963	43.1387925	0	0.2	20.8	34	12	0	78.8	Forest
Montaut	25/04/2018	-0.1686493	43.1386995	0	0.3	20.3	65	8	0	78.9	Forest
Montaut	25/04/2018	-0.1685993	43.1388455	0	0.8	20.1	24	9	0	78.8	Forest
Montaut	25/04/2018	-0.1683395	43.1384888	0	0.2	20.4	2	2	0	78.8	Forest
Montaut	25/04/2018	-0.165906	43.138088	0	0	19.9	73	9	0	79.4	Forest
Montaut	04/05/2018	-0.1686902	43.1389622	0	5.7	20.3	2	0	0	79.4	Forest
Montaut	04/05/2018	-0.1683057	43.1382958	0	0.1	20.3	1	0	0	79.4	Forest
Montaut	04/05/2018	-0.1659067	43.1382203	0	0	20.5	1	0	0	79.1	Forest
Montaut	16/05/2018	-0.164457	43.137754	0.1	0	20.3	1	0	0	79.4	Forest
Montaut	16/05/2018	-0.168492	43.138661	0	0.1	20.4	1	0	0	79.2	Forest
Montaut	16/05/2018	-0.168428	43.138497	0.1	0	20.4	1	0	0	79.2	Forest
Montaut	16/05/2018	-0.167975	43.138244	0	0	20.5	0	0	0	79.2	Forest
Castetnau-Camblong	16/05/2018	-0.7897172	43.3239003	0	0.6	20.1	7	0	0	79.1	Grassland
Turon de la Técouère	20/06/2018	-0.4945167	43.0631987	0.3	0.1	19.9	0	0	0	79.7	Meadow
Turon de la Técouère	20/06/2018	-0.4945737	43.0633133	0.2	0.1	19.5	1	0	0	80.2	Meadow
Turon de la Técouère	20/06/2018	-0.4945313	43.0631845	0.2	0.1	19.1	0	0	0	80.6	Meadow
Turon de la Técouère	20/06/2018	-0.4945693	43.063233	0.2	0.1	18.8	17	7	0	80.9	Meadow
Turon de la Técouère	20/06/2018	-0.4944077	43.0632138	0.1	1	17	300	11	1	81.5	Meadow
Turon de la Técouère	20/06/2018	-0.4946103	43.0634592	0	0.2	17.9	130	3	1	81.1	Meadow
Turon de la Técouère	20/06/2018	-0.4946233	43.0634558	0	0.3	18.3	93	3	1	81	Meadow
Turon de la Técouère	20/06/2018	-0.4944435	43.0636402	0	1.1	18.3	22	0	0	80.7	Meadow
Turon de la Técouère	20/06/2018	-0.4944555	43.063598	0.1	1.1	19	111	2	0	80	Meadow
Turon de la Técouère	20/06/2018	-0.4942145	43.0641563	0.2	4.1	16.6	612	23	0	79.6	Meadow
Turon de la Técouère	20/06/2018	-0.4942358	43.0641743	0.1	2.9	16.8	333	12	0	79.8	Meadow
Turon de la Técouère	20/06/2018	-0.4936763	43.0642122	0	1.1	18	174	6	0	80.5	Meadow
Turon de la Técouère	20/06/2018	-0.4933843	43.0641078	0	2.3	18.9	405	13	1	80.2	Meadow
Turon de la Técouère	20/06/2018	-0.4923743	43.0646652	0	1.2	19.3	142	5	0	79.7	Meadow
Turon de la Técouère	20/06/2018	-0.4925355	43.0646657	0	3.4	19.7	750	19	1	80.1	Meadow
Turon de la Técouère	20/06/2018	-0.4923217	43.0651015	0.1	5.3	15.6	120	2	0	78.7	Meadow
Turon de la Técouère	20/06/2018	-0.4921712	43.065022	0.1	5.5	16.3	228	12	0	78.8	Meadow
Turon de la Técouère	20/06/2018	-0.4921788	43.0652115	0.1	3.5	18.9	205	15	0	78.8	Meadow
Turon de la Técouère	20/06/2018	-0.4918437	43.0654473	0	1.2	19.3	105	4	0	79.3	Meadow
Turon de la Técouère	20/06/2018	-0.4918172	43.0656038	0	0.2	19.2	365	4	0	79.6	Meadow
Turon de la Técouère	20/06/2018	-0.4915328	43.0657285	0	0.1	18.8	736	12	1	79.9	Meadow
Turon de la Técouère	20/06/2018	-0.4914363	43.0658517	0	0	17.1	1000	20	2	79.9	Meadow
Turon de la Técouère	20/06/2018	-0.4914632	43.0658952	0	0	20.1	1000	1	0	79.8	Meadow
Turon de la Técouère	20/06/2018	-0.4914962	43.0657058	0	0	18.6	800	7	1	80	Meadow
Turon de la Técouère	20/06/2018	-0.4908852	43.0666567	0	1.3	19.9	67	5	0	79.5	Meadow
Turon de la Técouère	20/06/2018	-0.4909217	43.0666983	0	1	19.9	17	2	0	79.3	Meadow
Turon de la Técouère	20/06/2018	-0.489865	43.0646607	0	2.4	11.6	37	1	0	79.3	Meadow
Turon de la Técouère	20/06/2018	-0.4898323	43.0646528	0	0.3	20.2	217	4	0	79.4	Meadow
Turon de la Técouère	20/06/2018	-0.491625	43.0619573	0	2.5	20.3	159	6	0	79.3	Meadow
Turon de la Técouère	20/06/2018	-0.495814	43.0620837	0	1.8	20.2	2	1	0	78.9	Meadow
Turon de la Técouère	20/06/2018	-0.4961447	43.0622418	0	1.8	20	23	6	0	78.6	Meadow
Nord Baigts-de-Béarn	02/05/2019	-0.829677	43.5231383	0	0.3	20.3	152	2	0	79.1	Forest
Nord Baigts-de-Béarn	02/05/2019	-0.8296143	43.5231413	0.2	0.8	20.1	107	1	0	79	Forest
Nord Baigts-de-Béarn	02/05/2019	-0.8291317	43.5234377	0	0.2	20.7	92	6	1	79.1	Forest
Nord Baigts-de-Béarn	02/05/2019	-0.8291422	43.5233227	0.1	0.3	19.9	734	10	1	79	Forest

Nord Baigts-de-Béarn	02/05/2019	-0.8289763	43.5233127	0.1	0.1	20	350	9	1	79	Forest
Nord Baigts-de-Béarn	02/05/2019	-0.8284305	43.5224712	0	0.1	20.4	44	2	0	78.7	Forest
Nord Baigts-de-Béarn	02/05/2019	-0.8286693	43.5227893	0	0.7	20.4	221	6	0	78.7	Forest
Est Baigts-de-béarn	02/05/2019	-0.8152538	43.5133895	0	0.1	21.1	27	3	0	78.7	Grassland
Est Baigts-de-béarn	02/05/2019	-0.8152843	43.5134165	0	0.4	21	74	2	0	78.6	Grassland
Labordes	02/05/2019	-0.9088855	43.4354812	0	0.3	20.5	221	2	0	79.4	Grassland
Labordes	02/05/2019	-0.9094275	43.441804	0	0.1	20.8	722	4	1	79.2	Grassland
Labordes	02/05/2019	-0.9093278	43.4418713	0	1.6	19.5	70	2	0	79.1	Grassland
Labordes	02/05/2019	-0.90945	43.4417805	0	0.9	19.4	49	2	0	79.4	Grassland
Labordes	02/05/2019	-0.9201248	43.4612637	0	0.1	18.9	80	0	0	79.4	Grassland
Labordes	02/05/2019	-0.9185263	43.46016	0	3	18.6	284	3	0	79.1	Grassland
Labordes	02/05/2019	-0.9184595	43.4600703	0.6	3.8	16.8	1000	0	3	80.9	Grassland
Labordes	02/05/2019	-0.9076387	43.4416495	0.3	0.4	20.2	20	3	0	79.2	Grassland
Sussaute	02/05/2019	-0.9874452	43.3688172	0	0.1	21.2	12	1	0	79.2	Grassland
Sussaute	02/05/2019	-0.9873432	43.3687193	0	0.6	20.1	36	14	0	79.1	Grassland
Arbouet-Sussaute	02/05/2019	-0.9821332	43.3850248	0	0.1	21.1	0	0	0	78.8	Grassland
Arbouet-Sussaute	02/05/2019	-0.9821667	43.3851167	0	0.1	21	17	3	0	78.9	Grassland
Arbouet-Sussaute	02/05/2019	-0.982216	43.3846762	0	0.1	20.9	43	10	0	79	Grassland
Montaut	16/05/2019	-0.1689808	43.139159	0	0.2	20.2	25	0	0	79.3	Forest
Montaut	16/05/2019	-0.1662492	43.1385372	0	0.9	20.5	15	0	0	79.1	Forest
Montaut	16/05/2019	-0.169671	43.140192	0	0.6	20.6	140	6	0	79.2	Forest
Montaut	16/05/2019	-0.169671	43.140192	0	0.2	19.5	7	2	0	79.2	Forest
Sommet de Moncaut	16/05/2019	-0.31586	43.0759962	0	0.1	21.3	0	0	0	78.6	Meadow
Sommet de Moncaut	16/05/2019	-0.3161847	43.0766237	0	0.1	21.2	2	1	0	78.6	Meadow
Sommet de Moncaut	16/05/2019	-0.316552	43.0768237	0	0	21.2	1	2	0	78.7	Meadow
Sommet de Moncaut	16/05/2019	-0.3164798	43.0770513	0	0.1	21.1	1	1	0	78.8	Meadow
Sommet de Moncaut	16/05/2019	-0.3164035	43.0770528	0	0	21.1	1	0	0	78.8	Meadow
Sud Col d'Apanice	19/06/2019	-1.071121	43.0990375	0	0.2	19.9	3	0	0	79.5	Meadow
Sud Col d'Apanice	19/06/2019	-1.0446587	43.0928573	0	0.2	20.7	3	2	0	78.9	Meadow
Sud Col d'Apanice	19/06/2019	-1.044579	43.0927805	0	0.1	20.9	7	2	0	78.8	Meadow
Baigts de Bearn Est	19/09/2019	-0.8139493	43.5140765	0	0.4	20.7	5	1	0	79	grassland
Baigts de Bearn Est	19/09/2019	-0.8141292	43.5139402	0	0.8	20.1	8	2	0	79.1	grassland
Baigts de Bearn Est	19/09/2019	-0.8140948	43.514101	0	0.6	20.4	4	0	0	78.8	grassland
Baigts de Bearn Est	19/09/2019	-0.8140807	43.514104	0	0.8	20.4	1	0	0	78.8	grassland
Baigts de Bearn Est	19/09/2019	-0.8139442	43.5140843	0	0.8	20.5	11	0	0	78.9	grassland
Baigts de Bearn Est	19/09/2019	-0.8141342	43.5140173	0	1.6	20.3	8	1	0	78.6	grassland
Baigts de Bearn Est	19/09/2019	-0.8140668	43.5140525	0	0.8	20.5	23	0	0	78.8	grassland
Baigts de Bearn Est	19/09/2019	-0.813908	43.5141053	0	0.6	20.7	7	0	0	78.9	grassland
Baigts de Bearn Est	19/09/2019	-0.8152402	43.514263	0	3	18.8	10	1	0	78.3	grassland
Baigts de Bearn Est	19/09/2019	-0.8156937	43.5142735	0	3.2	18.9	44	3	0	78.6	grassland
Baigts de Bearn Est	19/09/2019	-0.8154822	43.5143583	0	2.4	19.1	36	1	0	78.5	grassland
Baigts de Bearn Est	19/09/2019	-0.8156817	43.5141447	0	2.5	19	25	6	0	79.1	grassland
Baigts de Bearn Est	19/09/2019	-0.8153205	43.5140208	0	0.4	20.2	481	9	0	79.2	grassland
Baigts de Bearn Est	19/09/2019	-0.8155012	43.5142307	0	0.3	20.6	272	1	0	79.1	grassland
Baigts de Bearn Est	19/09/2019	-0.8155028	43.514072	0	3.2	18.9	180	7	0	79	grassland
Baigts de Bearn Est	19/09/2019	-0.8156273	43.514094	0	1.1	20	37	8	0	79.1	grassland
Baigts de Bearn Est	19/09/2019	-0.8154692	43.5139885	0	0.6	20.2	36	3	0	79	grassland
Baigts de Bearn Est	19/09/2019	-0.8158915	43.5141927	0	2	20.4	90	3	0	79	grassland
Baigts de Bearn Est	19/09/2019	-0.8158785	43.5139147	0	0.3	20.7	21	3	0	78.9	grassland
Baigts de Bearn Est	19/09/2019	-0.815701	43.5140095	0	0	21.1	3	0	0	78.9	grassland
Baigts de Bearn Est	19/09/2019	-0.8157095	43.5139962	0	0.6	20.7	7	1	0	78.8	grassland
Baigts de Bearn Est	19/09/2019	-0.8154442	43.5140443	0	2.1	19.8	29	7	0	78.9	grassland
Baigts de Bearn Est	19/09/2019	-0.8152568	43.514007	0	3.1	19.4	21	7	0	78.5	grassland
Baigts de Bearn Est	19/09/2019	-0.8151516	43.514204	0	1.4	20	11	3	0	78.7	grassland
Baigts de Bearn Est	19/09/2019	-0.8147607	43.5143007	0	1.1	20.7	39	2	0	78.8	grassland
Baigts de Bearn Est	19/09/2019	-0.8147937	43.514253	0	0.8	20.6	17	2	0	78.8	grassland
Baigts de Bearn Est	19/09/2019	-0.8147307	43.5143948	0	2.9	19.7	34	4	0	78.8	grassland
Baigts de Bearn Est	19/09/2019	-0.8147143	43.5141988	0	0.5	20.3	43	3	0	79	grassland
Baigts de Bearn Est	19/09/2019	-0.8137635	43.514367	0	2.8	18.8	12	2	0	78.4	grassland
Baigts de Bearn Est	19/09/2019	-0.8131142	43.5144187	0	2.7	18.8	3	1	0	78.7	grassland
Baigts de Bearn Est	19/09/2019	-0.8130212	43.5144518	0	2.3	19.1	37	2	0	79.2	grassland
Baigts de Bearn Est	19/09/2019	-0.8134487	43.5143572	0	0.9	20.1	27	4	0	78.9	grassland
Baigts de Bearn Est	19/09/2019	-0.8154588	43.514164	0	0.9	20.2	17	3	0	78.8	grassland
Baigts de Bearn Est	19/09/2019	-0.815536	43.5142368	0	0.9	20.4	43	2	0	78.8	grassland
Baigts de Bearn Est	19/09/2019	-0.815549	43.5143868	0	2.5	19.1	46	6	0	78.6	grassland
Baigts de Bearn Est	19/09/2019	-0.815498	43.5144052	0	2.1	19.2	14	1	0	78.7	grassland
Baigts de Bearn Est	19/09/2019	-0.8155877	43.5145433	0	2.2	19.1	4	2	0	78.7	grassland

Baigts de Bearn Est	19/09/2019	-0.8153997	43.514522	0	5	17.4	198	14	0	78.6	grassland
Baigts de Bearn Est	19/09/2019	-0.8152367	43.514587	0	1.4	19.9	10	1	0	78.8	grassland
Baigts de Bearn Est	19/09/2019	-0.8155757	43.5149555	0	4.2	18.4	12	2	0	78.3	grassland
Baigts de Bearn Est	19/09/2019	-0.8156217	43.5150095	0	2.8	18.8	84	7	0	78.9	grassland
Baigts de Bearn Est	19/09/2019	-0.8157892	43.5152818	0	0.5	20.4	55	6	0	78.9	grassland
Baigts de Bearn Est	19/09/2019	-0.8155323	43.5151345	0	0.6	20.3	51	5	0	78.8	grassland
Baigts de Bearn Est	19/09/2019	-0.8150347	43.5136577	0	0.1	21	9	1	0	78.8	grassland
Baigts de Bearn Est	19/09/2019	-0.8149928	43.5134932	0	1.2	20.4	5	2	0	78.6	grassland
Baigts de Bearn Est	19/09/2019	-0.8146185	43.5134188	0	0	20.6	0	0	0	78.9	grassland
Baigts de Bearn Est	19/09/2019	-0.8147987	43.51366	0	1	21.1	0	0	0	78.7	grassland
Baigts de Bearn Est	19/09/2019	-0.8147367	43.5138038	0	3.1	20.7	0	1	0	78.3	grassland
	17/06/2020			0.1	0.1	20.6	0	0	0	79.2	Forest
	17/06/2020	-0.1686737	43.1388272	0	0.1	19.6	90	1	0	79.4	Forest
	17/06/2020	-0.168824	43.1387493	0	0.2	20.5	25	0	0	79.4	Forest
	17/06/2020	-0.1686475	43.1384858	0	0.7	19.7	0	0	0	79.1	Forest
	17/06/2020	-0.168565	43.1382072	0	0.4	20.2	0	0	0	79	Forest
	17/06/2020	-0.1686077	43.1379268	0	1.3	20.7	3	0	0	78.9	Forest
	17/06/2020	-0.1684727	43.1376778	0.1	0.5	20.7	2	0	1	78.9	Forest
	17/06/2020	-0.1684282	43.1375073	0.1	0.2	20.8	0	0	1	78.9	Grassland
	17/06/2020	-0.1684327	43.1374603	0.1	0.2	20.8	2	0	0	79.1	Grassland
	17/06/2020	-0.168434	43.1375377	0	1.2	20.8	1	1	0	79	Grassland
	17/06/2020	-0.1684568	43.137183	0	0.6	19.9	2	1	0	79	Grassland
	17/06/2020	-0.1683153	43.1371375	0	0.7	20.6	3	0	0	79.1	Grassland
	17/06/2020	-0.274979	43.131488	0	0.4	20.6	19	1	0	79.4	Grassland
	17/06/2020	-0.275243	43.131462	0	1.2	19.6	24	2	0	79.4	Grassland
	17/06/2020	-0.2751	43.131639	0	0.8	19.6	20	0	0	79.4	Grassland
	17/06/2020	-0.275041	43.13134	0	1	20.2	164	6	0	79.4	Grassland
	17/06/2020	-0.275039	43.131297	0	0.6	19.8	62	2	0	79.4	Grassland
	17/06/2020	-0.274652	43.131318	0	2	18.3	57	2	0	79.4	Grassland
	17/06/2020	-0.3242408	43.1116397	0	1.1	20.3	5	0	0	79.9	Grassland
	17/06/2020	-0.3238962	43.1116088	0	0.1	19.5	2	0	0	79.8	Grassland
	17/06/2020	-0.350998	43.108082	0	0.1	20.2	2	0	0	79.7	Grassland
	17/06/2020	-0.351282	43.1081138	0	1.2	18.7	6	1	0	79.7	Grassland
	17/06/2020	-0.3516793	43.1082883	0	1.3	17.4	7	0	0	79.9	Grassland
	17/06/2020	-0.3517823	43.1081693	0	0.2	19.9	4	0	0	79.7	Grassland
	17/06/2020	-0.3510108	43.1081807	0	2.1	18.4	5	1	0	80	Grassland
	17/06/2020	-0.3967335	43.088725	0.4	0.6	19	11	1	0	80	Grassland
	17/06/2020	-0.3968948	43.0887727	0	0.8	19.6	7	0	0	79.6	Grassland
	17/06/2020	-0.3971612	43.0885787	0	1.4	18.9	6	1	0	79.8	Grassland
	17/06/2020	-0.3974758	43.0886067	0	0.6	19.1	3	0	0	79.3	Grassland
	17/06/2020	-0.422498	43.211217	0	0.6	20.8	25	1	0	79.1	Grassland
	17/06/2020	-0.4223792	43.2110345	0	0.3	20.7	7	1	0	79	Grassland
	17/06/2020	-0.4221492	43.211113	0	0.1	20.8	63	2	0	79.4	Grassland
	17/06/2020	-0.4220678	43.2110465	0	0.8	18.9	43	4	0	79	Grassland
Caubiou (Gan)	17/06/2020	-0.422629	43.2111117	0	0.4	20.7	129	8	0	79.1	Grassland
Mounicq	22/06/2020	-0.813991	43.514026	0	0.1	20.3	1	0	0	79.6	Grassland
Mounicq	22/06/2020	-0.814011	43.513997	0	0.3	20.1	8	0	0	79.6	Grassland
Mounicq	22/06/2020	-0.813992	43.514023	0	0.1	20.2	5	0	0	79.6	Grassland
Mounicq	22/06/2020	-0.814035	43.51399	0	0.5	20	4	0	0	79.6	Grassland
Mounicq	22/06/2020	-0.813942	43.514036	0	0.2	20.2	1	0	0	79.5	Grassland
Mounicq	22/06/2020	-0.8139	43.514049	0	0.1	20.2	8	0	0	79.5	Grassland
Mounicq	22/06/2020	-0.814312	43.513882	0	5.1	18.5	7	1	0	79.5	Grassland
Mounicq	22/06/2020	-0.814352	43.513889	0	2.2	20.2	0	0	0	79	Grassland
Mounicq	22/06/2020	-0.814668	43.513798	0	0.7	19	3	0	0	79.5	Grassland
Mounicq	22/06/2020	-0.814722	43.513795	0	1.5	19.3	0	0	0	79.2	Grassland
Mounicq	22/06/2020	-0.815489	43.51414	0	0.3	19.3	0	0	0	79.4	Grassland
Mounicq	22/06/2020	-0.815467	43.514114	0	0.1	20.6	4	0	0	79.4	Grassland
Mounicq	22/06/2020	-0.81541	43.514573	0	1.6	19.6	1	0	0	79.1	Grassland
Mounicq	22/06/2020	-0.815893	43.513909	0	1	19.7	1	0	0	79.2	Grassland
Mounicq	22/06/2020	-0.815893	43.513909	0	0.1	20.6	2	0	0	79.2	Grassland
Mounicq	22/06/2020	-0.815845	43.513948	0	0.1	20.6	1	0	0	79.2	Grassland
Mounicq	22/06/2020	-0.8147932	43.5138833	0	9.6	9.8	20	3	0	80.3	Grassland
Mounicq	22/06/2020	-0.8146985	43.5139297	0	1.6	18.7	44	23	0	79.8	Grassland
Mounicq	22/06/2020	-0.8140223	43.5140058	0	0.5	20.5	27	2	0	79.2	Grassland
Mounicq	22/06/2020	-0.8139583	43.513992	0	0.4	20.6	25	3	0	79.1	Grassland
Mounicq	22/06/2020	-0.81397	43.5139398	0	0.7	20.5	43	6	0	79.1	Grassland
Col d'Aubisque	23/06/2020	-0.3314065	42.9855167	0	0.5	19.3	6	0	0	80.3	Meadow

Col d'Aubisque	23/06/2020	-0.3312992	42.9855188	0	0.7	19	15	1	0	80.3	Meadow
Col d'Aubisque	23/06/2020	-0.3311102	42.9855005	0	0.8	19.1	14	1	0	80.2	Meadow
Col d'Aubisque	23/06/2020	-0.3308743	42.9854392	0	0.4	19.1	17	1	0	80.5	Meadow
Col d'Aubisque	23/06/2020	-0.3301202	42.9862565	0	0.2	19	0	0	0	80.8	Meadow
Col d'Aubisque	23/06/2020	-0.330007	42.9862497	0	0.2	19	0	0	0	80.8	Meadow
Col d'Aubisque	23/06/2020	-0.3300337	42.9870337	0	4.2	16.1	18	1	0	80.3	Meadow
Col d'Aubisque	23/06/2020	-0.3300568	42.9870158	0	5.5	14.5	24	1	0	80.5	Meadow
Col d'Aubisque	23/06/2020	-0.3303867	42.9873523	0	1.7	17.9	6	1	0	80.2	Meadow
Col d'Aubisque	23/06/2020	-0.330407	42.9874262	0	1.8	18.1	43	3	0	80.5	Meadow
Col d'Aubisque	23/06/2020	-0.3303015	42.9875025	0	2.9	17	23	2	0	80.5	Meadow
Col d'Aubisque	23/06/2020	-0.3302602	42.9867458	0	0.9	18.6	17	2	0	81.8	Meadow
Col d'Aubisque	23/06/2020	-0.3303795	42.9864895	0	1.2	15.1	12	2	0	79.9	Meadow
Col d'Aubisque	23/06/2020	-0.3324132	42.9858352	0	0.3	19	11	1	0	80.1	Meadow
Barrage eaux bonnes	23/06/2020	-0.382173	42.9708527	61.9	0.1	2.9	3	2	0	35.1	Meadow
Barrage eaux bonnes	23/06/2020	-0.3821882	42.9708515	62.2	0.1	2.3	4	1	0	35.5	Meadow
Barrage eaux bonnes	23/06/2020	-0.4057928	42.9740153	0	0	20.3	0	0	0	79.6	Meadow
Barrage eaux bonnes	23/06/2020	-0.4052458	42.9739172	0	0.4	19.9	5	34	0	73.6	Meadow
Barrage eaux bonnes	23/06/2020	-0.4052932	42.9738957	0	0.4	19.6	11	4	0	79.6	Meadow
Col de jaut	24/06/2020	-0.3891853	43.2247428	0	0.1	20.4	0	0	0	79.5	Meadow
Col de jaut	24/06/2020	-0.3891973	43.2247343	0	0.1	20.4	0	0	0	79.6	Meadow
Col de jaut	24/06/2020	-0.339386	43.0370277	0	0.5	20.1	3	1	0	79.8	Meadow
Col de jaut	24/06/2020	-0.3393897	43.036715	0	0.3	19.9	2	1	0	80.3	Meadow
Col de jaut	24/06/2020	-0.3393977	43.0367558	0	0.5	19.5	3	1	0	80.4	Meadow
Col de jaut	24/06/2020	-0.3397915	43.0365232	0	0.1	19.5	0	0	0	80.2	Meadow
Col de jaut	24/06/2020	-0.3397945	43.0364357	0	0	19.6	1	1	0	80.4	Meadow
Col de jaut	24/06/2020	-0.3392862	43.036025	0	0.1	19.6	1	0	0	80.3	Meadow
Col de jaut	24/06/2020	-0.3394853	43.0355605	0	0.3	19.8	12	3	0	79.9	Meadow
Col de jaut	24/06/2020	-0.3366683	43.035912	0	0.1	20	5	1	0	79.6	Meadow
Col de jaut	24/06/2020	-0.3358932	43.0372987	0	0.2	20.5	42	5	0	79.4	Meadow
Col de jaut	24/06/2020	-0.3360022	43.0371123	0	0.1	20.5	4	1	0	79.6	Meadow
Col de jaut	24/06/2020	-0.3358238	43.0369422	0	0.2	20.1	1	0	0	79.7	Meadow
Col de jaut	24/06/2020	-0.3357442	43.0367185	0	0.1	20.2	0	1	0	79.8	Meadow
Col de jaut	24/06/2020	-0.3352825	43.0364007	0	0.2	20.2	14	1	0	79.8	Meadow
Col de jaut	24/06/2020	-0.3351892	43.0361442	0	0.1	20	0	0	0	79.7	Meadow
Col de jaut	24/06/2020	-0.3350595	43.0361437	0	0.1	20.1	0	0	0	79.8	Meadow
Col de jaut	24/06/2020	-0.3350325	43.0356312	0	0.1	20.1	1	1	0	79.8	Meadow
Col de jaut	24/06/2020	-0.3347173	43.0350217	0	0.2	20	2	1	0	79.8	Meadow
Col de jaut	24/06/2020	-0.3432125	43.0357407	0	0	20.3	11	4	0	79.8	Meadow
Col de jaut	24/06/2020	-0.3513557	43.0360637	0	0.4	19.9	2	2	0	79.7	Meadow
Col de jaut	24/06/2020	-0.3654518	43.04735	0	0.1	20.6	2	0	0	79.2	Meadow
Col de jaut	24/06/2020	-0.3644613	43.0464123	0	0.3	20.5	3	1	0	79.4	Meadow
Col de jaut	24/06/2020	-0.3642105	43.0461813	0	0.1	20.6	1	1	0	79.3	Meadow
Col de jaut	24/06/2020	-0.3640315	43.045905	0	0.2	20.6	1	1	0	79.2	Meadow
Col de jaut	24/06/2020	-0.364038	43.045446	0	0.1	20.8	0	0	0	79.1	Meadow
Col de jaut	24/06/2020	-0.3648683	43.0462642	0	0.3	20.7	0	2	0	79	Meadow
Col de jaut	24/06/2020	-0.3653627	43.0465802	0	0.2	20.9	0	2	0	78.9	Meadow
Col de jaut	24/06/2020	-0.3654045	43.0466162	0	0.3	20.7	4	2	0	79	Meadow
Col de jaut	24/06/2020	-0.3652797	43.0466392	0	0.3	20.9	2	1	0	78.8	Meadow
Col de jaut	24/06/2020	-0.3657247	43.0476127	0	0.1	21.1	0	1	0	78.3	Meadow
Col de jaut	24/06/2020	-0.3657883	43.0476217	0	2	19.6	1	0	0	78.4	Meadow
Col de jaut	24/06/2020	-0.3657617	43.0475088	0	1.9	19.7	4	2	0	78.9	Meadow
Col de jaut	24/06/2020	-0.3658627	43.0476513	0	2.6	20.6	5	2	0	77.8	Meadow
Col de jaut	24/06/2020	-0.3668763	43.0526087	0	0.3	21	0	0	0	78.9	Meadow
Sauveterre	25/06/2020	-0.9520922	43.406295	0	0.1	20.4	17	0	0	79.7	Grassland
Sauveterre	25/06/2020	-0.9521858	43.4063655	0	0.8	19.5	161	11	0	79.7	Grassland
Sauveterre	25/06/2020	-0.9521783	43.4065052	0	1.4	19.1	162	3	1	79.8	Grassland
Sauveterre	25/06/2020	-0.9521377	43.406458	0	0.3	19.7	6	1	1	80.1	Grassland
Sauveterre	25/06/2020	-0.9521225	43.4064745	0	1.6	18.8	3	1	1	79.8	Grassland
Sauveterre	25/06/2020	-0.9523353	43.4062347	0	1.3	18.9	102	3	1	79.8	Grassland
Sauveterre	25/06/2020	-0.9524217	43.4061208	0	0.7	19.5	71	2	1	80.1	Grassland
Sauveterre	25/06/2020	-0.9529282	43.4060822	0	0.2	19.7	24	1	0	80	Grassland
Sauveterre	25/06/2020	-0.9528947	43.4058283	0	0.2	19.8	4	0	0	79.9	Grassland
Sauveterre	25/06/2020	-0.9535103	43.4054635	0	0.5	19.8	24	1	0	79.8	Grassland
Sauveterre	25/06/2020	-0.9535352	43.4054753	0	0.2	19.8	31	0	0	79.9	Grassland
Sauveterre	25/06/2020	-0.9539707	43.4052873	0	0.2	19.9	15	1	0	79.8	Grassland
Sauveterre	25/06/2020	-0.953287	43.406069	0	0.1	20.1	60	2	0	79.7	Grassland
Sauveterre	25/06/2020	-0.9529755	43.4061397	0	0.7	19.7	16	1	0	79.7	Grassland

Sauveterre	25/06/2020	-0.952546	43.4064295	0	0.3	20	113	7	0	79	Grassland
Sauveterre	25/06/2020	-0.9523878	43.4063012	0	2.4	18.6	77	7	0	79.4	Grassland
Sauveterre	25/06/2020	-0.9520887	43.4062378	0	0.7	19.9	69	7	0	79.3	Grassland
Sauveterre	25/06/2020	-0.952216	43.4064185	0	2.3	18.8	244	16	0	79.1	Grassland
Sauveterre	25/06/2020	-0.9519558	43.4061882	0	0.8	20.1	126	5	0	79.6	Grassland
Sauveterre	25/06/2020	-0.9519832	43.4060688	0	0.3	19.7	78	3	0	79.8	Grassland
Sauveterre	25/06/2020	-0.9513603	43.4056862	0	2.2	18.8	239	15	1	79.8	Grassland
Sauveterre	25/06/2020	-0.950819	43.4057462	0	0.4	19.8	15	4	0	79.8	Grassland
Sauveterre	25/06/2020	-0.9473397	43.4062242	0	0.1	20.3	37	5	0	79.4	Grassland
Sauveterre	25/06/2020	-0.9476132	43.405744	0	0.1	20.5	123	2	0	79.3	Grassland
Sauveterre	25/06/2020	-0.9474778	43.4057787	0	0	20.7	140	2	0	79.3	Grassland
Sauveterre	25/06/2020	-0.9477565	43.4050293	0	0	20.7	96	2	0	79.2	Grassland
Sauveterre	25/06/2020	-0.9478438	43.4049567	0	0	20.7	136	2	0	79.1	Grassland
Sauveterre	25/06/2020	-0.9475672	43.4050935	0	0.1	20.8	22	1	0	79.1	Grassland
Sauveterre	25/06/2020	-0.9477357	43.4048065	0	0.1	20.6	28	2	0	79.2	Grassland
Sauveterre	25/06/2020	-0.9484418	43.404909	0	0	20.7	24	7	0	79.3	Grassland
Sauveterre	25/06/2020	-0.9484315	43.4049743	0	2.9	19	53	5	0	79.1	Grassland
Sauveterre	25/06/2020	-0.9485057	43.4050042	0	0.2	20.2	179	11	0	79.1	Grassland
Sauveterre	25/06/2020	-0.948584	43.4050827	0	0.5	20.4	140	13	0	79.1	Grassland
Sauveterre	25/06/2020	-0.9484705	43.4050778	0	10.3	13.7	63	4	0	79.1	Grassland
Sauveterre	25/06/2020	-0.9484563	43.4052608	0	1.1	19.8	63	7	0	79.2	Grassland
Sauveterre	25/06/2020	-0.9497502	43.4049063	0	1.3	20.1	50	2	0	79	Grassland
Sauveterre	25/06/2020	-0.9500558	43.4048073	0	1.2	20.8	98	6	0	79	Grassland
Sauveterre	25/06/2020	-0.949978	43.404701	0	1.8	19.8	40	4	0	79	Grassland
Sauveterre	25/06/2020	-0.9500803	43.4050028	0	3.2	20.8	80	5	0	78.1	Grassland
Sauveterre	25/06/2020	-0.950135	43.4051152	0	3.8	18.6	46	5	0	78.2	Grassland
Sauveterre	25/06/2020	-0.9186425	43.4601945	0	1.4	20.4	9	1	0	79.5	Grassland
Salies	25/06/2020	-0.9185095	43.4600637	0	2.1	19.4	58	4	0	79.6	Grassland
Salies	25/06/2020	-0.9184705	43.4599923	0	3.7	20	127	6	0	79.6	Grassland
Salies	25/06/2020	-0.9183578	43.4598017	0	0.1	18.9	10	1	0	79.7	Grassland
Salies	25/06/2020	-0.918518	43.45982	0	0.3	19.9	35	3	0	79.7	Grassland
Salies	25/06/2020	-0.9199343	43.461049	0	2.1	20.1	28	3	0	79.5	Grassland
Salies	25/06/2020	-0.9198873	43.4609913	0	0.4	18.4	52	2	0	79.6	Grassland
Salies	25/06/2020	-0.9200742	43.4614787	0	1	20.3	47	4	0	79.5	Grassland
Salies	25/06/2020	-0.9199088	43.4615705	0	0.2	19.6	112	5	0	79.5	Grassland
Salies	25/06/2020	-0.9096175	43.4418002	0	0.6	20.5	0	0	0	79.1	Grassland
Salies	25/06/2020	-0.9093172	43.441686	0	0.3	20.2	0	0	0	79.1	Grassland
Salies	25/06/2020	-0.9093002	43.4416507	0	0.3	20.8	1	3	0	79.2	Grassland
Salies	25/06/2020	-0.9088832	43.441461	0	0.9	20.6	5	5	0	79.3	Grassland
Peyroraide	30/06/2020	-1.1110078	43.5322783	0	2.5	20.8	16	0	0	78.9	Grassland
Peyroraide	30/06/2020	-1.1113287	43.532243	0	6	16.9	33	1	0	79.1	Grassland
Peyroraide	30/06/2020	-1.1111785	43.5320515	0	0.6	19.4	3	1	0	79.3	Grassland
Peyroraide	30/06/2020	-1.110923	43.5321095	0	0.5	20.2	21	1	0	79.3	Grassland
Peyroraide	30/06/2020	-1.1105643	43.5317287	0	0.3	20.4	49	13	0	78.2	Grassland
Peyroraide	30/06/2020	-1.110602	43.5317122	0	8.4	14.9	62	5	0	78.2	Grassland
La Bourgade	30/06/2020	-1.1872112	43.519447	2.2	2.3	17.1	5	1	0	79	Forest
La Bourgade	30/06/2020	-1.1868265	43.51985	0	0.5	18.9	0	0	0	79.2	Forest
La Bourgade	30/06/2020	-1.18639	43.5197185	0	3.1	20.5	10	1	0	78.8	Forest
La Bourgade	30/06/2020	-1.1861458	43.5196368	0	2.7	18.7	11	2	0	79	Forest
La Bourgade	30/06/2020	-1.1857685	43.5190767	0	1.5	20	13	6	0	79	Forest
Sud Bardos	30/06/2020	-1.1929778	43.4454512	0	0.4	20.8	13	1	0	79	Grassland
Sud Bardos	30/06/2020	-1.1927538	43.445497	0	0.3	20	3	0	0	79.2	Grassland
Sud Bardos	30/06/2020	-1.192511	43.4455457	0	0.4	20.6	56	6	0	79.4	Grassland
Sud Bardos	30/06/2020	-1.1920682	43.4455953	0	2.4	20.3	85	1	0	79.1	Grassland
Sud Bardos	30/06/2020	-1.1918822	43.4457232	0	1.1	19.7	11	1	0	79.2	Grassland
Isturitz	30/06/2020	-1.2023857	43.3583435	0	0.4	20.4	6	1	0	79.2	Grassland
Isturitz	30/06/2020	-1.2024238	43.3583735	0	1.2	20.4	23	3	0	79.4	Grassland
Isturitz	30/06/2020	-1.2023182	43.358348	0	0.9	19.6	43	3	0	79.3	Grassland
Isturitz	30/06/2020	-1.2020327	43.3584147	0	0.2	20	8	0	0	79.4	Grassland
Isturitz	30/06/2020	-1.2018648	43.3583502	0	2.2	19	2	1	0	79.1	Grassland
Iholdy	30/06/2020	-1.197437	43.267639	0	0.2	20.4	2	1	0	79.4	Grassland
Iholdy	30/06/2020	-1.197617	43.2674747	0	0.5	20	0	0	0	79.4	Grassland
Iholdy	30/06/2020	-1.1971837	43.2676587	0	0.9	19.8	0	1	0	79.5	Grassland
Iholdy	30/06/2020	-1.1969072	43.267653	0	2.5	19	2	1	0	79.1	Grassland
Iholdy	30/06/2020	-1.1968197	43.267733	0	1.3	19.4	3	2	0	79.4	Grassland
Bois d'Ostabat	30/06/2020	-1.0636998	43.2823257	0	3.1	20.6	9	1	0	79.1	Meadow
Bois d'Ostabat	30/06/2020	-1.0637965	43.2822602	0	0.9	19.5	4	2	0	79.5	Meadow

Bois d'Ostabat	30/06/2020	-1.0640533	43.2816455	0	0.4	20.3	2	1	0	79.6	Meadow
Bois d'Ostabat	30/06/2020	-1.0640897	43.2816602	0	0.3	20.3	1	2	0	79.6	Meadow
Bois d'Ostabat	30/06/2020	-1.063956	43.2814052	0	0.2	20.2	0	1	0	79.6	Meadow
Gabat	30/06/2020	-1.0727082	43.3735083	0	0.2	20.6	0	0	0	79.4	Grassland
Gabat	30/06/2020	-1.0725687	43.3732838	0	0.4	20.4	1	1	0	79.4	Grassland
Gabat	30/06/2020	-1.0725618	43.373425	0	0.9	20.4	4	1	0	79.5	Grassland
Gabat	30/06/2020	-1.0725313	43.3733603	0	3.4	20.3	3	2	0	79.4	Grassland
Gabat	30/06/2020	-1.0723843	43.3732188	0	0.4	20.1	1	1	0	79.8	Grassland
Arancour	30/06/2020	-1.0723475	43.3730985	0	0.2	17.4	4	3	0	79.7	Grassland
Arancour	30/06/2020	-1.0562008	43.4457292	0	0.6	20.5	7	1	0	79.5	Grassland
Arancour	30/06/2020	-1.0562312	43.4456137	0	0.1	20.3	25	4	0	79.6	Grassland
Arancour	30/06/2020	-1.0562222	43.4456773	0	3.4	17.3	33	5	0	79.2	Grassland
Arancour	30/06/2020	-1.0561183	43.4456302	0	0.6	18.3	22	5	0	79.7	Grassland
Arancour	30/06/2020	-1.0562003	43.4455257	0	0.3	20	19	3	0	79.9	Grassland
Pouillot	30/06/2020	-0.9448968	43.5461978	0	1.8	19.2	7	2	0	79.3	Grassland
Pouillot	30/06/2020	-0.944911	43.5462223	0	0.3	19.8	18	1	0	79.5	Grassland
Pouillot	30/06/2020	-0.9446598	43.546087	0	0.3	20.2	25	2	0	79.5	Grassland
Pouillot	30/06/2020	-0.944765	43.5461423	0	0.2	20.3	13	1	0	79.5	Grassland
Pouillot	30/06/2020	-0.9448292	43.5462638	0	0.1	20.4	9	0	0	79.6	Grassland
Salies de Bearn	25/06/2020	-0.9185095	43.4600637	0	2.1	19.4	58	4	0	79.6	Grassland
Salies de Bearn	25/06/2020	-0.9184705	43.4599923	0	3.7	20	127	6	0	79.6	Grassland
Salies de Bearn	25/06/2020	-0.9183578	43.4598017	0	0.1	18.9	10	1	0	79.7	Grassland
Salies de Bearn	25/06/2020	-0.918518	43.45982	0	0.3	19.9	35	3	0	79.7	Grassland
Salies de Bearn	25/06/2020	-0.9199343	43.461049	0	2.1	18.4	28	3	0	79.5	Grassland
Saint Laurent Bretagne	03/07/2020	-0.196688	43.382039	0	0.4		2	0	0	79.2	Grassland
Saint Laurent Bretagne	03/07/2020	-0.1968628	43.3822223	0	0.3	20.5	0	0	0	79.2	Grassland
Saint Laurent Bretagne	03/07/2020	-0.196851	43.3823007	0	0.2	20.6	0	0	0	79.2	Grassland
Saint Laurent Bretagne	03/07/2020	-0.1970817	43.382455	0	0.9	20.6	2	2	0	79.1	Grassland
Saint Laurent Bretagne	03/07/2020	-0.1972187	43.3823552	0	0.4	19.7	10	1	0	79.2	Grassland
Lannecaube	03/07/2020	-0.2106413	43.482156	0	4.2	20.9	47	8	0	78.2	Grassland
Lannecaube	03/07/2020	-0.2107055	43.4823757	0	0.9	17.7	17	1	0	79.3	Grassland
Lannecaube	03/07/2020	-0.2110172	43.4826915	0	0.7	20.1	20	3	0	79.4	Grassland
Lannecaube	03/07/2020	-0.2112873	43.4825608	0	1.2	20.1	8	1	0	79.6	Grassland
Lannecaube	03/07/2020	-0.2111628	43.4826923	0	0.5	20	37	2	0	79.6	Grassland
Castetpugon	03/07/2020	-0.221285	43.56341	0	0.1	20.8	0	1	0	79.1	Grassland
Castetpugon	03/07/2020	-0.221293	43.563205	0	0.1	20.8	1	2	0	79.1	Grassland
Castetpugon	03/07/2020	-0.221096	43.5635	0	0.1	20.8	9	2	0	79.1	Grassland
Castetpugon	03/07/2020	-0.220018	43.563712	0	0.1	20.8	13	3	0	78.9	Grassland
Castetpugon	03/07/2020	-0.220687	43.563496	0	0.7	20.6	5	1	0	78.8	Grassland
Sensacq	03/07/2020	-0.3498228	43.581888	0	1.5	21.1	25	2	0	78.7	Grassland
Sensacq	03/07/2020	-0.3496455	43.5818815	0.2	0.6	20.8	29	3	0	79	Grassland
Sensacq	03/07/2020	-0.349664	43.5819003	0.2	1.7	20.8	52	5	0	78.8	Grassland
Sensacq	03/07/2020	-0.3496043	43.5817715	0	0.9	19.7	16	3	0	79	Grassland
Sensacq	03/07/2020	-0.3493813	43.5818272	0.5	1.9	20.7	7	2	0	79	Grassland
Méracq	03/07/2020	-0.3937743	43.5127292	0	1.9	21	9	2	0	78.7	Grassland
Méracq	03/07/2020	-0.3936115	43.5126915	0	0.4	20.1	7	2	0	79	Grassland
Méracq	03/07/2020	-0.3937737	43.5127433	0	0.6	20.7	13	2	0	79	Grassland
Méracq	03/07/2020	-0.3938117	43.5127513	0	0.3	20.8	13	3	0	79.1	Grassland
Méracq	03/07/2020	-0.3939523	43.5127779	0	0.1	20.8	1	0	0	79	Grassland
Navailles-Angos	03/07/2020	-0.3460903	43.4048048	0	0.1	20.8	20	2	0	79.2	Grassland
Navailles-Angos	03/07/2020	-0.3459295	43.4049242	0	0.1	20.6	4	1	0	79.3	Grassland
Navailles-Angos	03/07/2020	-0.3458833	43.4051278	0	0.1	20.6	3	1	0	79.4	Grassland
Navailles-Angos	03/07/2020	-0.3458775	43.4051463	0	0.1	20.5	2	0	0	79.3	Grassland
Navailles-Angos	03/07/2020	-0.34561	43.4052283	0	0.1	20.5	0	1	0	79.4	Grassland
Uzein	03/07/2020	-0.4413152	43.3963883	0	0.3	20.8	1	1	0	79.1	Grassland
Uzein	03/07/2020	-0.4411737	43.3964923	0	0.3	20.6	1	0	0	79.1	Grassland
Uzein	03/07/2020	-0.4411445	43.3965125	0	0.8	20.7	2	0	0	79.2	Grassland
Uzein	03/07/2020	-0.441101	43.3967053	0	0.9	20.5	3	1	0	79.1	Grassland
Uzein	03/07/2020	-0.4407933	43.3967993	0	1.2	20.4	12	1	0	79.2	Grassland
Esterencuby	07/07/2020	-1.186444	43.10543	0	1.7	21.4	102	2	0	78.6	Meadow
Esterencuby	07/07/2020	-1.1865923	43.1050473	0	0.6	21.2	22	2	0	78.5	Meadow
Esterencuby	07/07/2020	-1.186745	43.1050828	0	1.9	21	44	1	0	78.4	Meadow
Esterencuby	07/07/2020	-1.1869062	43.1051638	0	0.8	20.6	0	0	0	78.3	Meadow
Esterencuby	07/07/2020	-1.1873122	43.1053518	0	1.1	20.8	20	1	0	78.5	Meadow
Errozate	07/07/2020	-1.1512307	43.0421115	0.1	1.3	20.7	23	0	0	78.2	Meadow
Errozate	07/07/2020	-1.151153	43.0420832	0	0.5	21.5	22	1	0	78.1	Meadow
Errozate	07/07/2020	-1.1509862	43.042063	0	0	21.5	7	0	0	78	Meadow

Errozate	07/07/2020	-1.1508618	43.0420977	0	1	21.8	20	0	0	77.9	Meadow
Errozate	07/07/2020	-1.1510965	43.0422695	0.3	3.8	21.4	757	2	1	79.2	Meadow
Zazpigain	07/07/2020	-1.0381133	43.010437	0	1.5	21.4	21	1	0	78.1	Meadow
Zazpigain	07/07/2020	-1.0380397	43.0103353	0	2.2	21	23	1	0	78.2	Meadow
Zazpigain	07/07/2020	-1.0379608	43.0103772	0	3.2	21	24	2	0	78	Meadow
Zazpigain	07/07/2020	-1.0377065	43.0103283	0	2.2	20.4	29	1	0	78.1	Meadow
Zazpigain	07/07/2020	-1.0379102	43.0103827	0	1.8	20.7	36	1	0	78.1	Meadow
Pic d'Apanice	07/07/2020	-1.0606428	43.1007105	0	0	21.2	0	2	0	78.7	Meadow
Pic d'Apanice	07/07/2020	-1.0605382	43.1008053	0	0.1	21.1	0	0	1	78.7	Meadow
Pic d'Apanice	07/07/2020	-1.0605448	43.1009075	0	0	21.2	0	1	1	78.7	Meadow
Pic d'Apanice	07/07/2020	-1.0603988	43.100888	0	0.1	19.6	0	1	1	78.8	Meadow
Pic d'Apanice	07/07/2020	-1.0605342	43.1010298	0	0.2	21.2	0	2	1	78.7	Meadow
Alcay	07/07/2020	-0.9151655	43.0955535	0	0.6	21.1	0	0	1	78.7	Meadow
Alcay	07/07/2020	-0.9150953	43.095646	0	0.5	20.9	0	0	1	79	Meadow
Alcay	07/07/2020	-0.9149188	43.095548	0	2.9	20.6	18	1	1	79.2	Meadow
Alcay	07/07/2020	-0.9147098	43.0958222	0	0.9	20.3	8	0	1	79.3	Meadow
Alcay	07/07/2020	-0.9145617	43.0957707	0	2.9	20.5	0	0	1	79.4	Meadow
Logibaria	07/07/2020	-0.9260017	43.0201807	0	0.7	21.1	0	1	1	78.9	Meadow
Logibaria	07/07/2020	-0.9260115	43.0201342	0	0.9	20.4	7	1	1	78.8	Meadow
Logibaria	07/07/2020	-0.9261505	43.0200582	0	0.1	21	0	0	1	78.9	Meadow
Logibaria	07/07/2020	-0.9259948	43.0199327	0	0.3	20.9	11	0	1	78.9	Meadow
Logibaria	07/07/2020	-0.9260442	43.0198845	0	0.4	20.8	21	1	1	78.9	Meadow
Pic d'issarbe	07/07/2020	-0.795446	43.0182895	0	2.8	21.1	56	10	1	78.7	Meadow
Pic d'issarbe	07/07/2020	-0.7954132	43.0182295	0	0.2	20.7	50	0	1	78.5	Meadow
Pic d'issarbe	07/07/2020	-0.7954387	43.0181163	0	2.3	21.4	90	2	1	78.3	Meadow
Pic d'issarbe	07/07/2020	-0.7952148	43.0180052	0	1.6	21.2	52	0	1	78.5	Meadow
Pic d'issarbe	07/07/2020	-0.7951137	43.0178907	0	2.9	20.5	80	2	1	78.6	Meadow
Montorry	07/07/2020	-0.8203107	43.096771	0	0.3	21.4	0	0	1	78.4	Grassland
Montorry	07/07/2020	-0.8203222	43.0968048	0	0	21.2	0	0	1	78.7	Grassland
Montorry	07/07/2020	-0.8203387	43.096962	0	1.1	21.1	0	0	1	78.8	Grassland
Montorry	07/07/2020		43.0969963	0	0.1	20.9	0	0	1	78.8	Grassland
Montorry	07/07/2020	-0.8201883	43.0968983	0	1.1	21.1	0	0	1	78.7	Grassland
Arette	07/07/2020	-0.70735	43.108289	0	0.1	20.9	0	0	1	78.9	Grassland
Arette	07/07/2020	-0.7073155	43.1083345	0	0	20.9	0	0	1	79	Grassland
Arette	07/07/2020	-0.7074055	43.1082457	0	0.5	20.9	0	0	2	78.8	Grassland
Arette	07/07/2020	-0.7074155	43.108146	0	6.7	20.9	0	0	2	78.7	Grassland
Arette	07/07/2020	-0.7075103	43.1081888	0	0.1	16	0	0	1	79	Grassland
Lourdios Ichère	07/07/2020	-0.6689227	43.0470052	0	0	20.9	0	0	1	79	Meadow
Lourdios Ichère	07/07/2020	-0.6690297	43.0469728	0	0	20.9	0	0	1	78.9	Meadow
Lourdios Ichère	07/07/2020	-0.669014	43.046963	0	0.1	20.9	0	0	1	78.9	Meadow
Lourdios Ichère	07/07/2020	-0.6689962	43.0470198	0	0.1	20.8	0	0	2	78.9	Meadow
Lourdios Ichère	07/07/2020	-0.6689493	43.0470943	0	0.6	20.8	0	0	1	79	Meadow
Bustince Iribéry	08/07/2020	-1.1851082	43.1919467	0	0.1	21.3	7	0	1	78.6	Grassland
Bustince Iribéry	08/07/2020	-1.1850668	43.1920278	0	0.2	21.2	17	1	1	78.6	Grassland
Bustince Iribéry	08/07/2020	-1.185128	43.1919393	0	0	21.1	16	0	1	78.6	Grassland
Bustince Iribéry	08/07/2020	-1.1849463	43.1919885	0	0.1	21.1	14	1	1	78.6	Grassland
Bustince Iribéry	08/07/2020	-1.1849278	43.1919803	0.1	0.4	21.2	29	1	1	78.6	Grassland
Saint Juste Ibarre	08/07/2020	-1.0560507	43.1893288	0	1	21.4	0	0	1	78.3	Grassland
Saint Juste Ibarre	08/07/2020	-1.0561777	43.1891588	0	0.1	20.6	0	1	1	78.8	Grassland
Saint Juste Ibarre	08/07/2020	-1.0561238	43.1891283	0	1.3	20.6	0	1	1	78.7	Grassland
Saint Juste Ibarre	08/07/2020	-1.056144	43.1891835	0	0.1	20.7	0	0	1	78.9	Grassland
Saint Juste Ibarre	08/07/2020	-1.0560793	43.1890845	0	0.1	20.9	0	0	1	78.9	Grassland
Ordiarp	08/07/2020	-0.942392	43.1842272	0	0.9	21	0	0	1	78.9	Grassland
Ordiarp	08/07/2020	-0.9425965	43.1843442	0	0.3	20.7	0	0	1	79	Grassland
Ordiarp	08/07/2020	-0.9424638	43.1844137	0	0.5	20.6	0	0	1	79	Grassland
Ordiarp	08/07/2020	-0.9424373	43.1844495	0	0.9	20.6	9	1	1	79	Grassland
Ordiarp	08/07/2020	-0.9424438	43.1843845	0	0.5	20.6	17	0	1	79	Grassland
Barcus	08/07/2020	-0.786773	43.1888432	0	0.5	21	22	2	1	78.9	Grassland
Barcus	08/07/2020	-0.78683	43.1888657	0	0.4	20.8	19	5	1	78.9	Grassland
Barcus	08/07/2020	-0.786783	43.1887922	0	0.3	20.6	27	4	1	79	Grassland
Barcus	08/07/2020	-0.786666	43.188861	0	1.6	20.4	43	5	1	79.3	Grassland
Barcus	08/07/2020	-0.7865522	43.1888778	0	0.2	20.4	3	0	1	78.9	Grassland
Esquiule	08/07/2020	-0.7047513	43.194978	0	0.2	21.1	0	0	1	78.8	Grassland
Esquiule	08/07/2020	-0.7048108	43.1950685	0	0.2	20.8	0	0	1	78.7	Grassland
Esquiule	08/07/2020	-0.7049313	43.1949078	0	0.7	21.1	0	0	1	78.5	Grassland
Esquiule	08/07/2020	-0.7049657	43.194932	0	0.2	20.7	0	0	1	78.7	Grassland
Esquiule	08/07/2020	-0.704992	43.1948027	0	0.5	20.9	0	0	1	78.6	Grassland

Lamidou	08/07/2020	-0.716618	43.2856242	0.1	1.5	20.2	50	1	1	78.6	Grassland
Lamidou	08/07/2020	-0.7167892	43.285512	0	0.4	20.8	0	0	1	78.9	Grassland
Lamidou	08/07/2020	-0.7170097	43.285714	0	0.4	20.4	5	0	1	79.1	Grassland
Lamidou	08/07/2020	-0.7169382	43.2854897	0	1.7	20.7	10	2	1	79.1	Grassland
Lamidou	08/07/2020	-0.7169202	43.2855413	0	0.5	20.3	11	0	1	79.1	Grassland
Moncayolle	08/07/2020	-0.8433655	43.2643478	0	1.6	20.9	0	0	1	79.1	Grassland
Moncayolle	08/07/2020	-0.843489	43.2642078	0	1.2	20.4	0	0	1	79.2	Grassland
Moncayolle	08/07/2020	-0.843462	43.2641115	0	0.1	20.8	0	1	1	79	Grassland
Moncayolle	08/07/2020	-0.8433647	43.2641637	0	0.1	20.8	0	0	2	79.1	Grassland
Moncayolle	08/07/2020	-0.8433527	43.2640985	0	0.1	20.9	0	1	2	79.1	Grassland
Ainharp	08/07/2020	-0.927217	43.268141	0	0.8	20.6	0	0	1	79	Grassland
Ainharp	08/07/2020	-0.9271743	43.2680478	0	1.5	19.5	0	0	2	79.4	Grassland
Ainharp	08/07/2020	-0.9273727	43.2680798	0	0.7	20	0	0	2	79.3	Grassland
Ainharp	08/07/2020	-0.927421	43.2679237	0	0.2	20.4	0	0	1	79.4	Grassland
Ainharp	08/07/2020	-0.9272805	43.2679278	0	0.3	20.2	0	0	2	79.5	Grassland
Osserain	08/07/2020	-0.9603708	43.3777653	0	0	20.7	0	0	1	79.3	Grassland
Osserain	08/07/2020	-0.9605305	43.3777913	0	0	20.5	0	0	2	79.3	Grassland
Osserain	08/07/2020	-0.9603815	43.3776778	0	0.3	20.4	0	0	2	79.2	Grassland
Osserain	08/07/2020	-0.9605468	43.3776765	0	0.2	20.3	0	0	2	79.3	Grassland
Osserain	08/07/2020	-0.9606743	43.3776078	0	1.4	19.3	3	1	2	79.3	Grassland
Laas	08/07/2020	-0.8469535	43.3797703	0	0.9	20.1	21	0	2	79.2	Grassland
Laas	08/07/2020	-0.8468893	43.3797992	0	0.2	20.5	7	0	1	79.1	Grassland
Laas	08/07/2020	-0.8470072	43.3798455	0	0.2	20.5	7	0	1	79.1	Grassland
Laas	08/07/2020	-0.8470685	43.3798265	0	0	20.8	0	0	1	79	Grassland
Laas	08/07/2020	-0.8471782	43.3798552	0	0.1	20.5	2	0	2	79.2	Grassland
Laneplaa	09/07/2020	-0.8237082	43.4606745	0	3.2	21.4	15	1	1	78.1	Grassland
Laneplaa	09/07/2020	-0.8236125	43.4607163	0	0.1	19.6	22	0	1	78.7	Grassland
Laneplaa	09/07/2020	-0.8234998	43.4607182	0	0.5	20.6	97	2	1	78.7	Grassland
Laneplaa	09/07/2020	-0.8234677	43.4607868	0	0.1	21.1	0	0	1	78.7	Grassland
Laneplaa	09/07/2020	-0.8234995	43.4607725	0	0.1	21	95	0	1	78.8	Grassland
Hourquebie	09/07/2020	-0.8419558	43.5343427	0	0.6	20.7	0	4	1	78.5	Grassland
Hourquebie	09/07/2020	-0.8420748	43.5343442	0	0.2	20.7	3	2	1	78.7	Grassland
Hourquebie	09/07/2020	-0.841934	43.534342	0	0.5	20.8	0	0	1	78.6	Grassland
Hourquebie	09/07/2020	-0.8413635	43.5340672	0	1.3	20.8	0	0	1	78.6	Grassland
Hourquebie	09/07/2020	-0.8413937	43.5342613	0	0.5	20.9	0	0	1	78.7	Grassland
Pibole	09/07/2020	-0.7324702	43.550446	0	0	21.3	0	3	1	78.6	Grassland
Pibole	09/07/2020	-0.7325418	43.5503357	0	0	21.3	8	1	1	78.7	Grassland
Pibole	09/07/2020	-0.732416	43.55032	0	0.7	20.7	5	0	1	78.8	Grassland
Pibole	09/07/2020	-0.7325057	43.5503698	0	0	21.1	7	2	1	78.8	Grassland
Pibole	09/07/2020	-0.7325305	43.5504167	0	0	21.1	1	0	1	78.8	Grassland
Biron	09/07/2020	-0.7488428	43.4642157	0	0	21.1	0	0	1	78.9	Grassland
Biron	09/07/2020	-0.7489237	43.4641007	0	0	21	0	0	1	79	Grassland
Biron	09/07/2020	-0.7488008	43.4642248	0	0	20.9	0	1	1	79.1	Grassland
Biron	09/07/2020	-0.7488147	43.4642887	0	0	20.8	0	0	1	79.1	Grassland
Biron	09/07/2020	-0.7485837	43.4644183	0	0	20.7	0	0	1	79.2	Grassland
Sauvelade	09/07/2020	-0.705163	43.3962125	0	1.6	20.9	10	2	1	78.7	Grassland
Sauvelade	09/07/2020	-0.7052283	43.396039	0	1.6	20.6	3	3	1	78.6	Grassland
Sauvelade	09/07/2020	-0.705286	43.395915	0	0.4	20.3	6	4	1	78.9	Grassland
Sauvelade	09/07/2020	-0.7049287	43.3961467	0	3.7	20.7	0	0	1	78.5	Grassland
Sauvelade	09/07/2020	-0.7049072	43.39601	0	2.2	18.3	0	3	1	79.1	Grassland
Abidos	09/07/2020	-0.6056157	43.3950678	0	0.5	20.8	0	1	1	78.9	Grassland
Abidos	09/07/2020	-0.605545	43.3949777	0	9	21	0	0	1	79	Grassland
Abidos	09/07/2020	-0.6056177	43.3948862	0	0.6	21	0	0	1	78.7	Grassland
Abidos	09/07/2020	-0.6054488	43.3949517	0	0.1	20.6	0	1	1	79.1	Grassland
Abidos	09/07/2020	-0.6054287	43.3948967	0	0.1	20.8	0	0	1	79.1	Grassland
Arthez de Bearn	09/07/2020	-0.597732	43.4636332	0	1	20.9	14	0	0	78.9	Grassland
Arthez de Bearn	09/07/2020	-0.597897	43.46366	0	0.5	20.9	28	1	1	79	Grassland
Arthez de Bearn	09/07/2020	-0.5978707	43.4637567	0	2	21	32	2	1	78.8	Grassland
Arthez de Bearn	09/07/2020	-0.5980078	43.46356	0	1.1	20.5	22	0	2	79.1	Grassland
Arthez de Bearn	09/07/2020	-0.598034	43.4634362	0	0.3	20.8	27	1	2	79	Grassland
Castlener	09/07/2020	-0.577049	43.5468982	0	0	21.1	4	0	2	78.9	Grassland
Castlener	09/07/2020	-0.5767332	43.5468945	0	0	21	0	0	2	78.8	Grassland
Castlener	09/07/2020	-0.576904	43.5468503	0	0	21	0	0	2	79.1	Grassland
Castlener	09/07/2020	-0.5769538	43.5467868	0	0.6	20.7	0	1	1	79	Grassland
Castlener	09/07/2020	-0.5769292	43.5468853	0	0.3	20.6	7	2	1	78.9	Grassland
Philondenx	09/07/2020	-0.44067	43.564424	0	0.8	20.7	0	1	1	79	Grassland
Philondenx	09/07/2020	-0.440689	43.5644567	0	0.6	20.6	0	2	1	79.1	Grassland

Philondenx	09/07/2020	-0.4405407	43.5645893	0	0.7	20.6	6	3	1	79.1	Grassland
Philondenx	09/07/2020	-0.4405942	43.5646397	0	1.7	19.9	7	3	1	79.3	Grassland
Philondenx	09/07/2020	-0.4406463	43.5645373	0	1	20.5	9	3	1	79.2	Grassland
Momas	09/07/2020	-0.4497342	43.4506322	1.1	3.6	18.5	50	4	2	78.8	Grassland
Momas	09/07/2020	-0.4497613	43.4505695	0	5.4	20.5	29	4	2	79.2	Grassland
Momas	09/07/2020	-0.449645	43.4504837	0	2.5	19.6	34	4	2	79	Grassland
Momas	09/07/2020	-0.4497067	43.4505138	0	0.2	19.7	5	0	2	78.9	Grassland
Momas	09/07/2020	-0.4496625	43.4504768	0	0.8	20.9	0	1	1	79	Grassland
Mifaget	16/07/2020	-0.3079433	43.1104982	0	0.3	20.6	0	0	0	79.2	Grassland
Mifaget	16/07/2020	-0.3079528	43.1104522	0	0.1	20.6	0	0	0	79.3	Grassland
Mifaget	16/07/2020	-0.3079753	43.1103947	0	0.1	20.6	0	1	0	79.3	Grassland
Mifaget	16/07/2020	-0.3079797	43.1103518	0	0.1	20.6	0	0	0	79.3	Grassland
Mifaget	16/07/2020	-0.3080518	43.1102753	0	0.3	15.9	2	0	0	79.3	Grassland
Montaut	16/07/2020	-0.191059	43.119682	0	0.5	20.4	0	0	0	79.2	Forest
Montaut	16/07/2020	-0.190968	43.119638	0	3.1	18.8	2	1	0	78.9	Forest
Montaut	16/07/2020	-0.1910827	43.119651	0	1.6	19.4	15	0	0	79.2	Forest
Montaut	16/07/2020	-0.1910897	43.119648	0	0.7	20.4	4	0	0	79.2	Forest
Montaut	16/07/2020	-0.1912137	43.1195893	0	2.3	19.7	2	2	0	79.1	Forest
Soum de las Escures	16/07/2020	-0.1720875	43.0229472	0	0.4	20.5	3	0	0	79.4	Forest
Soum de las Escures	16/07/2020	-0.1718538	43.0228075	0	0.3	20.3	3	1	0	79.4	Meadow
Soum de las Escures	16/07/2020	-0.1717842	43.0228087	0	0.9	20.1	6	0	0	79.3	Meadow
Soum de las Escures	16/07/2020	-0.1716142	43.0228122	0	0.3	20.4	4	1	0	79.4	Meadow
Soum de las Escures	16/07/2020	-0.1715298	43.0229227	0	0.3	20.4	0	0	0	79.3	Meadow
Agos Vidalos	16/07/2020	-0.0679817	43.0386507	0	1.5	19.9	0	1	0	78.8	Grassland
Agos Vidalos	16/07/2020	-0.0680287	43.0386297	0	1.5	20	4	0	0	79	Grassland
Agos Vidalos	16/07/2020	-0.0679295	43.0386697	0	1.2	20	4	1	0	79.3	Grassland
Agos Vidalos	16/07/2020	-0.0678297	43.0388415	0	1.3	19.9	2	1	0	78.9	Grassland
Agos Vidalos	16/07/2020	-0.0678745	43.0389642	0	1.7	19.6	2	0	0	78.9	Grassland
Germs-sur-l'oussouet	16/07/2020	0.0547172	43.0546203	0	0.6	20.3	1	0	0	79.2	Meadow
Germs-sur-l'oussouet	16/07/2020	0.0549063	43.0546337	0	4.7	17.4	1	1	0	80.7	Meadow
Germs-sur-l'oussouet	16/07/2020	0.0548062	43.0546612	0	6.8	14.8	4	0	0	79.2	Meadow
Germs-sur-l'oussouet	16/07/2020	0.0547015	43.0546057	0	4.9	20.4	1	0	0	79.1	Meadow
Germs-sur-l'oussouet	16/07/2020	0.0547975	43.054637	0	1.8	18.9	1	0	0	79.4	Meadow
Orincles	16/07/2020	0.0411485	43.1223628	0	0.3	20.5	2	0	0	79.3	Grassland
Orincles	16/07/2020	0.0411733	43.1222295	0	1.4	19.8	15	1	0	79.6	Grassland
Orincles	16/07/2020	0.0410952	43.1220618	0	1.9	19.6	8	1	0	79.6	Grassland
Orincles	16/07/2020	0.0411063	43.1220938	0	1.9	19.5	8	1	0	79.4	Grassland
Orincles	16/07/2020	0.0411383	43.1224583	0	1.1	19.7	5	0	0	79.6	Grassland
Juillian	16/07/2020	0.0179692	43.2050957	0	0.5	20.2	4	1	0	79.4	Grassland
Juillian	16/07/2020	0.0179888	43.2051602	0	0.4	20.2	4	0	0	79.4	Grassland
Juillian	16/07/2020	0.0179372	43.2051828	0	0.5	20.3	2	0	0	79.4	Grassland
Juillian	16/07/2020	0.017816	43.2051542	0	0.9	19.8	2	1	0	79.4	Grassland
Juillian	16/07/2020	0.017756	43.2052563	0	0.5	19.8	2	0	0	79.5	Grassland
Pontacq	16/07/2020	-0.0916387	43.1938932	0	0.1	20.4	1	0	0	79.4	Grassland
Pontacq	16/07/2020	-0.0918295	43.193722	0	1	20	42	3	0	79.4	Grassland
Pontacq	16/07/2020	-0.091808	43.1935247	0	0.2	20.3	1	0	0	79.5	Grassland
Pontacq	16/07/2020	-0.091647	43.1935458	0	2.4	19.5	2	1	0	79.6	Grassland
Pontacq	16/07/2020	-0.0917788	43.1935427	0	1.3	20.4	11	2	0	79.6	Grassland
Loubajac	16/07/2020	-0.070349	43.1354765	0	0.2	20.5	3	1	0	79.3	Grassland
Loubajac	16/07/2020	-0.0703357	43.1354148	0	0.3	20.5	16	2	0	79.3	Grassland
Loubajac	16/07/2020	-0.0703358	43.13548	0	1.5	20.6	28	3	0	79.2	Grassland
Loubajac	16/07/2020	-0.0702738	43.135329	0	1.9	19.8	19	2	0	79.1	Grassland
Loubajac	16/07/2020	-0.0702692	43.135459	0	4	19	43	3	0	79.2	Grassland
Bénéjac	16/07/2020	-0.19699	43.199649	0	0.6	20.3	7	1	0	79.3	Grassland
Bénéjac	16/07/2020	-0.197034	43.19965	0	0.9	20.3	9	1	0	79.2	Grassland
Bénéjac	16/07/2020	-0.196885	43.199721	0	0.8	20.3	8	1	0	79.1	Grassland
Bénéjac	16/07/2020	-0.196624	43.199563	0	0.5	20.3	1	0	0	79.2	Grassland
Bénéjac	16/07/2020	-0.196718	43.199592	0	0.2	20.6	3	0	0	79.2	Grassland
Lesquerre	16/07/2020	-0.3421668	43.193199	0	0.9	20.3	3	0	0	79	Grassland
Lesquerre	16/07/2020	-0.3420142	43.193045	0	0.4	20.6	0	0	0	79.1	Grassland
Lesquerre	16/07/2020	-0.3419785	43.1930263	0	0.7	20.4	19	0	0	79.1	Grassland
Lesquerre	16/07/2020	-0.3420807	43.1930437	0	0.3	20.5	34	13	0	79.2	Grassland
Lesquerre	16/07/2020	-0.3418658	43.1931167	0	0.3	20.7	4	1	0	79.2	Grassland
Limendous	17/07/2020	-0.184942	43.2732077	0	1.8	20.7	8	0	0	79	Grassland
Limendous	17/07/2020	-0.1849852	43.273242	0	0.9	20.1	11	1	0	79.3	Grassland
Limendous	17/07/2020	-0.18485	43.2732618	0	1.4	20.1	24	2	0	78.9	Grassland
Limendous	17/07/2020	-0.1845785	43.2734148	0	0.4	20.3	20	1	0	79.2	Grassland

Limendous	17/07/2020	-0.1846843	43.2732183	0	0.9	20.1	4	1	0	79.1	Grassland
AAST	17/07/2020	-0.0905755	43.2812423	0	0.8	20.6	0	0	0	78.8	Grassland
AAST	17/07/2020	-0.0906192	43.28133	0	0.5	20.7	1	2	0	79	Grassland
AAST	17/07/2020	-0.0906485	43.2813792	0	0.8	20.8	4	1	0	78.8	Grassland
AAST	17/07/2020	-0.090692	43.2813773	0	0.1	20.4	3	0	0	79.1	Grassland
AAST	17/07/2020	-0.090754	43.2811532	0	0.5	20.5	13	1	0	79	Grassland
Lagarde	17/07/2020	0.028728	43.29708	0.1	0.3	20.7	3	0	0	79.1	Grassland
Lagarde	17/07/2020	0.0286485	43.2972113	0	0.2	20.6	5	1	0	79.1	Grassland
Lagarde	17/07/2020	0.0288807	43.297156	0	1	20.2	6	1	0	79.1	Grassland
Lagarde	17/07/2020	0.028839	43.2971893	0	0.4	20.4	5	1	0	79.3	Grassland
Lagarde	17/07/2020	0.0291008	43.2971365	0	0.2	20.4	3	0	0	79.4	Grassland
Saint Lézer	17/07/2020	0.0255307	43.3782162	0	0.3	20.6	1	2	0	79.3	Grassland
Saint Lézer	17/07/2020	0.0255418	43.3781755	0	0.8	20.2	1	2	0	79.2	Grassland
Saint Lézer	17/07/2020	0.0256272	43.3781927	0	0.2	20.2	2	0	0	79.4	Grassland
Saint Lézer	17/07/2020	0.02554	43.3781095	0	0.8	20.5	0	1	0	79.2	Grassland
Saint Lézer	17/07/2020	0.0255788	43.3779572	0	0.6	20.1	5	1	0	79.4	Grassland
Maubourget	17/07/2020	0.0251748	43.4800077	0	0.4	20.2	0	0	0	79.4	Grassland
Maubourget	17/07/2020	0.0251938	43.480026	0	0.2	20.2	1	0	0	79.5	Grassland
Maubourget	17/07/2020	0.0251963	43.4800633	0	0.5	19.7	3	0	0	79.5	Grassland
Maubourget	17/07/2020	0.0251822	43.4801192	0	0.2	20.2	2	0	0	79.5	Grassland
Maubourget	17/07/2020	0.0251663	43.4801543	0	0.1	20.2	3	1	0	79.6	Grassland
Hères	17/07/2020	0.0047642	43.5438105	0	3.2	17.8	3	0	0	79.6	Grassland
Hères	17/07/2020	0.0047792	43.5436597	0	0.7	19.9	1	0	0	79.6	Grassland
Hères	17/07/2020	0.0047897	43.5437658	0	1.1	19.7	2	0	0	79.4	Grassland
Hères	17/07/2020	0.0048278	43.5437758	0	0.5	20	2	0	0	79.6	Grassland
Hères	17/07/2020	0.0048217	43.543793	0	0.8	20.2	4	0	0	79.6	Grassland
Arrossès	17/07/2020	-0.1044333	43.5366138	0	0.3	20	1	1	0	79.5	Grassland
Arrossès	17/07/2020	-0.104399	43.5365902	0	0.5	20.3	1	0	0	79.5	Grassland
Arrossès	17/07/2020	-0.1043697	43.536653	0	0.1	20.3	0	0	0	79.6	Grassland
Arrossès	17/07/2020	-0.1042582	43.5366695	0	0.2	20.1	0	0	0	79.7	Grassland
Arrossès	17/07/2020	-0.1041008	43.5365278	0	0.4	20	4	1	0	79.8	Grassland
Séméacq Blachon	17/07/2020	-0.1237073	43.4946453	0	0.3	19.9	1	2	0	79.8	Grassland
Séméacq Blachon	17/07/2020	-0.1236198	43.4946773	0	0.2	20	2	1	0	79.7	Grassland
Séméacq Blachon	17/07/2020	-0.1233745	43.4945723	0	0.7	20.2	5	1	0	79.7	Grassland
Séméacq Blachon	17/07/2020	-0.1236595	43.494567	0	0.3	20.2	8	1	0	79.6	Grassland
Séméacq Blachon	17/07/2020	-0.1234102	43.494553	0	0.1	20.2	6	1	0	79.6	Grassland
Lucaré	17/07/2020	-0.078102	43.415144	0	1.6	19.6	2	2	0	79.8	Grassland
Lucaré	17/07/2020	-0.078102	43.415144	0	0.7	19.8	0	1	0	79.7	Grassland
Lucaré	17/07/2020	-0.078102	43.415144	0	0.4	20	0	0	0	79.7	Grassland
Lucaré	17/07/2020	-0.077827	43.412965	0	1.2	19.5	0	0	0	79.6	Grassland
Lucaré	17/07/2020	-0.077872	43.413032	0	0.2	20	0	0	0	79.8	Grassland
Bedous	22/07/2020	-0.558885	42.996271	0	0.8	20.3	2	0	0	79.1	Meadow
Bedous	22/07/2020	-0.580959	42.998354	0	0.4	20.4	3	0	0	79.2	Meadow
Bedous	22/07/2020	-0.55879	42.996059	0	0.6	20.3	3	0	0	79.1	Meadow
Bedous	22/07/2020	-0.5591932	42.996031	0	0.3	20.3	3	0	0	79.3	Meadow
Bedous	22/07/2020	-0.558908	42.996065	0	0.3	20.6	13	1	0	79.2	Meadow
Gère Belestin	22/07/2020	-0.421927	43.024804	0	1.4	20	3	1	0	79.1	Meadow
Gère Belestin	22/07/2020	-0.422018	43.024752	0	0.9	19.9	2	1	0	79.4	Meadow
Gère Belestin	22/07/2020	-0.4218915	43.0247782	0	0.4	20.2	1	1	0	79.5	Meadow
Gère Belestin	22/07/2020	-0.4219123	43.0247222	0	0.8	20	7	2	0	79.7	Meadow
Gère Belestin	22/07/2020	-0.4218905	43.0246917	0	1	19.8	2	0	0	79.8	Meadow
Arudy	22/07/2020	-0.4376092	43.1105303	0	1.9	20.1	2	0	0	79.6	Grassland
Arudy	22/07/2020	-0.4374483	43.1105577	0	1.7	19.1	1	1	0	79.4	Grassland
Arudy	22/07/2020	-0.4378262	43.1102668	0	1.4	19.3	0	0	0	79.5	Grassland
Arudy	22/07/2020	-0.4378197	43.1101688	0	1.3	19.1	1	1	0	79.7	Grassland
Arudy	22/07/2020	-0.4377137	43.110243	0	0.9	19.5	0	1	0	79.8	Grassland
Misériou	22/07/2020	-0.5533892	43.1155277	0	1.8	19.6	1	0	0	79.3	Meadow
Misériou	22/07/2020	-0.553402	43.1155778	0	2.6	18.8	3	0	0	79	Meadow
Misériou	22/07/2020	-0.5535452	43.1156187	0	7.9	19.7	5	1	0	77.9	Meadow
Misériou	22/07/2020	-0.553397	43.1154353	0	1	17.2	2	0	0	79.5	Meadow
Misériou	22/07/2020	-0.553475	43.1155432	0	1.2	19.8	3	1	0	79.4	Meadow
Précilhon	22/07/2020	-0.573282	43.1977083	0	0.1	20.4	4	0	0	79.6	Grassland
Précilhon	22/07/2020	-0.5732382	43.197551	0	0.7	19.8	8	1	0	79.6	Grassland
Précilhon	22/07/2020	-0.573247	43.1977563	0	0.1	20.2	6	0	0	79.7	Grassland
Précilhon	22/07/2020	-0.5732867	43.1977603	0	0.1	20.1	3	1	0	79.7	Grassland
Précilhon	22/07/2020	-0.5732755	43.197754	0	0.1	20.1	2	1	0	79.8	Grassland
Labarcat	22/07/2020	-0.4235382	43.205561	0	0.1	20.1	4	1	0	79.8	Grassland

Labarcat	22/07/2020	-0.4233417	43.2054665	0	0.1	20	5	1	0	79.8	Grassland
Labarcat	22/07/2020	-0.4232645	43.2054848	0	1.2	19.6	2	1	0	79.6	Grassland
Labarcat	22/07/2020	-0.4232525	43.2054667	0	0.6	19.7	2	1	0	79.7	Grassland
Labarcat	22/07/2020	-0.4234	43.205556	0	0.1	20	5	1	0	79.7	Grassland
Lesquerré	22/07/2020	-0.3421668	43.193199	0	0.9	20.3	3	0	0	79	Grassland
Lesquerré	22/07/2020	-0.3420142	43.193045	0	0.4	20.6	0	0	0	79.1	Grassland
Lesquerré	22/07/2020	-0.3419785	43.1930263	0	0.7	20.4	19	0	0	79.1	Grassland
Lesquerré	22/07/2020	-0.3420807	43.1930437	0	0.3	20.5	34	13	0	79.2	Grassland
Lesquerré	22/07/2020	-0.3418658	43.1931167	0	0.3	20.7	4	1	0	79.2	Grassland
Bizanos	22/07/2020	-0.352381	43.2808795	0	0.6	20.2	1	0	0	79.7	Grassland
Bizanos	22/07/2020	-0.3524877	43.2809692	0	0.8	19.3	5	0	0	79.8	Grassland
Bizanos	22/07/2020	-0.3524802	43.2808342	0	0.9	19.2	8	1	0	80	Grassland
Bizanos	22/07/2020	-0.3523057	43.2808578	0	0.8	19.5	3	1	0	80.1	Grassland
Bizanos	22/07/2020	-0.352358	43.2808867	0	0.5	19.4	2	1	0	80.3	Grassland
Laroïn	22/07/2020	-0.4377835	43.304135	0	0	19.7	1	0	0	80.3	Grassland
Laroïn	22/07/2020	-0.4377865	43.3041003	0	0	19.7	2	0	0	80.2	Grassland
Laroïn	22/07/2020	-0.4378673	43.3041963	0	0	19.7	2	1	0	80.3	Grassland
Laroïn	22/07/2020	-0.4377183	43.304082	0	0.1	19.6	6	2	0	80.2	Grassland
Laroïn	22/07/2020	-0.4378415	43.3042063	0	0.4	19.6	3	1	0	80.1	Grassland
Laroïn	22/07/2020	-0.4379217	43.3042235	0	0.3	19.4	7	1	0	80.3	Grassland
Haurrot	22/07/2020	-0.5678612	43.3082782	0	0.2	20	3	1	0	79.8	Grassland
Haurrot	22/07/2020	-0.5679992	43.3081078	0	0.3	20.1	2	0	0	79.6	Grassland
Haurrot	22/07/2020	-0.5678602	43.3082385	0	0.5	19.9	5	1	0	79.7	Grassland
Haurrot	22/07/2020	-0.5678013	43.308289	0	0.3	20	4	1	0	79.8	Grassland
Haurrot	22/07/2020	-0.5677583	43.308181	0	0.1	20	3	1	0	79.8	Grassland
Gaujacq	11/08/2020	-0.711854	43.661172	0	0.2	20.6	8	1	0	79.4	Grassland
Gaujacq	11/08/2020	-0.711818	43.661121	0	0.3	20.4	5	1	0	79.4	Grassland
Gaujacq	11/08/2020	-0.71181	43.661096	0	0.6	20.2	5	1	0	79.3	Grassland
Gaujacq	11/08/2020	-0.711829	43.661142	0	0.6	20	16	1	0	79.4	Grassland
Gaujacq	11/08/2020	-0.71198	43.66121	0	2.8	19.1	3	0	0	79	Grassland
Peyredère	11/08/2020	-0.7198242	43.7328115	0	0.1	20.8	1	0	0	79.1	Grassland
Peyredère	11/08/2020	-0.7199733	43.7327623	0	0.4	20.6	1	0	0	79.1	Grassland
Peyredère	11/08/2020	-0.7198872	43.7327407	0	0.3	20.6	1	0	0	79	Grassland
Peyredère	11/08/2020	-0.7199125	43.7326877	0	0.4	20.5	0	0	0	79.3	Grassland
Peyredère	11/08/2020	-0.7199673	43.7327285	0	0.4	20.6	2	2	0	79.4	Grassland
Gamarde-les-Bains	11/08/2020	-0.8617692	43.7397787	0	0.5	20.9	13	0	0	79.1	Grassland
Gamarde-les-Bains	11/08/2020	-0.8618607	43.7396248	0	0.6	20.5	15	0	0	79	Grassland
Gamarde-les-Bains	11/08/2020	-0.8616661	43.7396663	0	0.9	20.7	45	1	0	79.1	Grassland
Gamarde-les-Bains	11/08/2020	-0.8613703	43.7396463	0	0.6	20.7	19	0	0	79.2	Grassland
Gamarde-les-Bains	11/08/2020	-0.861776	43.7396423	0	0.2	20.5	2	0	0	79.3	Grassland
Candresse	11/08/2020	-0.9759565	43.723164	0	0.5	20.5	2	0	0	79	Grassland
Candresse	11/08/2020	-0.9760732	43.7231787	0	0.7	20.4	1	1	0	79.1	Grassland
Candresse	11/08/2020	-0.9759162	43.723125	0.1	0.6	20.3	0	1	0	79.1	Grassland
Candresse	11/08/2020	-0.9758305	43.7231423	0	0.6	20.3	0	0	0	79.2	Grassland
Candresse	11/08/2020	-0.9756418	43.7231338	0	0.7	20.3	1	0	0	79.1	Grassland
Eyrasse	11/08/2020	-1.1011817	43.7253257	0	1.1	20.4	2	1	0	79.2	Grassland
Eyrasse	11/08/2020	-1.1009842	43.7252965	0	1	19.7	11	3	0	79.3	Grassland
Eyrasse	11/08/2020	-1.1009377	43.7253348	0.1	1	19.7	13	3	0	79.3	Grassland
Eyrasse	11/08/2020	-1.1009972	43.7251972	0	0.9	19.8	5	1	0	79.4	Grassland
Eyrasse	11/08/2020	-1.1008223	43.7252723	0	0.7	19.7	4	1	0	79.5	Grassland
Balenton	11/08/2020	-1.228461	43.7222162	0	0.4	20.3	0	0	0	79.3	Grassland
Balenton	11/08/2020	-1.2283947	43.7222538	0	0.4	20.2	0	0	0	79.4	Grassland
Balenton	11/08/2020	-1.2282937	43.722274	0	0.4	20.2	0	0	0	79.4	Grassland
Balenton	11/08/2020	-1.2284365	43.7222422	0	0.2	20.2	19	2	0	79.5	Grassland
Balenton	11/08/2020	-1.2283322	43.7222807	0	0.4	20.3	10	0	0	79.4	Grassland
Josse	11/08/2020	-1.2201365	43.6384445	0	0.2	20.3	2	0	0	79.3	Grassland
Josse	11/08/2020	-1.2201792	43.6385422	0	0.2	20.4	5	0	0	79.3	Grassland
Josse	11/08/2020	-1.2199942	43.6385935	0	0.5	20	7	1	0	79.4	Grassland
Josse	11/08/2020	-1.2199308	43.6384893	0	0.1	20.4	9	0	0	79.4	Grassland
Josse	11/08/2020	-1.2201363	43.6385252	0	0.2	20.3	13	1	0	79.4	Grassland
Heugas	11/08/2020	-1.090996	43.631865	0	0.4	20.1	2	1	0	79.6	Grassland
Heugas	11/08/2020	-1.091223	43.631791	0	0.2	20.1	6	1	0	79.8	Grassland
Heugas	11/08/2020	-1.09121	43.63183	0	0.1	20.1	8	1	0	79.8	Grassland
Heugas	11/08/2020	-1.09098	43.631847	0	0.6	20	4	1	0	79.9	Grassland
Heugas	11/08/2020	-1.091198	43.631744	0	0.4	19.8	3	1	0	79.9	Grassland
Mimbaste	11/08/2020	-0.9652445	43.6469152	0	0.3	20.2	2	0	0	79.8	Grassland
Mimbaste	11/08/2020	-0.965301	43.6468947	0	0.3	20	5	0	0	79.9	Grassland

Mimbaste	11/08/2020	-0.965351	43.64686	0	0.4	19.8	3	2	0	79.9	Grassland
Mimbaste	11/08/2020	-0.9654008	43.6469332	0	0.2	19.7	3	1	0	80	Grassland
Mimbaste	11/08/2020	-0.9652538	43.6469303	0	0.3	19.8	8	1	0	80	Grassland
Romarez	11/08/2020	-0.838045	43.6329775	0	0.3	20	3	0	0	79.9	Grassland
Romarez	11/08/2020	-0.8381438	43.6329355	0	0.2	19.8	3	0	0	80	Grassland
Romarez	11/08/2020	-0.8380463	43.6330792	0	0.2	19.7	11	1	0	80	Grassland
Romarez	11/08/2020	-0.8379175	43.6330263	0	0.2	19.9	7	1	0	80	Grassland
Romarez	11/08/2020	-0.8380027	43.6330245	0	0.1	19.9	2	0	0	80	Grassland
Bahus soubiran	14/08/2020	-0.363096	43.666309	0	0.4	20.7	0	0	0	79.3	Grassland
Bahus soubiran	14/08/2020	-0.363166	43.666453	0	0.2	20.6	0	1	0	79.4	Grassland
Bahus soubiran	14/08/2020	-0.363088	43.66637	0	0.4	20.2	12	0	0	79.4	Grassland
Bahus soubiran	14/08/2020	-0.363002	43.666293	0	0.5	20.5	2	1	0	79.3	Grassland
Bahus soubiran	14/08/2020	-0.362971	43.666469	0	0.3	20.5	1	1	0	79.4	Grassland
Bernède	14/08/2020	-0.228397	43.669555	0	0.2	20.7	3	0	0	79.1	Grassland
Bernède	14/08/2020	-0.231667	43.669264	0	0.7	20.5	3	0	0	78.9	Grassland
Bernède	14/08/2020	-0.2317108	43.6692927	0	0.3	20.6	3	0	0	79.1	Grassland
Bernède	14/08/2020	-0.2317098	43.6692878	0	0.2	20.7	4	0	0	79.1	Grassland
Bernède	14/08/2020	-0.231682	43.6693105	0	0.1	20.6	8	1	0	79.2	Grassland
Tarsac	14/08/2020	-0.1047977	43.6670352	0	0.5	20.5	0	0	0	79.1	Grassland
Tarsac	14/08/2020	-0.1046757	43.6669787	0	0.4	20.4	8	0	0	79.1	Grassland
Tarsac	14/08/2020	-0.1046098	43.667035	0	0.1	20.6	3	0	0	79.2	Grassland
Tarsac	14/08/2020	-0.1046848	43.6670573	0	0.1	20.6	2	0	0	79.3	Grassland
Tarsac	14/08/2020	-0.1046477	43.6670395	0	0.1	20.6	7	0	0	79.3	Grassland
Arblade le haut	14/08/2020	-0.0639412	43.7436748	0	0.2	20.8	6	1	0	79.2	Grassland
Arblade le haut	14/08/2020	-0.0640433	43.7437165	0	0.1	20.6	2	0	0	79.3	Grassland
Arblade le haut	14/08/2020	-0.0640572	43.7436472	0	0.3	20.6	7	0	0	79.3	Grassland
Arblade le haut	14/08/2020	-0.06405	43.743551	0	0.1	20.6	0	0	0	79.4	Grassland
Arblade le haut	14/08/2020	-0.0639667	43.7435555	0	0.1	20.5	0	0	0	79.4	Grassland
Lussagnet	14/08/2020	-0.230921	43.7748162	0	0.1	20.7	3	0	0	79.2	Grassland
Lussagnet	14/08/2020	-0.2310398	43.7749073	0	0.1	20.6	0	0	0	79.2	Grassland
Lussagnet	14/08/2020	-0.2310505	43.774818	0	0.1	20.7	8	0	0	79.3	Grassland
Lussagnet	14/08/2020	-0.2311072	43.7749108	0	0.4	20.6	1	0	0	79.3	Grassland
Lussagnet	14/08/2020	-0.23099	43.7748947	0	0.1	20.6	1	0	0	79.3	Grassland
Lussagnet	14/08/2020	-0.231062	43.7749715	0	0.4	20.3	0	0	0	79.4	Grassland
Renung	14/08/2020	-0.3554283	43.7404603	0	0.1	20.7	0	0	0	79.6	Grassland
Renung	14/08/2020	-0.3554055	43.740559	0	0.3	20.1	0	1	0	79.6	Grassland
Renung	14/08/2020	-0.3553953	43.7405038	0	0.7	20	9	0	0	79.6	Grassland
Renung	14/08/2020	-0.3553823	43.7405203	0	1.5	20.2	3	0	0	79.6	Grassland
Renung	14/08/2020	-0.3554242	43.7404992	0	0.9	20.2	12	1	0	79.8	Grassland
Renung	14/08/2020	-0.3560313	43.7407593	0	0.7	20	3	0	0	79.7	Grassland
Montgaillard	14/08/2020	-0.481685	43.7377	0	0.8	19.9	11	1	0	79.4	Grassland
Montgaillard	14/08/2020	-0.4818232	43.7377322	0	1	19.7	15	2	0	79.4	Grassland
Montgaillard	14/08/2020	-0.4816722	43.7376365	0	1.4	19.6	32	2	0	79.3	Grassland
Montgaillard	14/08/2020	-0.4818088	43.7377325	0	0.4	20.3	17	2	0	79.4	Grassland
Montgaillard	14/08/2020	-0.4818938	43.7377943	0	1.2	19.8	27	2	0	79.4	Grassland
Audignon	14/08/2020	-0.5882988	43.7297888	0	0.1	20.7	0	0	0	79.2	Grassland
Audignon	14/08/2020	-0.5884475	43.729895	0	1.8	19.5	2	0	0	79.1	Grassland
Audignon	14/08/2020	-0.58841	43.7299447	0	0.5	19.8	3	0	0	79.3	Grassland
Audignon	14/08/2020	-0.5883987	43.7298453	0	0.7	20.6	10	1	0	79.3	Grassland
Audignon	14/08/2020	-0.5885272	43.729939	0	3.8	20.5	19	0	0	79.2	Grassland
Magetmau	14/08/2020	-0.6096252	43.6519425	0	1.5	20.5	32	2	0	79.5	Grassland
Magetmau	14/08/2020	-0.6095663	43.65185	0	0.8	19.8	14	2	0	79.4	Grassland
Magetmau	14/08/2020	-0.6096323	43.6518175	0	1.4	19.6	3	0	0	79.1	Grassland
Magetmau	14/08/2020	-0.6096772	43.651997	0	0.9	19.4	0	0	0	79.2	Grassland
Magetmau	14/08/2020	-0.6097428	43.6518995	0	0.7	19.2	35	1	0	79.7	Grassland
Bats	14/08/2020	-0.4601553	43.6514042	0	0.7	20.2	2	1	0	79.3	Grassland
Bats	14/08/2020	-0.4601502	43.6514328	0	0.6	20.5	4	0	0	79.2	Grassland
Bats	14/08/2020	-0.4600367	43.6515062	0	0.4	20.4	6	1	0	79.3	Grassland
Bats	14/08/2020	-0.4600917	43.6514823	0	0.8	20	5	1	0	79.3	Grassland
Bats	14/08/2020	-0.4599673	43.6516208	0	0.7	20	6	1	0	79.4	Grassland
Lecumberry	18/08/2020	-1.1393383	43.1440442	0	0.7	20.6	0	0	0	79.2	Meadow
Lecumberry	18/08/2020	-1.1393143	43.144071	0	0.3	20	0	0	0	79.4	Meadow
Lecumberry	18/08/2020	-1.1392185	43.1441372	0	0.3	20.2	0	1	0	79.4	Meadow
Lecumberry	18/08/2020	-1.139389	43.1439758	0	0.1	20.2	0	0	0	79.6	Meadow
Lecumberry	18/08/2020	-1.1393502	43.1439783	0	1.2	19.7	0	1	0	79	Meadow
Pierraene. col de Napole	18/08/2020	-0.9862093	43.1541787	0	0.2	20.5	0	0	0	79.5	Meadow
Pierraene. col de Napole	18/08/2020	-0.9861945	43.1542212	0	0.1	20.2	0	1	0	79.6	Meadow

Pierraene. col de Napole	18/08/2020	-0.9861342	43.1541937	0	0.1	20.3	0	0	0	79.6	Meadow
Pierraene. col de Napole	18/08/2020	-0.9861055	43.1542472	0	0.1	20.2	0	0	0	79.7	Meadow
Pierraene. col de Napole	18/08/2020	-0.986105	43.154076	0	0.1	20.1	0	0	0	79.8	Meadow
Sauguis saint Etienne	18/08/2020	-0.8938353	43.1539908	0	0.1	20.1	0	1	0	79.8	Grassland
Sauguis saint Etienne	18/08/2020	-0.8937287	43.1537652	0	0.5	19.9	5	1	0	79.8	Grassland
Sauguis saint Etienne	18/08/2020	-0.8937233	43.1537592	0	0.3	20	4	0	0	79.8	Grassland
Sauguis saint Etienne	18/08/2020	-0.8938668	43.1537913	0	0.6	19.7	2	0	0	79.9	Grassland
Sauguis saint Etienne	18/08/2020	-0.8939265	43.1537747	0	0.6	19.7	2	1	0	79.9	Grassland
Mauléon Licharre	18/08/2020	-0.890561	43.2317192	0	0.1	20	0	0	0	79.9	Grassland
Mauléon Licharre	18/08/2020	-0.8906138	43.2317945	0	0.1	19.9	1	0	0	79.9	Grassland
Mauléon Licharre	18/08/2020	-0.8905575	43.2317268	0	0.2	20	1	1	0	79.9	Grassland
Mauléon Licharre	18/08/2020	-0.8906512	43.2317132	0	0.1	19.9	0	1	0	80	Grassland
Mauléon Licharre	18/08/2020	-0.8906273	43.2316172	0	0.1	19.9	1	0	0	79.9	Grassland
Charre	18/08/2020	-0.8790327	43.319389	0	0.1	20.2	3	0	0	79.7	Grassland
Charre	18/08/2020	-0.8787977	43.3194755	0	0.1	20.1	3	1	0	79.7	Grassland
Charre	18/08/2020	-0.878745	43.3194802	0	1	19.4	5	2	0	79.6	Grassland
Charre	18/08/2020	-0.8786887	43.3194895	0	0.4	19.4	5	2	0	79.7	Grassland
Charre	18/08/2020	-0.878809	43.3195378	0	1.6	19.2	51	4	0	79.7	Grassland
Béhasque Lapiste	18/08/2020	-1.0008585	43.3238257	0	0.1	20.2	1	1	0	79.7	Grassland
Béhasque Lapiste	18/08/2020	-1.0011103	43.3239293	0	0.1	20.3	2	1	0	79.6	Grassland
Béhasque Lapiste	18/08/2020	-1.0010653	43.324019	0	0.1	20.3	3	0	0	79.6	Grassland
Béhasque Lapiste	18/08/2020	-1.0010308	43.3240365	0	0.3	20.1	1	1	0	79.7	Grassland
Béhasque Lapiste	18/08/2020	-1.001026	43.3240528	0	0	20.2	1	0	0	79.7	Grassland
Pagolle	18/08/2020	-0.9886803	43.2312965	0	0	20.3	1	0	0	79.5	Grassland
Pagolle	18/08/2020	-0.9885677	43.231297	0	0	20.1	2	1	0	79.7	Grassland
Pagolle	18/08/2020	-0.9885308	43.2313123	0	0	20.3	1	0	0	79.8	Grassland
Pagolle	18/08/2020	-0.9886507	43.2313498	0	0.1	20	0	0	0	79.9	Grassland
Pagolle	18/08/2020	-0.9886485	43.2313662	0	0.1	20	5	1	0	79.8	Grassland
Saint Etienne Lantabat	18/08/2020	-1.1477432	43.2460792	0	0.5	20.6	1	1	0	79.1	Grassland
Saint Etienne Lantabat	18/08/2020	-1.1477332	43.2461235	0	0.4	20.6	3	1	0	79.3	Grassland
Saint Etienne Lantabat	18/08/2020	-1.147671	43.246028	0	0.1	20.4	2	0	0	79.4	Grassland
Saint Etienne Lantabat	18/08/2020	-1.1478353	43.2461753	0	0.2	20.4	2	0	0	79.3	Grassland
Saint Etienne Lantabat	18/08/2020	-1.1478137	43.246235	0	0.1	20.5	2	0	0	79.3	Grassland
Méharin	18/08/2020	-1.1391313	43.3301618	0	0	20.6	2	0	0	79.3	Grassland
Méharin	18/08/2020	-1.1392758	43.3302353	0	0.1	20.6	1	0	0	79.3	Grassland
Méharin	18/08/2020	-1.1392132	43.3302238	0	0.1	20.5	1	2	0	79.5	Grassland
Méharin	18/08/2020	-1.139184	43.3301962	0	0.1	20.5	2	0	0	79.4	Grassland
Méharin	18/08/2020	-1.1391825	43.3301988	0	0.1	20.4	1	0	0	79.5	Grassland
Orègue	18/08/2020	-1.1354657	43.3960803	0	0.4	20.3	1	0	0	79.5	Grassland
Orègue	18/08/2020	-1.1353967	43.3959845	0	0.2	20.1	1	0	0	79.6	Grassland
Orègue	18/08/2020	-1.1354163	43.396036	0	0.4	20	1	0	0	79.6	Grassland
Orègue	18/08/2020	-1.1355102	43.3960882	0	0.3	20	2	0	0	79.7	Grassland
Orègue	18/08/2020	-1.135339	43.396099	0	0.2	20.1	1	0	0	79.7	Grassland
Abitain	19/08/2020	-0.9951383	43.4123457	0	0.2	20.8	0	0	0	79.2	Grassland
Abitain	19/08/2020	-0.9950187	43.4123527	0	0.3	20.4	0	1	0	79.2	Grassland
Abitain	19/08/2020	-0.9951878	43.4123408	0	0.5	20.3	4	0	0	79.2	Grassland
Abitain	19/08/2020	-0.995109	43.4122615	0	0.2	20.4	2	0	0	79.2	Grassland
Abitain	19/08/2020	-0.9952165	43.4123142	0	0.2	20.5	0	0	0	79.3	Grassland
Orion	19/08/2020	-0.8620758	43.4184547	0	0.3	20.4	0	1	0	79.2	Grassland
Orion	19/08/2020	-0.8621823	43.4184223	0	0.9	20	1	1	0	79.1	Grassland
Orion	19/08/2020	-0.8621642	43.4183978	0	0.2	20	1	0	0	79.3	Grassland
Orion	19/08/2020	-0.862236	43.418376	0	0.4	20.3	3	0	0	79.5	Grassland
Orion	19/08/2020	-0.8621105	43.4184047	0	0.3	20	1	0	0	79.7	Grassland
Sauveterre	26/08/2020	-0.949009	43.4044013	0	0.1	20.6	37	2	0	79.4	Grassland
Sauveterre	26/08/2020	-0.9492777	43.4046993	0	0.7	19.9	11	0	0	79.8	Grassland
Sauveterre	26/08/2020	-0.949078	43.4048273	0	0.4	19.8	14	1	0	79.6	Grassland
Sauveterre	26/08/2020	-0.9490692	43.4050965	0	0.7	19.6	27	2	0	79.6	Grassland
Sauveterre	26/08/2020	-0.949107	43.4052518	0	1	19.5	5	0	0	79.7	Grassland
Sauveterre	26/08/2020	-0.9491238	43.4055235	0	0.3	20.1	29	2	0	79.6	Grassland
Sauveterre	26/08/2020	-0.9502338	43.4052952	0	0.3	18.9	50	4	0	79.5	Grassland
Sauveterre	26/08/2020	-0.952655	43.4064735	0	0.3	20.3	24	4	0	79.3	Grassland
Sauveterre	26/08/2020	-0.9517605	43.4062013	0	0.3	20.3	37	2	0	79.4	Grassland
Sauveterre	26/08/2020	-0.9512172	43.405307	0	0	20.7	55	6	0	79.4	Grassland
Sauveterre	26/08/2020	-0.9512	43.4050485	0	0.2	20.4	119	6	0	79.4	Grassland
Sauveterre	26/08/2020	-0.9512997	43.4047612	0	0.2	20.3	50	4	0	79.5	Grassland
Sauveterre	26/08/2020	-0.9511887	43.4042962	0	0.3	20.2	60	5	0	79.5	Grassland
Sauveterre	26/08/2020	-0.951668	43.4039612	0	0.5	20	6	1	0	79.3	Grassland

Sauveterre	26/08/2020	-0.951744	43.403663	0	0.4	20.2	18	3	0	79.5	Grassland
Sauveterre	26/08/2020	-0.9508555	43.4039783	0	0.3	20.3	1	0	0	79.5	Grassland
Sauveterre	26/08/2020	-0.948133	43.4044467	0	0	20.6	4	2	0	79.2	Grassland
Sauveterre	26/08/2020	-0.9481632	43.4046447	0	0.6	20.2	12	3	0	79.3	Grassland
Sauveterre	26/08/2020	-0.9479597	43.404895	0	0.5	20.3	12	5	0	79.3	Grassland
Sauveterre	26/08/2020	-0.9490157	43.404403	0	0	20.6	0	0	0	79.4	Grassland
Sauveterre	26/08/2020	-0.9489653	43.4044825	0	0	20.5	0	0	0	79.5	Grassland
Sauveterre	26/08/2020	-0.9490845	43.4043915	0	0	20.5	0	0	0	79.4	Grassland
Sauveterre	27/08/2020	-0.9490627	43.4044773	0	0	20.5	36	3	0	79.5	Grassland
Sauveterre	27/08/2020	-0.9491138	43.4045195	0	0.6	19.9	33	1	0	79.7	Grassland
Sauveterre	27/08/2020	-0.9491623	43.4044675	0	0.5	19.8	21	3	0	79.7	Grassland
Sauveterre	27/08/2020	-0.949107	43.4045245	0	0	20.1	16	1	0	79.6	Grassland
Sauveterre	27/08/2020	-0.9510023	43.405638	0	0	20.4	108	4	0	79.6	Grassland
Sauveterre	27/08/2020	-0.9511262	43.4054517	0	0.2	20.2	50	6	0	79.8	Grassland
Sauveterre	27/08/2020	-0.9511938	43.405433	0	0	20.4	70	12	0	79.8	Grassland
Sauveterre	27/08/2020	-0.952225	43.4062175	0	0.4	19.8	19	5	0	79.6	Grassland
Sauveterre	27/08/2020	-0.9527828	43.407021	0	1.2	19.1	57	9	0	79.6	Grassland
Sauveterre	27/08/2020	-0.9528128	43.40704	0	0.5	19.8	76	5	0	79.8	Grassland
Sauveterre	27/08/2020	-0.9514777	43.4077955	0	0.2	20	17	2	0	79.7	Grassland
Sauveterre	27/08/2020	-0.9497565	43.4081968	0	0.7	19.4	94	12	0	80	Grassland
Sauveterre	27/08/2020	-0.9496363	43.4081757	0	0.3	19.7	39	2	0	80	Grassland
Sauveterre	27/08/2020	-0.950099	43.408015	0	0.1	19.8	55	4	0	80.4	Grassland
Sauveterre	27/08/2020	-0.9506942	43.4075002	0	0.2	19.5	30	5	0	80.3	Grassland
Sauveterre	27/08/2020	-0.9522057	43.4062082	0	0	20.2	51	1	0	79.7	Grassland
Sauveterre	03/09/2020	-0.949258	43.4043885	0	0.1	20.6	18	2	0	79.4	Grassland
Sauveterre	03/09/2020	-0.9487715	43.4043638	0	0.4	20.2	9	3	0	79.6	Grassland
Sauveterre	03/09/2020	-0.9500323	43.4047862	0	0.2	20.1	11	4	0	79.9	Grassland
Sauveterre	03/09/2020	-0.9499057	43.4047035	0	0	19.9	4	2	0	80.2	Grassland
Sauveterre	03/09/2020	-0.9513742	43.4050517	0	0.2	19.8	26	6	0	80.4	Grassland
Sauveterre	03/09/2020	-0.9514117	43.4049842	0	0.2	19.3	18	3	0	80.5	Grassland
Sauveterre	10/09/2020	-0.9491003	43.4045207	0	0.1	20.5	3	2	0	79.3	Grassland
Sauveterre	10/09/2020	-0.9500913	43.4048885	0	0.1	20.2	0	1	0	79.8	Grassland
Sauveterre	10/09/2020	-0.9500235	43.4048148	0	0.2	20.1	0	1	0	79.6	Grassland
Sauveterre	10/09/2020	-0.9512205	43.4051647	0	0	20.2	5	5	0	79.8	Grassland
Sauveterre	10/09/2020	-0.9513072	43.405079	0	0.1	20.1	68	0	0	79.6	Grassland
Sauveterre	10/09/2020	-0.949369	43.405088	0	0.1	20.6	2	1	0	79.3	Grassland